tions of aquifer thickness, velocity of groundwater in the aquifer, concentration gradients in the aquitards, and diffusion coefficients, determine conditions under which the water chemistry in the aquifer would be controlled by the vertical flux by molecular diffusion of dissolved solids from the shale into the aquifer. Assume that dissolved solids that enter the aquifer are distributed uniformly over the aquifer thickness as a result of dispersion. Do you think such conditions could occur in nature?

20. Groundwater *A*, at $P_{CO_2} = 10^{-2}$, has a composition that results from the open-system dissolution of siderite ($FeCO_3$) in a stratum with no calcite or dolomite. Groundwater *B*, at the same P_{CO_2}, has a composition that results from open-system dissolution of calcite in a stratum with no siderite or dolomite. These two waters, each having been in equilibrium with their respective solid phase, are intercepted by a well in which they are mixed in equal proportions as pumping occurs. The system has a temperature of 25°C.

(a) Compute the cation and anion concentrations and pH of each of these waters.
(b) Compute the composition of the mixed water in the well.
(c) Is this mixture capable of producing calcite or siderite by precipitation?
(d) After discharge from the well into an open-air storage tank at 25°C, would calcite and/or siderite precipitate?

CHAPTER 8

Groundwater Resource Evaluation

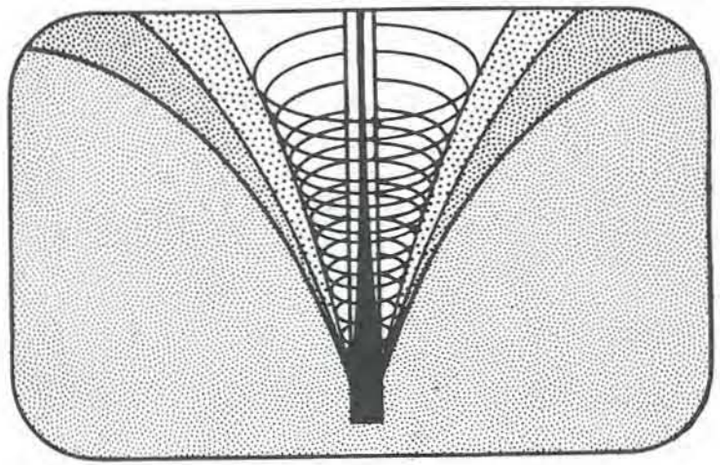

In the first seven chapters of this book we have examined the physical and chemical principles that govern groundwater flow and we have investigated the interrelationships that exist between the geological environment, the hydrologic cycle, and natural groundwater flow. In this chapter and the two that follow, we will turn to the interactions between groundwater and man. We will look at the utilization of groundwater as a resource, we will examine its role as an agent for subsurface contamination, and we will assess the part it plays in a variety of geotechnical problems.

8.1 Development of Groundwater Resources

Exploration, Evaluation, and Exploitation

The development of groundwater resources can be viewed as a sequential process with three major phases. First, there is an *exploration* stage, in which surface and subsurface geological and geophysical techniques are brought to bear on the search for suitable aquifers. Second, there is an *evaluation* stage that encompasses the measurement of hydrogeologic parameters, the design and analysis of wells, and the calculation of aquifer yields. Third, there is an *exploitation*, or *management* phase, which must include consideration of optimal development strategies and an assessment of the interactions between groundwater exploitation and the regional hydrologic system.

It is worth placing these three phases in a historical perspective. In North America and Europe, nearly all major aquifers have already been located and are being used to some extent. The era of true exploration for regional aquifers is over. We are now in a period in which detailed evaluation of known aquifers and careful management of known resources will take on greater importance. The layout of this chapter reflects this interpretation of current needs. We will treat

aquifer exploration in a single section, and place heavier emphasis on the evaluation and management stages.

Let us assume that we have located an aquifer that has some apparent potential. The scope of groundwater resource evaluation and management studies might best be indicated by the following series of questions:

1. Where should the wells be located? How many wells are needed? What pumping rates can they sustain?
2. What will be the effect of the proposed pumping scheme on regional water levels?
3. What are the long-term yield capabilities of the aquifer?
4. Will the proposed development have any detrimental influence on other components of the hydrologic cycle?
5. Are there likely to be any undesirable side effects of development, such as land subsidence or seawater intrusion, that could serve to limit yields?

This chapter is designed to provide the methodology needed to answer questions of this type. The measurement and estimation of hydrogeologic parameters is treated in Sections 8.4 through 8.7. Predictions of drawdown in an aquifer under a proposed pumping scheme can be carried out for simple situations with the analytical methods presented in Section 8.3. More complex hydrogeological environments may require the application of numerical-simulation techniques, as presented in Section 8.8, or electrical-analog techniques, as presented in Section 8.9. Land subsidence is discussed in Section 8.12, and seawater intrusion in Section 8.13.

Well Yield, Aquifer Yield, and Basin Yield

The techniques of groundwater resource evaluation require an understanding of the concept of *groundwater yield*, and, perhaps surprisingly, this turns out to be a difficult and ambiguous term to address. The concept is certainly pertinent, in that one of the primary objectives of most groundwater resource studies is the determination of the maximum possible pumping rates that are compatible with the hydrogeologic environment from which the water will be taken. This need for compatibility implies that yields must be viewed in terms of a balance between the benefits of groundwater pumpage and the undesirable changes that will be induced by such pumpage. The most ubiquitous change that results from pumping is lowered water levels, so in the simplest cases groundwater yield can be defined in terms of the maximum rate of pumpage that can be allowed while ensuring that water-level declines are kept within acceptable limits.

This concept of yield can be applied on several scales. If our unit of study is a single well, we can define a well yield; if our unit of study is an aquifer, we can define an aquifer yield; and if our unit of study is a groundwater basin, we can define a basin yield. *Well yield* can be defined as the maximum pumping rate that can be supplied by a well without lowering the water level in the well below the pump intake. *Aquifer yield* can be defined as the maximum rate of withdrawal that

can be sustained by an aquifer without causing an unacceptable decline in the hydraulic head in the aquifer. *Basin yield* can be defined as the maximum rate of withdrawal that can be sustained by the complete hydrogeologic system in a groundwater basin without causing unacceptable declines in hydraulic head in the system or causing unacceptable changes to any other component of the hydrologic cycle in the basin. In light of the effects of well interference that are discussed in Section 8.3, it is clear that aquifer yield is highly dependent on the number and spacing of wells tapping an aquifer. If all the wells in a highly developed aquifer pump at a rate equal to their well yield, it is likely that the aquifer yield will be exceeded. In light of the effects of aquitard leakage and aquifer interference that are also discussed in Section 8.3, it is clear that basin yield is highly dependent on the number and spacing of exploited aquifers in a basin. If all the aquifers are pumped at a rate equal to their aquifer yield, it is likely that the basin yield will be exceeded.

These simple concepts should prove useful to the reader in the early sections of this chapter. However, the concept of basin yield deserves reconsideration in greater depth, and this is presented in Section 8.10.

8.2 Exploration for Aquifers

An aquifer is a geological formation that is capable of yielding economic quantities of water to man through wells. It must be porous, permeable, and saturated. While aquifers can take many forms within the wide variety of existing hydrogeological environments, a perusal of the permeability and porosity data of Tables 2.2 and 2.4 and consideration of the discussions of Chapter 4 make it clear that certain geological deposits are of recurring interest as aquifers. Among the most common are unconsolidated sands and gravels of alluvial, glacial, lacustrine, and deltaic origin; sedimentary rocks, especially limestones and dolomites, and sandstones and conglomerates; and porous or fractured volcanic rocks. In most cases, aquifer exploration becomes a search for one or other of these types of geological deposits. The methods of exploration can be grouped under four headings: surface geological, subsurface geological, surface geophysical, and subsurface geophysical.

Surface Geological Methods

The initial steps in a groundwater exploration program are carried out in the office rather than in the field. Much can be learned from an examination of available maps, reports, and data. There are published geologic maps on some scale for almost all of North America; there are published soils maps or surficial geology maps for most areas; and there are published hydrogeological maps for some areas. Geologic maps and reports provide the hydrogeologist with an initial indication of the rock formations in an area, together with their stratigraphic and structural interrelationships. Soils maps or surficial geology maps, together with topographic maps, provide an introduction to the distribution and genesis of the

surficial unconsolidated deposits and their associated landforms. Hydrogeologic maps provide a summarized interpretation of the topographic, geologic, hydrogeologic, geochemical, and water resource data available in an area.

Airphoto interpretation is also widely used in groundwater exploration. It is usually possible to prepare maps of landforms, soils, land use, vegetation, and drainage from the airphoto coverage of an area. Each of these environmental properties leads to inferences about the natural groundwater flow systems and/or the presence of potential aquifers. Way (1973) and Mollard (1973) each provide a handbook-style treatment of airphoto-interpretation methods, and both include a large number of interpreted photos, many of which illustrate significant hydrogeological features.

However, even in areas where there is a considerable amount of published information, it is usually necessary to carry out geologic mapping in the field. In view of the importance of unconsolidated sands and gravels as potential aquifers, special attention must be paid to geomorphic landforms and to the distribution of glacial and alluvial deposits. Where sand and gravel deposits are sparse, or where these deposits are shallow and unsaturated, more detailed attention must be paid to the lithology, stratigraphy, and structure of the bedrock formations.

The methods of hydrogeologic mapping outlined in Section 6.1 are useful in determining the scale and depth of natural groundwater flow systems and in mapping the extent of their recharge and discharge areas.

Subsurface Geological Methods

It is seldom sufficient to look only at the surficial manifestations of a hydrogeological environment. It is unlikely that subsurface stratigraphic relationships will be fully revealed without direct subsurface investigation. Once again, the initial step usually involves scanning the available records. Many state and provincial governments now require that geological logs of all water wells be filed in a central bank for the use of other investigators. These data, while varying widely in quality, can often provide the hydrogeologist with considerable information on past successes and failures in a given region.

In most exploration programs, especially those for large-scale industrial or municipal water supplies, it is necessary to carry out test-drilling to better delineate subsurface conditions. Test holes provide the opportunity for geological and geophysical logging and for the coring or sampling of geological materials. Test holes can also be used to obtain water samples for chemical analysis and to indicate the elevation of the water table at a site. Test-drilling programs, together with published geological maps and available well-log records, can be interpreted in terms of the local and regional lithology, stratigraphy, and structure. Their logs can be used to prepare stratigraphic cross sections, geological fence diagrams, isopach maps of overburden thickness or formation thickness, and lithofacies maps. Hydrogeological interpretations might include water-table contours and isopachs of saturated thickness of unconfined aquifers. The results of chemical analyses of groundwater samples, when graphically displayed using the methods

of Chapter 7, can provide important evidence on the natural geochemical environment as well as a direct measure of water quality.

Surface Geophysical Methods

There are two regional geophysical techniques that are used to some extent in the exploration for aquifers. These are the *seismic refraction* method and the *electrical resistivity* method. The design of geophysical surveys that utilize these approaches, and the interpretation of the resulting geophysical measurements, is a specialized branch of the earth sciences. It is not expected that a groundwater hydrologist become such a specialist, and for this reason our discussion is brief. On the other hand, it *is* necessary that the hydrogeologist be aware of the power and limitations of the methods. If this brief presentation fails to meet that objective, the reader is directed to a standard geophysics textbook such as Dobrin (1960), or to one of several review papers that deal specifically with geophysical applications in groundwater exploration, such as McDonald and Wantland (1961), Hobson (1967), or Lennox and Carlson (1967).

The *seismic refraction method* is based on the fact that elastic waves travel through different earth materials at different velocities. The denser the material, the higher the wave velocity. When elastic waves cross a geologic boundary between two formations with different elastic properties, the velocity of wave propagation changes and the wave paths are refracted according to Snell's law. In seismic exploration, elastic waves are initiated by an energy source, usually a small explosion, at the ground surface. A set of receivers, called *geophones*, is set up in a line radiating outward from the energy source. Waves initiated at the surface and refracted at the critical angle by a high-velocity layer at depth will reach the more distant geophones more quickly than waves that travel directly through the low-velocity surface layer. The time between the shock and the arrival of the elastic wave at a geophone is recorded on a *seismograph*. A set of seismograph records can be used to derive a graph of arrival time versus distance from shot point to geophone, and this, in turn, with the aid of some simple theory, can be used to calculate layer depths and their seismic velocities.

In groundwater investigations the seismic refraction method has been used to determine such features as the depth to bedrock, the presence of buried bedrock channels, the thickness of surficial fracture zones in crystalline rock, and the areal extent of potential aquifers. The interpretations are most reliable in cases where there is a simple two-layer or three-layer geological configuration in which the layers exhibit a strong contrast in seismic velocity. The velocities of the layers must increase with depth; the method cannot pick up a low-velocity layer (which might well be a porous potential aquifer) that underlies a high-velocity surface layer. The depth of penetration of the seismic method depends on the strength of the energy source. For shallow investigations (say, up to 30 m) hydrogeologists have often employed *hammer seismic* methods, in which the energy source is simply a hammer blow on a steel plate set on the ground surface.

The *electrical resistivity* of a geological formation is defined as $\rho = RA/L$, where R is the resistance to electrical current for a unit block of cross-sectional area A and length L. The resistivity controls the gradient in electrical potential that will be set up in a formation under the influence of an applied current. In a saturated rock or soil, the resistivity is largely dependent on the density and porosity of the material and on the salinity of the saturating fluid. In an electrical resistivity survey an electric current is passed into the ground through a pair of *current electrodes* and the potential drop is measured across a pair of *potential electrodes*. The spacing of the electrodes controls the depth of penetration. At each setup an apparent resistivity is calculated on the basis of the measured potential drop, the applied current, and the electrode spacing. Sets of measurements are taken either in the form of *lateral profiling* or *depth profiling*. In lateral profiling the electrode spacing is kept constant as electrodes are leapfrogged down a survey line. This method provides areal coverage at a given depth of penetration. It can be used to define aquifer limits or to map areal variations in groundwater salinity. In depth profiling a series of readings is taken at different electrode spacings at a single station. Apparent resistivities are plotted against electrode spacing, and stratigraphic interpretations are made by comparing the resulting curve against published theoretical curves for simple layered geometries. Depth profiling has been widely used to determine the thickness of sand and gravel aquifers that overlie bedrock. It can also be used to locate the saltwater-freshwater interface in coastal aquifers. It is often claimed that the method can "feel" the water table, but this is questionable except in very homogeneous deposits. In urban areas the method is often hampered by the presence of pipes, rails, and wires that interfere with the current fields.

Surface geophysical methods cannot replace test drilling, although by providing data that lead to a more intelligent selection of test-hole drilling, they may lead to a reduction in the amount of drilling required. Stratigraphic interpretations based on seismic or electrical resistivity measurements must be calibrated against test-hole information.

Subsurface Geophysical Methods

There is one geophysical approach that has now become a standard tool in groundwater exploration. This approach involves the logging of wells and test holes by the methods of *borehole geophysics*. The term encompasses all techniques in which a sensing device is lowered into a hole in order to make a record that can be interpreted in terms of the characteristics of the geologic formations and their contained fluids. The techniques of borehole geophysics were originally developed in the petroleum industry and the standard textbooks on the interpretation of geophysical logs (Pirson, 1963; Wyllie, 1963) emphasize petroleum applications. Fortunately, there are several excellent review articles (Jones and Skibitzke, 1956; Patton and Bennett, 1963; Keys, 1967, 1968) that deal specifically with the application of geophysical logging techniques to groundwater problems.

A complete borehole geophysics program as it is carried out in the petroleum industry usually includes two electric logs (spontaneous potential and resistivity), three radiation logs (natural gamma, neutron, and gamma-gamma), and a caliper log that indicates variations in hole diameter. In hydrogeological applications, emphasis is usually placed on the electric logs.

The simplest electric log is the *spontaneous potential* (or self-potential) log. It is obtained with the single-point electrode arrangement shown in Figure 8.1 with the current source disconnected. It provides a measure of the naturally occurring potential differences between the surface electrode and the borehole electrode. The origin of these natural electric potentials is not well understood, but they are apparently related to electrochemical interactions that take place between the borehole fluid and the *in situ* rock-water complex.

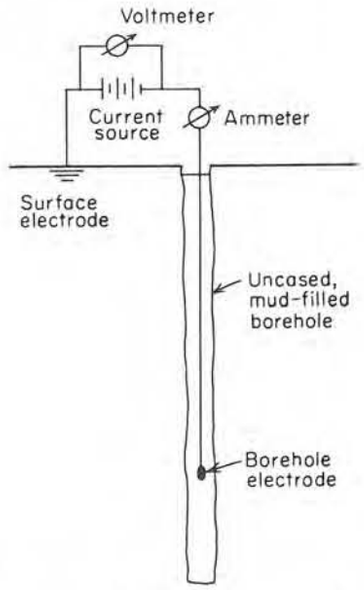

Figure 8.1 Single-point electrode arrangement for spontaneous potential and resistivity logging in a borehole.

The second electric log is a *resistivity* log. There are several electrode arrangements that can be used, but the simplest and the one most widely used in the water well industry is the single-point arrangement shown in Figure 8.1. The potential difference recorded at different depths for a given current strength leads to a log of apparent resistivity versus depth.

The two electric logs can be jointly interpreted in a qualitative sense in terms of the stratigraphic sequence in the hole. Figure 8.2 shows a pair of single-point electric logs measured in a test hole in an unconsolidated sequence of Pleistocene and Upper Cretaceous sediments in Saskatchewan. The geologic descriptions and

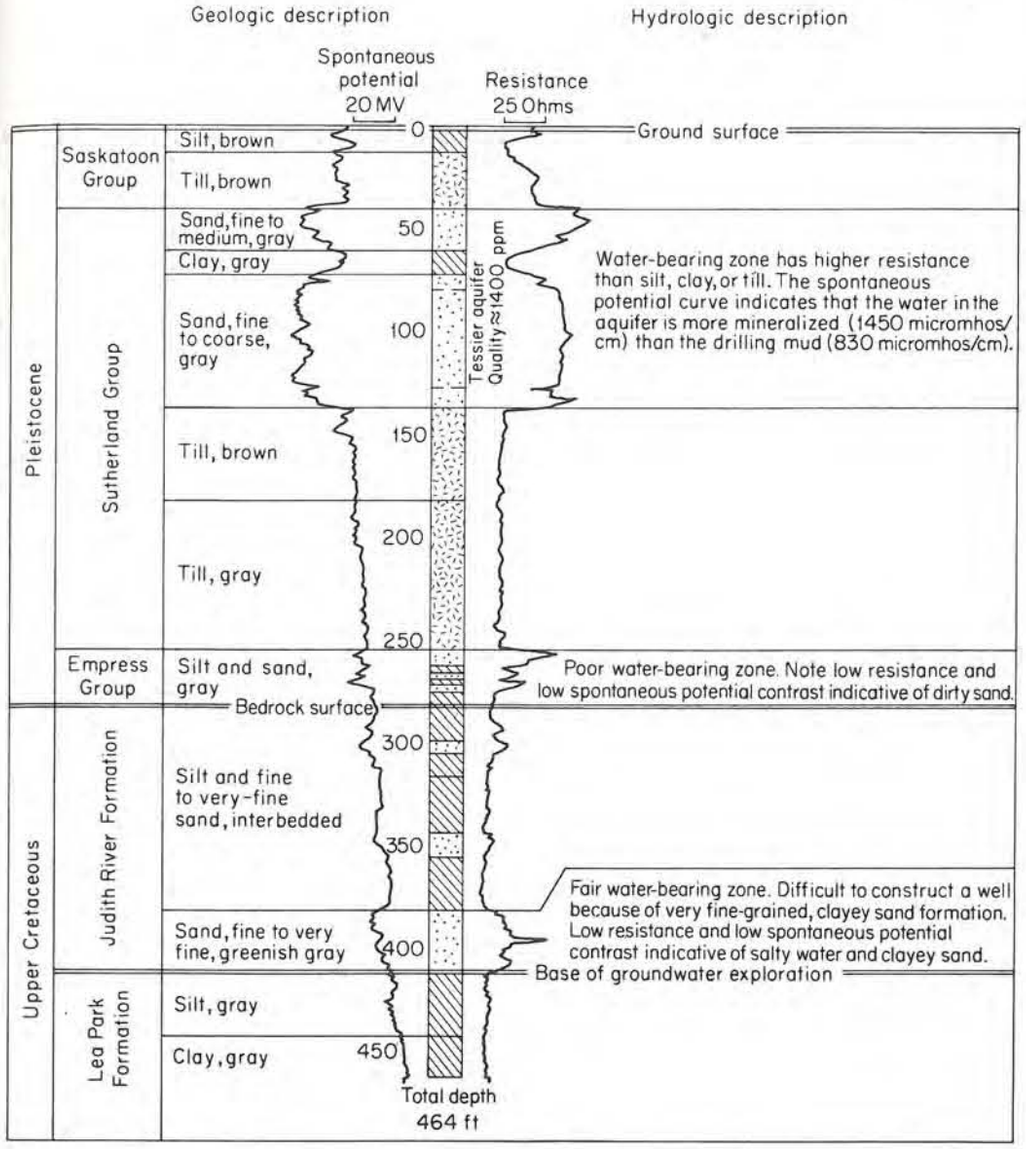

Figure 8.2 Geologic log, electric logs, geologic description, and hydrologic description of a test hole in Saskatchewan (after Christiansen et al., 1971).

the geologic log in the center are based on a core-sampling program. The hydrologic description of the potential aquifers at the site is based on a joint interpretation of the geologic and geophysical logs. In most common geological environments, the

best water-yielding zones have the highest resistivities. Electric logs often provide the most accurate detail for the selection of well-screen settings.

Dyck et al. (1972) pointed out three disadvantages to single-point electric logs. They do not provide quantitative values of formation resistivity; they are affected by hole diameter and borehole fluid resistivity; and they have only a shallow radius of investigation. To emphasize the first point, the resistivity log on Figure 8.2 records simply the resistance measured between the two electrodes rather than an apparent resistivity. Multiple-point electric logs are more versatile. They can be used for quantitative calculations of the resistivity of formation rocks and their enclosed fluids. These calculations lie beyond the scope of this presentation. Campbell and Lehr (1973) provide a good summary of the techniques. Dyck et al. (1972) provide some sample calculations in the context of a groundwater exploration program.

Keys (1967, 1968) has suggested that radiation logs, especially the natural gamma log, may have applications to groundwater hydrology. A logging suite that might be considered complete for hydrogeological purposes would include a driller's log (including drilling rate), a geologic log, a spontaneous potential log, a resistivity log, a natural gamma log, and a caliper log.

Drilling and Installation of Wells and Piezometers

The drilling of piezometers and wells, and their design, construction, and maintenance, is a specialized technology that rests only in part on scientific and engineering principles. There are many books (Briggs and Fiedler, 1966; Gibson and Singer, 1971; Campbell and Lehr, 1973; U.S. Environmental Protection Agency, 1973a, 1976) that provide a comprehensive treatment of water well technology. In addition, Walton (1970) presents material on the technical aspects of groundwater hydrology, and his text includes many case histories of water well installations and evaluations. Reeve (1965), Hvorslev (1951), Campbell and Lehr (1973), and Kruseman and de Ridder (1970) discuss methods of piezometer construction and installation. In this text we will limit ourselves to a brief overview of these admittedly important practical matters. Most of what follows is drawn from Campbell and Lehr (1973).

Water wells are usually classified on the basis of their method of construction. Wells may be *dug* by hand, *driven* or *jetted* in the form of well points, *bored* by an earth auger, or *drilled* by a drilling rig. The selection of the method of construction hinges on such questions as the purpose of the well, the hydrogeological environment, the quantity of water required, the depth and diameter envisaged, and economic factors. Dug, bored, jetted and driven wells are limited to shallow depths, unconsolidated deposits, and relatively small yields. For deeper, more productive wells in unconsolidated deposits, and for all wells in rock, drilling is the only feasible approach.

There are three main types of drilling equipment: *cable tool*, *rotary*, and *reverse rotary*. The cable tool drills by lifting and dropping a string of tools suspended on a cable. The bit at the bottom of the tool string rotates a few degrees between each stroke so that the cutting face of the bit strikes a different area of the hole bottom with each stroke. Drilling is periodically interrupted to bail out the cuttings. With medium- to high-capacity rigs, 40- to 60-cm-diameter holes can be drilled to depths of several hundred meters and smaller diameter holes to greater depths. The cable-tool approach is successful over a wide range of geological materials, but it is not capable of drilling as quickly or as deeply as rotary methods. With the conventional rotary method, drilling fluid is forced down the inside of a rapidly rotating drill stem and out through openings in the bit. The drilling fluid flows back to the surface, carrying the drill cuttings with it, by way of the annulus formed between the outside of the drill pipe and the hole wall. In a reverse rotary system, the direction of circulation is reversed. Reverse rotary is particularly well suited to drilling large-diameter holes in soft, unconsolidated formations.

The conventional rotary rig is generally considered to be the fastest, most convenient, and least expensive system to operate, expecially in unconsolidated deposits. Penetration rates for rotary rigs depend on such mechanical factors as the weight, type, diameter, and condition of the bit, and its speed of rotation; the circulation rate of the drilling fluid and its properties; and the physical characteristics of the geological formation. In rock formations, *drillability* (defined as depth of penetration per revolution) is directly related to the compressive strength of the rock.

The direct rotary method is heavily dependent on its hydraulic circulation system. The most widely used drilling fluid is a suspension of bentonitic clay in water, known as *drilling mud*. During drilling, the mud coats the hole wall and in so doing contributes to the hole stability and prevents losses of the drilling fluid to permeable formations. When even heavy drilling mud cannot prevent the caving of hole walls, well casing must be emplaced as drilling proceeds. Caving, lost circulation, and conditions associated with the encounter of flowing artesian water constitute the most common drilling problems.

The design of a deep-cased well in an unconsolidated aquifer must include consideration of the surface housing, the casing, the pumping equipment, and the intake. Of these, it is the intake that is most often of primary concern to groundwater hydrologists. In the first half of this century it was quite common to provide access for the water to the well by a set of perforations or hand-sawn slots in the casing. It is now recognized that well yields can be significantly increased by the use of *well screens*. The size of the intake slots in a properly designed well screen is related to the grain-size distribution of the aquifer. Development of a screened well by pumping, surging, or backwashing draws the fines out of the aquifer, through the well screen, and up to the surface. By removing the fines from the formation in the vicinity of the well, a *natural gravel pack* is created around the screen that increases the efficiency of the intake. In some cases, an *artificial gravel pack* is emplaced to improve intake properties. Figure 8.3 shows several typical designs for wells in consolidated and unconsolidated formations.

The productivity of a well is often expressed in terms of the *specific capacity*,

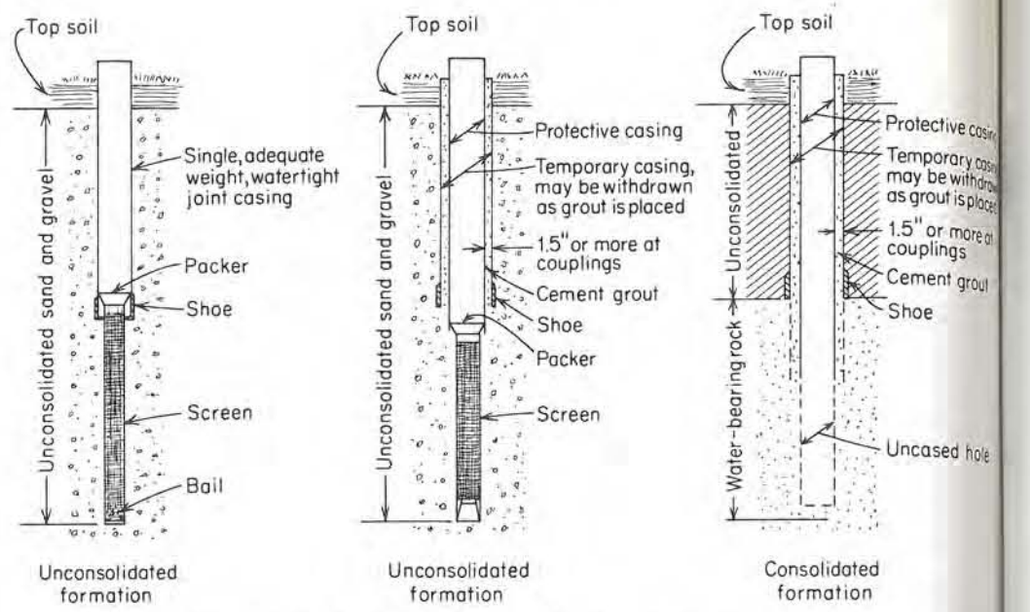

Figure 8.3 Typical well designs for consolidated and unconsolidated formations.

C_s, which is defined as $C_s = Q/\Delta h_w$, where Q is the pumping rate and Δh_w is the drawdown in the well. In this equation, $\Delta h_w = \Delta h + \Delta h_L$, where Δh is the drawdown in hydraulic head in the aquifer at the well screen boundary, and Δh_L is the *well loss* created by the turbulent flow of water through the screen and into the pump intake. Δh is calculated from the standard well-hydraulics equations developed in Section 8.3. Δh_L can be estimated by methods outlined in Walton (1970) and Campbell and Lehr (1973). In general, $\Delta h_L \ll \Delta h$.

8.3 The Response of Ideal Aquifers to Pumping

The exploitation of a groundwater basin leads to water-level declines that serve to limit yields. One of the primary goals of groundwater resource evaluation must therefore be the prediction of hydraulic-head drawdowns in aquifers under proposed pumping schemes. In this section, the theoretical response of idealized aquifers to pumping will be examined. We will investigate several types of aquifer configuration, but in each case the geometry will be sufficiently regular and the boundary conditions sufficiently simple to allow the development of an analytical solution to the boundary-value problem that represents the case at hand. These solutions, together with solutions to more complex boundary-value problems that describe less ideal conditions, constitute the foundation of the study of *well hydraulics*. This section provides an introduction to the topic, but the material covered is far from all-inclusive. There is a massive literature in the field and the committed reader is directed to Walton's (1970) comprehensive treatment, to Hantush's (1964) monograph, or to the excellent handbooks of Ferris et al. (1962) and Kruseman and de Ridder (1970).

Radial Flow to a Well

The theoretical analyses are based on an understanding of the physics of flow toward a well during pumping. All the necessary concepts have been introduced in Chapter 2. The distinction between *confined* and *unconfined* aquifers was explained there, as was the relation between the general concept of *hydraulic head* in a three-dimensional geologic system and the specific concept of the *potentiometric surface* on a two-dimensional, horizontal, confined aquifer. Definitions were presented for the fundamental hydrogeologic parameters: *hydraulic conductivity*, *porosity*, and *compressibility*; and for the derived aquifer parameters: *transmissivity* and *storativity*. It was explained there that pumping induces horizontal hydraulic gradients toward a well, and as a result hydraulic heads are decreased in the aquifer around a well during pumping. What is required now is that we take these fundamental concepts, put them into the form of a boundary-value problem that represents flow to a well in an aquifer, and examine the theoretical response.

At this point it is worth recalling from Section 2.10 that the definition of storativity invokes a one-dimensional concept of aquifer compressibility. The α in Eq. (2.63) is the aquifer compressibility in the vertical direction. The analyses that follow in effect assume that changes in effective stress induced by aquifer pumping are much larger in the vertical direction than in the horizontal.

The concept of aquifer storage inherent in the storativity term also implies an instantaneous release of water from any elemental volume in the system as the head drops in that element.

Let us begin our analysis with the simplest possible aquifer configuration. Consider an aquifer that is (1) horizontal, (2) confined between impermeable formations on top and bottom, (3) infinite in horizontal extent, (4) of constant thickness, and (5) homogeneous and isotropic with respect to its hydrogeological parameters.

For the purposes of our initial analysis, let us further limit our ideal system as follows: (1) there is only a single pumping well in the aquifer, (2) the pumping rate is constant with time, (3) the well diameter is infinitesimally small, (4) the well penetrates the entire aquifer, and (5) the hydraulic head in the aquifer prior to pumping is uniform throughout the aquifer.

The partial differential equation that describes saturated flow in two horizontal dimensions in a confined aquifer with transmissivity T and storativity S was developed in Section 2.11 as Eq. (2.77):

$$\frac{\partial^2 h}{\partial x^2} + \frac{\partial^2 h}{\partial y^2} = \frac{S}{T}\frac{\partial h}{\partial t}$$

Since it is clear that hydraulic-head drawdowns around a well will possess radial symmetry in our ideal system, it is advantageous to convert Eq. (2.77) into radial coordinates. The conversion is accomplished through the relation $r = \sqrt{x^2 + y^2}$ and the equation of flow becomes (Jacob, 1950)

$$\frac{\partial^2 h}{\partial r^2} + \frac{1}{r}\frac{\partial h}{\partial r} = \frac{S}{T}\frac{\partial h}{\partial t} \tag{8.1}$$

The mathematical region of flow, as illustrated in the plan view of Figure 8.4, is a horizontal one-dimensional line through the aquifer, from $r = 0$ at the well to $r = \infty$ at the infinite extremity.

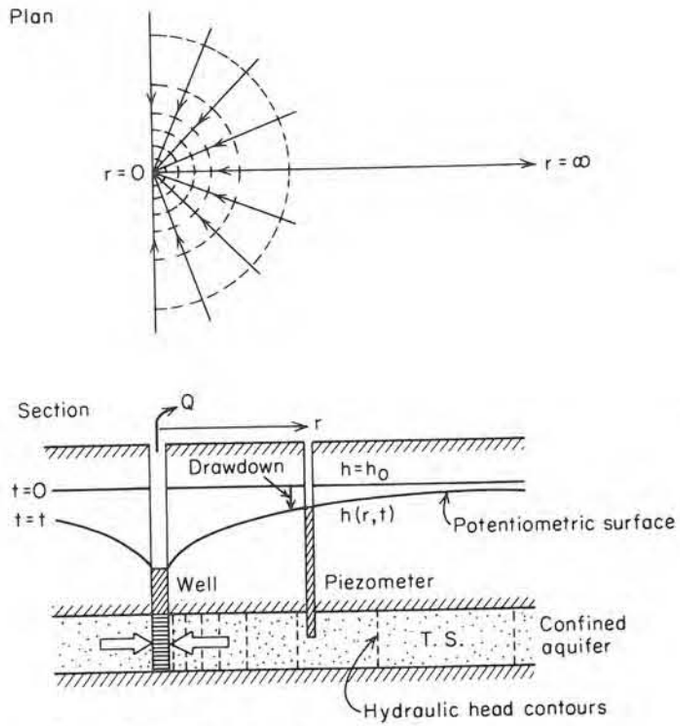

Figure 8.4 Radial flow to a well in a horizontal confined aquifer.

The initial condition is

$$h(r, 0) = h_0 \qquad \text{for all } r \tag{8.2}$$

where h_0 is the constant initial hydraulic head.

The boundary conditions assume no drawdown in hydraulic head at the infinite boundary:

$$h(\infty, t) = h_0 \qquad \text{for all } t \tag{8.3}$$

and a constant pumping rate Q $[L^3/T]$ at the well:

$$\lim_{r \to 0}\left(r\frac{\partial h}{\partial r}\right) = \frac{Q}{2\pi T} \qquad \text{for } t > 0 \tag{8.4}$$

Condition (8.4) is the result of a straightforward application of Darcy's law at the well face.

The solution $h(r, t)$ describes the hydraulic head field at any radial distance r at any time after the start of pumping. For reasons that should be clear from a perusal of Figure 8.4, solutions are often presented in terms of the drawdown in head $h_0 - h(r, t)$.

The Theis Solution

Theis (1935), in what must be considered one of the fundamental breakthroughs in the development of hydrologic methodology, utilized an analogy to heat-flow theory to arrive at an analytical solution to Eq. (8.1) subject to the initial and boundary conditions of Eqs. (8.2) through (8.4). His solution, written in terms of the drawdown, is

$$h_0 - h(r, t) = \frac{Q}{4\pi T}\int_u^\infty \frac{e^{-u}\,du}{u} \tag{8.5}$$

where

$$u = \frac{r^2 S}{4Tt} \tag{8.6}$$

The integral in Eq. (8.5) is well known in mathematics. It is called the *exponential integral* and tables of values are widely available. For the specific definition of u given by Eq. (8.6), the integral is known as the *well function*, $W(u)$. With this notation, Eq. (8.5) becomes

$$h_0 - h = \frac{Q}{4\pi T}W(u) \tag{8.7}$$

Table 8.1 provides values of $W(u)$ versus u, and Figure 8.5(a) shows the relationship $W(u)$ versus $1/u$ graphically. This curve is commonly called the *Theis curve*.

If the aquifer properties, T and S, and the pumping rate, Q, are known, it is possible to predict the drawdown in hydraulic head in a confined aquifer at any distance r from a well at any time t after the start of pumping. It is simply necessary to calculate u from Eq. (8.6), look up the value of $W(u)$ on Table 8.1, and calculate

Table 8.1 Values of $W(u)$ for Various Values of u

u	1.0	2.0	3.0	4.0	5.0	6.0	7.0	8.0	9.0
$\times 1$	0.219	0.049	0.013	0.0038	0.0011	0.00036	0.00012	0.000038	0.000012
$\times 10^{-1}$	1.82	1.22	0.91	0.70	0.56	0.45	0.37	0.31	0.26
$\times 10^{-2}$	4.04	3.35	2.96	2.68	2.47	2.30	2.15	2.03	1.92
$\times 10^{-3}$	6.33	5.64	5.23	4.95	4.73	4.54	4.39	4.26	4.14
$\times 10^{-4}$	8.63	7.94	7.53	7.25	7.02	6.84	6.69	6.55	6.44
$\times 10^{-5}$	10.94	10.24	9.84	9.55	9.33	9.14	8.99	8.86	8.74
$\times 10^{-6}$	13.24	12.55	12.14	11.85	11.63	11.45	11.29	11.16	11.04
$\times 10^{-7}$	15.54	14.85	14.44	14.15	13.93	13.75	13.60	13.46	13.34
$\times 10^{-8}$	17.84	17.15	16.74	16.46	16.23	16.05	15.90	15.76	15.65
$\times 10^{-9}$	20.15	19.45	19.05	18.76	18.54	18.35	18.20	18.07	17.95
$\times 10^{-10}$	22.45	21.76	21.35	21.06	20.84	20.66	20.50	20.37	20.25
$\times 10^{-11}$	24.75	24.06	23.65	23.36	23.14	22.96	22.81	22.67	22.55
$\times 10^{-12}$	27.05	26.36	25.96	25.67	25.44	25.26	25.11	24.97	24.86
$\times 10^{-13}$	29.36	28.66	28.26	27.97	27.75	27.56	27.41	27.28	27.16
$\times 10^{-14}$	31.66	30.97	30.56	30.27	30.05	29.87	29.71	29.58	29.46
$\times 10^{-15}$	33.96	33.27	32.86	32.58	32.35	32.17	32.02	31.88	31.76

SOURCE: Wenzel, 1942.

$h_0 - h$ from Eq. (8.7). Figure 8.5(b) shows a calculated plot of $h_0 - h$ versus t for the specific set of parameters noted on the figure. A set of field measurements of drawdown versus time measured in a piezometer that is set in an ideal confined aquifer with these properties would show this type of record.

The shape of the function $h_0 - h$ versus t, when plotted on log-log paper as in Figure 8.5(b), has the same form as the plot of $W(u)$ versus $1/u$ shown in Figure 8.5(a). This is a direct consequence of the relations embodied in Eqs. (8.6) and (8.7), where it can be seen that $h_0 - h$ and $W(u)$, and t and $1/u$, are related to one another through a constant term.

It is also possible to calculate values of $h_0 - h$ at various values of r at a given time t. Such a calculation leads to a plot of the *cone of depression* (or *drawdown cone*) in the potentiometric surface around a pumping well. Figure 8.4 provides a schematic example. The steepening of the slope of the cone near the well is reflected in the solution, Eq. (8.7). The physical explanation is clear if one carries out the simple flow-net construction shown in the plan view of Figure 8.4 and then carries the hydraulic head values down onto the section.

For a given aquifer the cone of depression increases in depth and extent with increasing time. Drawdown at any point at a given time is directly proportional to the pumping rate and inversely proportional to aquifer transmissivity and aquifer storativity. As shown in Figure 8.6, aquifers of low transmissivity develop tight, deep drawdown cones, whereas aquifers of high transmissivity develop shallow cones of wide extent. Transmissivity exerts a greater influence on drawdown than does storativity.

In that geologic configurations are seldom as ideal as that outlined above, the time-drawdown response of aquifers under pumpage often deviates from the

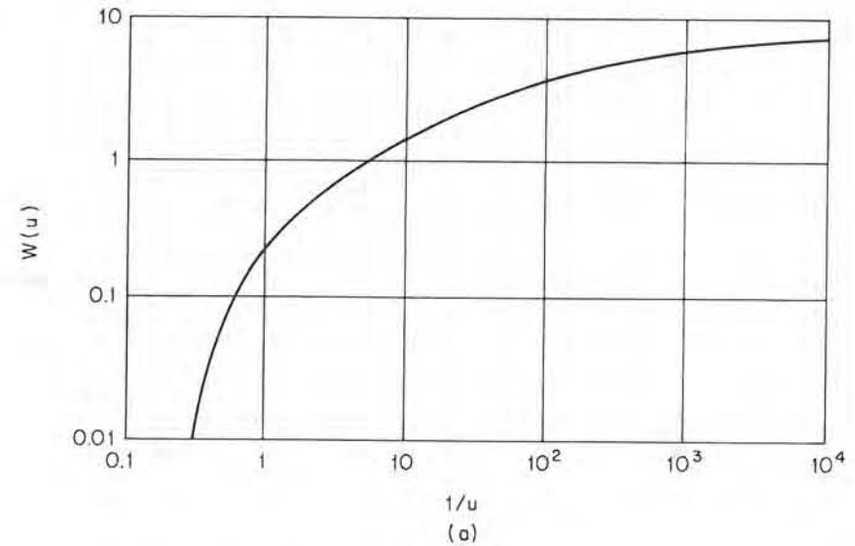

Figure 8.5 (a) Theoretical curve of $W(u)$ versus $1/u$. (b) Calculated curve of $h_0 - h$ versus t.

Theis solution shown in Figure 8.5. We will now turn to some of the theoretical response curves that arise in less ideal situations. Specifically, we will look at (1) leaky aquifers, (2) unconfined aquifers, (3) multiple-well systems, (4) stepped pumping rates, (5) bounded aquifers, and (6) partially penetrating wells.

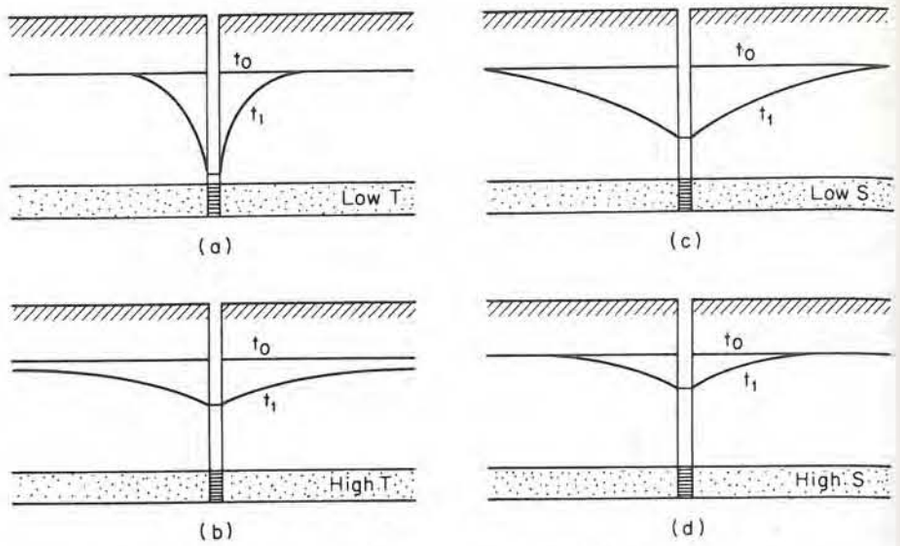

Figure 8.6 Comparison of drawdown cones at a given time for aquifers of (a) low transmissivity; (b) high transmissivity; (c) low storativity; (d) high storativity.

Leaky Aquifers

The assumption inherent in the Theis solution that geologic formations overlying and underlying a confined aquifer are completely impermeable is seldom satisfied. Even when production wells are screened only in a single aquifer, it is quite usual for the aquifer to receive a significant inflow from adjacent beds. Such an aquifer is called a *leaky aquifer*, although in reality it is the aquitard that is leaky. The aquifer is often just one part of a multiple-aquifer system in which a succession of aquifers are separated by intervening low-permeability aquitards. For the purposes of this section, however, it is sufficient for us to consider the three-layer case shown in Figure 8.7. Two aquifers of thickness b_1 and b_2 and horizontal hydraulic conductivities K_1 and K_2 are separated by an aquitard of thickness b' and vertical hydraulic conductivity K'. The specific storage values in the aquifers are S_{s_1} and S_{s_2}, while that in the aquitard is S'_s.

Since a rigorous approach to flow in multiple-aquifer systems involves boundary conditions that make the problem intractable analytically, it has been customary to simplify the mathematics by assuming that flow is essentially horizontal in the aquifers and vertical in the aquitards. Neuman and Witherspoon (1969a) report that the errors introduced by this assumption are less than 5% when the conductivities of the aquifers are more than 2 orders of magnitude greater than that of the aquitard.

The development of leaky-aquifer theory has taken place in two distinct sets of papers. The first, by Hantush and Jacob (1955) and Hantush (1956, 1960),

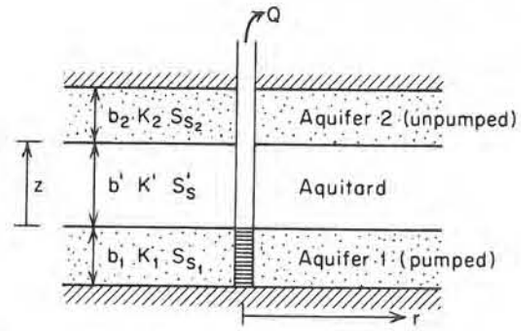

Figure 8.7 Schematic diagram of a two-aquifer "leaky" system. Recall that $T = Kb$ and $S = S_s b$.

provided the original differentiation between the Theis response and that for leaky aquifers. The second, by Neuman and Witherspoon (1969a, 1969b, 1972) evaluated the significance of the assumptions inherent in the earlier work and provided more generalized solutions.

The analytical solution of Hantush and Jacob (1955) can be couched in the same form as the Theis solution [Eq. (8.7)] but with a more complicated well function. In fact, Hantush and Jacob developed two analytical solutions, one valid only for small t and one valid only for large t, and then interpolated between the two solutions to obtain the complete response curve. Their solution is presented in terms of the dimensionless parameter, r/B, defined by the relation

$$\frac{r}{B} = r\sqrt{\frac{K'}{K_1 b_1 b'}} \tag{8.8}$$

In analogy with Eq. (8.7), we can write their solution as

$$h_0 - h = \frac{Q}{4\pi T} W(u, r/B) \tag{8.9}$$

where $W(u, r/B)$ is known as the *leaky well function.*

Hantush (1956) tabulated the values of $W(u, r/B)$. Figure 8.8 is a plot of this function against $1/u$. If the aquitard is impermeable, then $K' = 0$, and from Eq. (8.8), $r/B = 0$. In this case, as shown graphically in Figure 8.8, the Hantush-Jacob solution reduces to the Theis solution.

If T_1 $(= K_1 b_1)$ and S_1 $(= S_{s_1} b_1)$ are known for the aquifer and K' and b' are known for the aquitard, then the drawdown in hydraulic head in the pumped aquifer for any pumpage Q at any radial distance r at any time t can be calculated from Eq. (8.9), after first calculating u for the pumped aquifer from Eq. (8.6), r/B from Eq. (8.8), and $W(u, r/B)$ from Figure 8.9.

The original Hantush and Jacob (1955) solution was developed on the basis of two very restrictive assumptions. They assumed that the hydraulic head in the

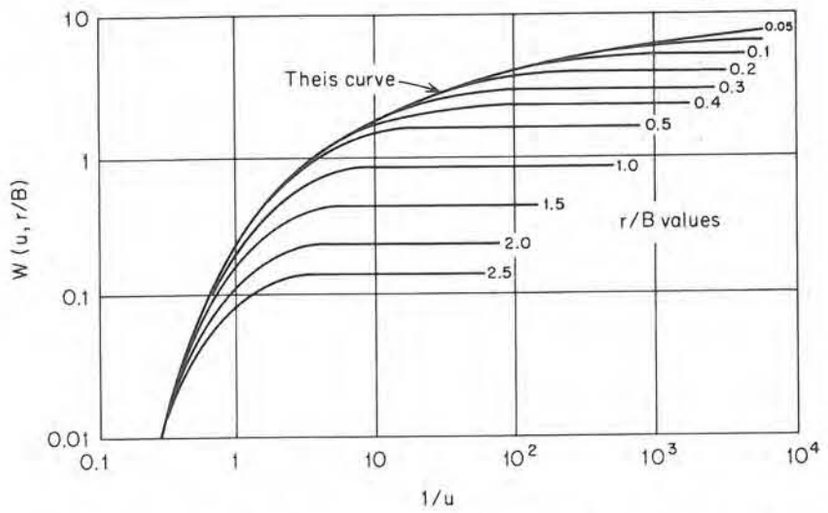

Figure 8.8 Theoretical curves of $W(u, r/B)$ versus $1/u$ for a leaky aquifer (after Walton, 1960).

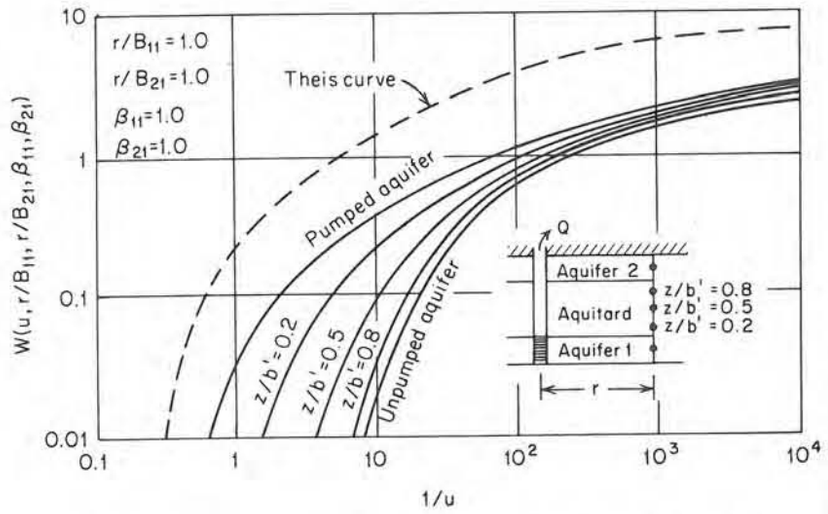

Figure 8.9 Theoretical curves of $W(u, r/B_{11}, r/B_{21}, \beta_{11}, \beta_{21})$ versus $1/u$ for a leaky two-aquifer system (after Neuman and Witherspoon, 1969a).

unpumped aquifer remains constant during the removal of water from the pumped aquifer and that the rate of leakage into the pumped aquifer is proportional to the hydraulic gradient across the leaky aquitard. The first assumption implies that the unpumped aquifer has an unlimited capacity to provide water for delivery

through the aquitard to the pumped aquifer. The second assumption completely ignores the effects of the storage capacity of the aquitard on the transient solution (i.e., it is assumed that $S'_s = 0$).

In a later paper, Hantush (1960) presented a modified solution in which consideration was given to the effects of storage in the aquitard. More recently, Neuman and Witherspoon (1969a, 1969b) presented a complete solution that includes consideration of both release of water from storage in the aquitard and head drawdowns in the unpumped aquifer. Their solutions require the calculation of four dimensionless parameters, which, with reference to Figure 8.7, are defined as follows:

$$\frac{r}{B_{11}} = r\sqrt{\frac{K'}{K_1 b_1 b'}}$$

$$\frac{r}{B_{21}} = r\sqrt{\frac{K'}{K_2 b_2 b'}}$$

$$\beta_{11} = \frac{r}{4b_1}\sqrt{\frac{K'S'_s}{K_1 S_{s_1}}} \qquad (8.10)$$

$$\beta_{21} = \frac{r}{4b_2}\sqrt{\frac{K'S'_s}{K_2 S_{s_2}}}$$

Neuman and Witherspoon's solutions provide the drawdown in both aquifers as a function of radial distance from the well, and in the aquitard as a function of both radial distance and elevation above the base of the aquitard. Their solutions can be described in a schematic sense by the relation

$$h_0 - h(r, z, t) = \frac{Q}{4\pi T} W(u, r/B_{11}, r/B_{21}, \beta_{11}, \beta_{21}) \qquad (8.11)$$

Tabulation of this well function would require many pages of tables, but an indication of the nature of the solutions can be seen from Figure 8.9, which presents the theoretical response curves for the pumped aquifer, the unpumped aquifer, and at three elevations in the aquitard, for a specific set of r/B and β values. The Theis solution is shown on the diagram for comparative purposes.

Because of its simplicity, and despite the inherent dangers of using a simple model for a complex system, the r/B solution embodied in Figure 8.8 is widely used for the prediction of drawdowns in leaky-aquifer systems. Figure 8.10 shows an $h_0 - h$ versus t plot for a specific case as calculated from Eq. (8.9) with the aid of Figure 8.8. The drawdown reaches a constant level after about 5×10^3 seconds. From this point on, the r/B solution indicates that steady-state conditions hold throughout the system, with the infinite storage capacity assumed to exist in the upper aquifer feeding water through the aquitard toward the well. If the overlying aquitard were impermeable rather than leaky, the response would follow the dotted line. As one would expect, drawdowns in leaky aquifers are less than those in non-

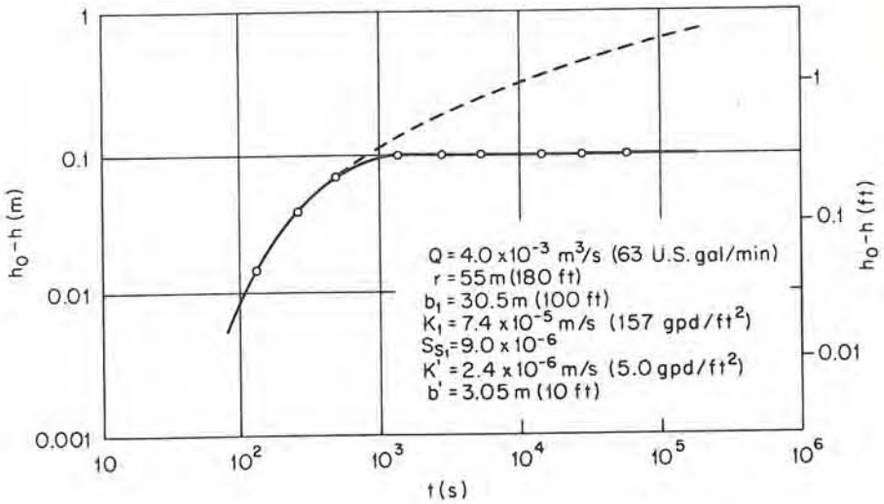

Figure 8.10 Calculated curve of $h_0 - h$ versus t for a leaky aquifer, based on Hantush-Jacob theory.

leaky aquifers, as there is now an additional source of water over and above that which can be supplied by the aquifer itself. Predictions based on the Theis equation therefore provide a conservative estimate for leaky systems; that is, they overpredict the drawdown, or, put another way, actual drawdowns are unlikely to reach the values predicted by the Theis equation for a given pumping scheme in a multiaquifer system.

Unconfined Aquifers

When water is pumped from a confined aquifer, the pumpage induces hydraulic gradients toward the well that create drawdowns in the potentiometric surface. The water produced by the well arises from two mechanisms: expansion of the water in the aquifer under reduced fluid pressures, and compaction of the aquifer under increased effective stresses (Section 2.10). There is no dewatering of the geologic system. The flow system in the aquifer during pumping involves only horizontal gradients toward the well; there are no vertical components of flow. When water is pumped from an unconfined aquifer, on the other hand, the hydraulic gradients that are induced by the pumpage create a drawdown cone in the water table itself and there are vertical components of flow (Figure 8.11). The water produced by the well arises from the two mechanisms responsible for confined delivery *plus* the actual dewatering of the unconfined aquifer.

There are essentially three approaches that can be used to predict the growth of unconfined drawdown cones in time and space. The first, which might be termed the complete analysis, recognizes that the unconfined well-hydraulics problem (Figure 8.11) involves a saturated-unsaturated flow system in which

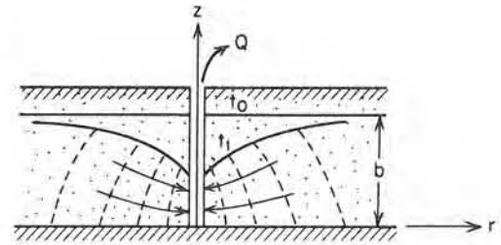

Figure 8.11 Radial flow to a well in an unconfined aquifer.

water-table drawdowns are accompanied by changes in the unsaturated moisture contents above the water table (such as those shown in Figure 2.23). The complete analysis requires the solution of a boundary-value problem that includes both the saturated and unsaturated zones. An analytical solution for this complete case was presented by Kroszynski and Dagan (1975) and several numerical mathematical models have been prepared (Taylor and Luthin, 1969; Cooley, 1971; Brutsaert et al., 1971). The general conclusion of these studies is that the position of the water table during pumpage is not substantially affected by the nature of the unsaturated flow above the water table. In other words, while it is conceptually more appealing to carry out a complete saturated-unsaturated analysis, there is little practical advantage to be gained, and since unsaturated soil properties are extremely difficult to measure *in situ*, the complete analysis is seldom used.

The second approach, which is by far the simplest, is to use the same equation as for a confined aquifer [Eq. (8.7)] but with the argument of the well function [Eq. (8.6)] defined in terms of the specific yield S_y rather than the storativity S. The transmissivity T must be defined as $T = Kb$, where b is the *initial* saturated thickness. Jacob (1950) has shown that this approach leads to predicted drawdowns that are very nearly correct as long as the drawdown is small in comparison with the saturated thickness. The method in effect relies on the Dupuit assumptions (Section 5.5) and fails when vertical gradients become significant.

The third approach, and the one most widely used in practice, is based on the concept of delayed water-table response. This approach was pioneered by Boulton (1954, 1955, 1963) and has been significantly advanced by Neuman (1972, 1973b, 1975a). It can be observed that water-level drawdowns in piezometers adjacent to pumping wells in unconfined aquifers tend to decline at a slower rate than that predicted by the Theis solution. In fact, there are three distinct segments that can be recognized in time-drawdown curves under water-table conditions. During the first segment, which covers only a short period after the start of pumping, an unconfined aquifer reacts in the same way as does a confined aquifer. Water is released instantaneously from storage by the compaction of the aquifer and by the expansion of the water. During the second segment, the effects of gravity drainage are felt. There is a decrease in the slope of the time-drawdown curve relative to the Theis curve because the water delivered to the well by the dewatering that

accompanies the falling water table is greater than that which would be delivered by an equal decline in a confined potentiometric surface. In the third segment, which occurs at later times, time-drawdown data once again tend to conform to a Theis-type curve.

Boulton (1963) produced a semiempirical mathematical solution that reproduces all three segments of the time-drawdown curve in an unconfined aquifer. His solution, although useful in practice, required the definition of an empirical *delay index* that was not related clearly to any physical phenomenon. In recent years there has been a considerable amount of research (Neuman, 1972; Streltsova, 1972; Gambolati, 1976) directed at uncovering the physical processes responsible for delayed response in unconfined aquifers. It is now clear that the delay index is not an aquifer constant, as Boulton had originally assumed. It is related to the vertical components of flow that are induced in the flow system and it is apparently a function of the radius r and perhaps the time t.

The solution of Neuman (1972, 1973b, 1975a) also reproduces all three segments of the time-drawdown curve and it does not require the definition of any empirical constants. Neuman's method recognizes the existence of vertical flow components, and the general solution for the drawdown, $h_0 - h$, is a function of both r and z, as defined in Figure 8.11. His general solution can be reduced to one that is a function of r alone if an *average drawdown* is considered. His complex analytical solution can be represented in simplified form as

$$h_0 - h = \frac{Q}{4\pi T} W(u_A, u_B, \eta) \tag{8.12}$$

where $W(u_A, u_B, \eta)$ is known as the *unconfined well function* and $\eta = r^2/b^2$. Figure 8.12 is a plot of this function for various values of η. The type A curves that grow out of the left-hand Theis curve of Figure 8.12, and that are followed at early time, are given by

$$h_0 - h = \frac{Q}{4\pi T} W(u_A, \eta) \tag{8.13}$$

where

$$u_A = \frac{r^2 S}{4Tt}$$

and S is the elastic storativity responsible for the instantaneous release of water to the well. The type B curves that are asymptotic to the right-hand Theis curve of Figure 8.12, and that are followed at later time, are given by

$$h_0 - h = \frac{Q}{4\pi T} W(u_B, \eta) \tag{8.14}$$

where

$$u_B = \frac{r^2 S_y}{4Tt}$$

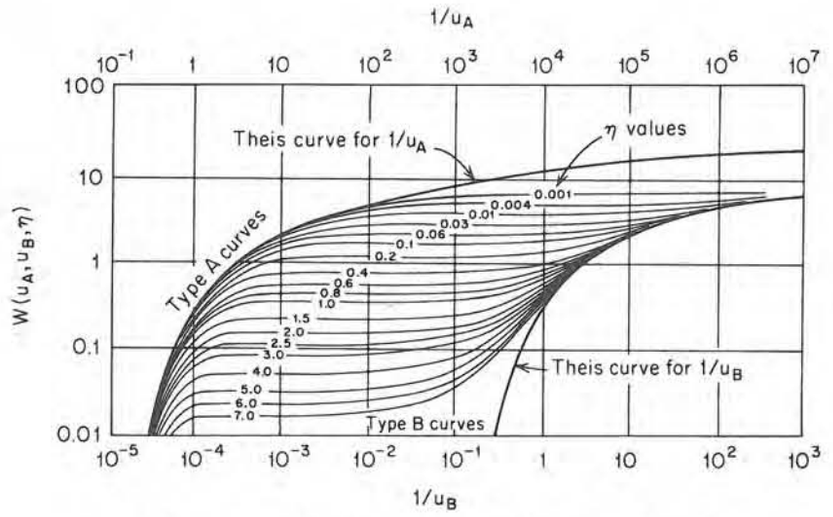

Figure 8.12 Theoretical curves of $W(u_A, u_B, \eta)$ versus $1/u_A$ and $1/u_B$ for an unconfined aquifer (after Neuman, 1975a).

and S_y is the specific yield that is responsible for the delayed release of water to the well.

For an anisotropic aquifer with horizontal hydraulic conductivity K_r and vertical hydraulic conductivity K_z, the parameter η is given by

$$\eta = \frac{r^2 K_z}{b^2 K_r} \tag{8.15}$$

If the aquifer is isotropic, $K_z = K_r$, and $\eta = r^2/b^2$. The transmissivity T is defined as $T = K_r b$. Equations (8.12) through (8.15) are only valid if $S_y \gg S$ and $h_0 - h \ll b$.

The prediction of the average drawdown at any radial distance r from a pumping well at any time t can be obtained from Eqs. (8.13) through (8.15) given Q, S, S_y, K_r, K_z, and b.

Multiple-Well Systems, Stepped Pumping Rates, Well Recovery, and Partial Penetration

The drawdown in hydraulic head at any point in a confined aquifer in which more than one well is pumping is equal to the sum of the drawdowns that would arise from each of the wells independently. Figure 8.13 schematically displays the drawdown $h_0 - h$ at a point B situated between two pumping wells with pumping rates $Q_1 = Q_2$. If $Q_1 \neq Q_2$, the symmetry of the diagram about the plane $A - A'$ would be lost but the principles remain the same.

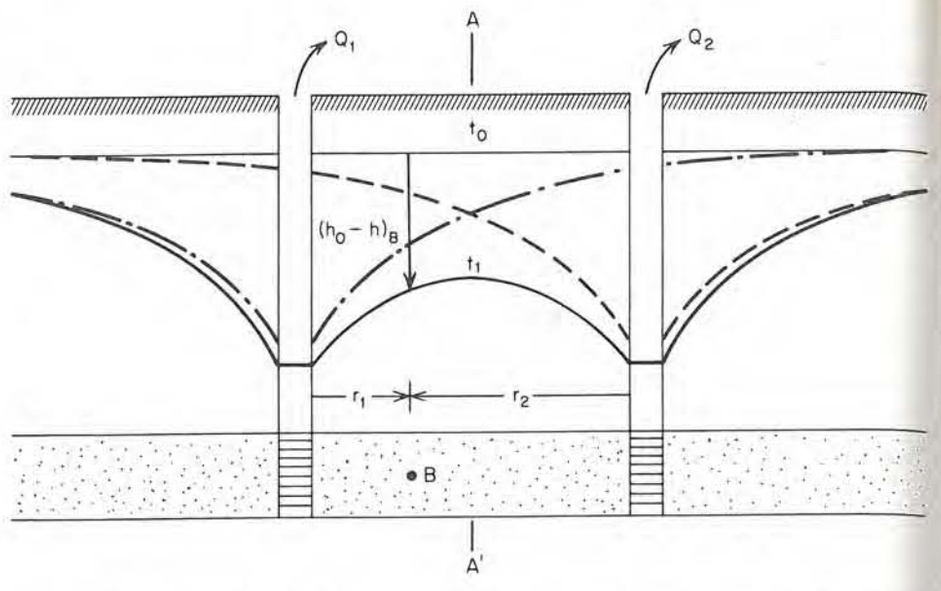

Figure 8.13 Drawdown in the potentiometric surface of a confined aquifer being pumped by two wells with $Q_1 = Q_2$.

For a system of n wells pumping at rates $Q_1, Q_2, \ldots, Q_n$, the arithmetic summation of the Theis solutions leads to the following predictive equation for the drawdown at a point whose radial distance from each well is given by $r_1, r_2, \ldots, r_n$

$$h_0 - h = \frac{Q_1}{4\pi T} W(u_1) + \frac{Q_2}{4\pi T} W(u_2) + \cdots + \frac{Q_n}{4\pi T} W(u_n) \qquad (8.16)$$

where

$$u_i = \frac{r_i^2 S}{4Tt_i} \qquad i = 1, 2, \ldots, n$$

and t_i is the time since pumping started at the well whose discharge is Q_i.

The summation of component drawdowns outlined above is an application of the principle of superposition of solutions. This approach is valid because the equation of flow [Eq. (8.1)] for transient flow in a confined aquifer is linear (i.e., there are no cross terms of the form $\partial h/\partial r \cdot \partial h/\partial t$). Another application of the principle of superposition is in the case of a single well that is pumped at an initial rate Q_0 and then increased to the rates $Q_1, Q_2, \ldots, Q_m$ in a stepwise fashion by the additions $\Delta Q_1, \Delta Q_2, \ldots, \Delta Q_m$. Drawdown at a radial distance r from the pumping well is given by

$$h_0 - h = \frac{Q_0}{4\pi T} W(u_0) + \frac{\Delta Q_1}{4\pi T} W(u_1) + \cdots + \frac{\Delta Q_m}{4\pi T} W(u_m) \qquad (8.17)$$

where

$$u_j = \frac{r^2 S}{4Tt_j} \qquad j = 0, 1, 2, \ldots, m$$

and t_j is the time since the start of the pumping rate Q_j.

A third application of the superposition principle is in the recovery of a well after pumping has stopped. If t is the time since the start of pumping and t' is the time since shutdown, then the drawdown at a radial distance r from the well is given by

$$h_0 - h = \frac{Q}{4\pi T}[W(u_1) - W(u_2)] \qquad (8.18)$$

where

$$u_1 = \frac{r^2 S}{4Tt} \quad \text{and} \quad u_2 = \frac{r^2 S}{4Tt'}$$

Figure 8.14 schematically displays the drawdowns that occur during the pumping period and the residual drawdowns that remain during the recovery period.

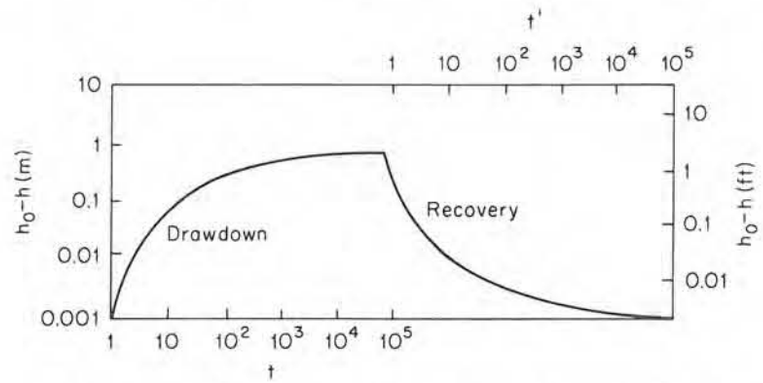

Figure 8.14 Schematic diagram of the recovery in hydraulic head in an aquifer after pumping is stopped.

It is not always possible, or necessarily desirable, to design a well that fully penetrates the aquifer under development. This is particularly true for unconfined aquifers, but may also be the case for thick confined aquifers. Even for wells that are fully penetrating, screens may be set over only a portion of the aquifer thickness.

Partial penetration creates vertical flow gradients in the vicinity of the well that render the predictive solutions developed for full penetration inaccurate. Hantush (1962) presented adaptations to the Theis solution for partially penetrating wells, and Hantush (1964) reviewed these solutions for both confined and leaky-confined aquifers. Dagan (1967), Kipp (1973), and Neuman (1974) considered the effects of partial penetration in unconfined aquifers.

Bounded Aquifers

When a confined aquifer is bounded on one side by a straight-line impermeable boundary, drawdowns due to pumping will be greater near the boundary [Figure 8.15(a)] than those that would be predicted on the basis of the Theis equation for an aquifer of infinite areal extent. In order to predict head drawdowns in such systems, the method of images, which is widely used in heat-flow theory, has been adapted for application in the groundwater milieu (Ferris et al., 1962). With this approach, the real bounded system is replaced for the purposes of analysis by an

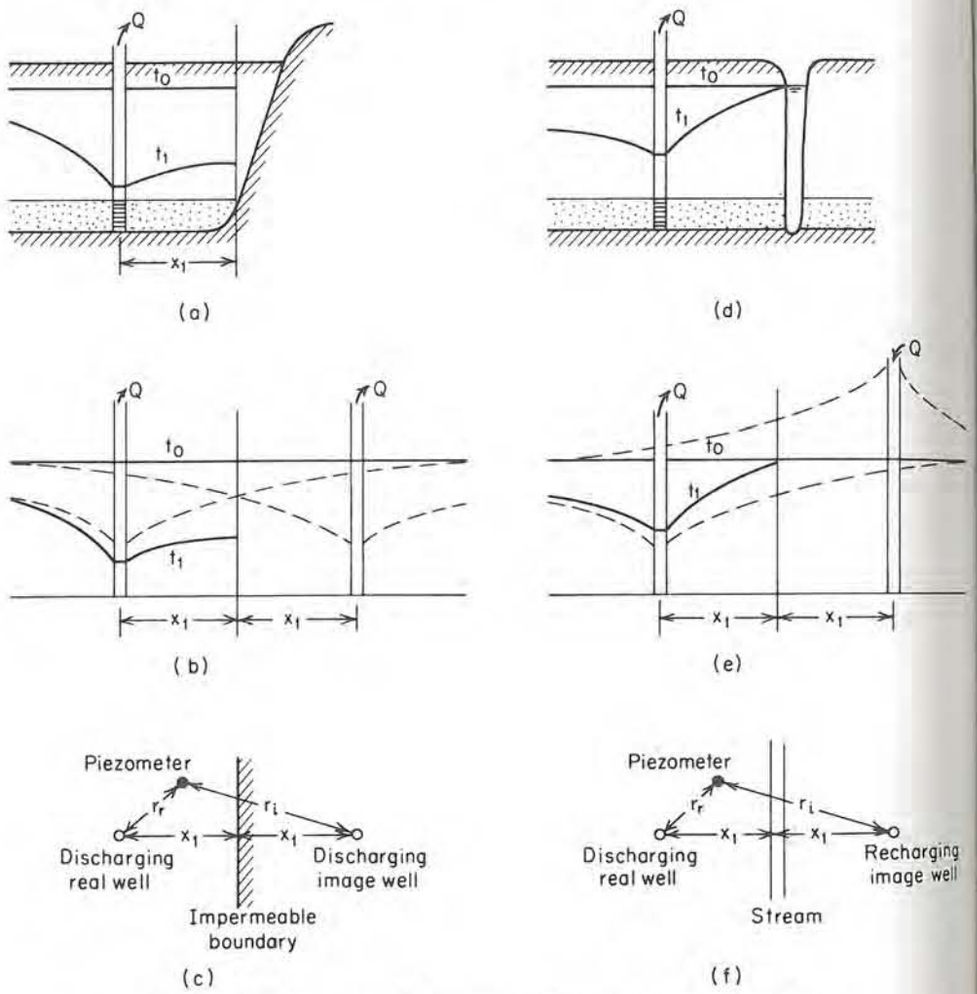

Figure 8.15 (a) Drawdown in the potentiometric surface of a confined aquifer bounded by an impermeable boundary; (b) equivalent system of infinite extent; (c) plan view.

imaginary system of infinite areal extent [Figure 8.15(b)]. In this system there are two wells pumping: the real well on the left and an image well on the right. The image well pumps at a rate, Q, equal to the real well and is located at an equal distance, x_1, from the boundary. If we sum the two component drawdowns in the infinite system (in identical fashion to the two-well case shown in Figure 8.13), it becomes clear that this pumping geometry creates an imaginary impermeable boundary (i.e., a boundary across which there is no flow) in the infinite system at the exact position of the real impermeable boundary in the bounded system. With reference to Figure 8.15(c), the drawdown in an aquifer bounded by an impermeable boundary is given by

$$h_0 - h = \frac{Q}{4\pi T}[W(u_r) + W(u_i)] \tag{8.19}$$

where

$$u_r = \frac{r_r^2 S}{4Tt} \quad \text{and} \quad u_i = \frac{r_i^2 S}{4Tt}$$

One can use the same approach to predict the decreased drawdowns that occur in a confined aquifer in the vicinity of a constant-head boundary, such as would be produced by the slightly unrealistic case of a fully penetrating stream [Figure 8.15(d)]. For this case, the imaginary infinite system [Figure 8.15(e)] includes the discharging real well and a recharging image well. The summation of the cone of depression from the pumping well and the cone of impression from the recharge well leads to an expression for the drawdown in an aquifer bounded by a constant-head boundary:

$$h_0 - h = \frac{Q}{4\pi T}[W(u_r) - W(u_i)] \tag{8.20}$$

where u_r and u_i are as defined in connection with Eq. (8.19).

It is possible to use the image well approach to provide predictions of drawdown in systems with more than one boundary. Ferris et al. (1962) discuss several geometric configurations. One of the more realistic (Figure 8.16) applies to a pumping well in a confined alluvial aquifer in a more-or-less straight river valley. For this case, the imaginary infinite system must include the real pumping well R, an image well I_1 equidistant from the left-hand impermeable boundary, and an image well I_2 equidistant from the right-hand impermeable boundary. These image wells themselves give birth to the need for further image wells. For example, I_3 reflects the effect of I_2 across the left-hand boundary, and I_4 reflects the effect of I_1 across the right-hand boundary. The result is a sequence of imaginary pumping wells stretching to infinity in each direction. The drawdown at point P in Figure 8.16 is the sum of the effects of this infinite array of wells. In practice, image wells need only be added until the most remote pair produces a negligible effect on water-level response (Bostock, 1971).

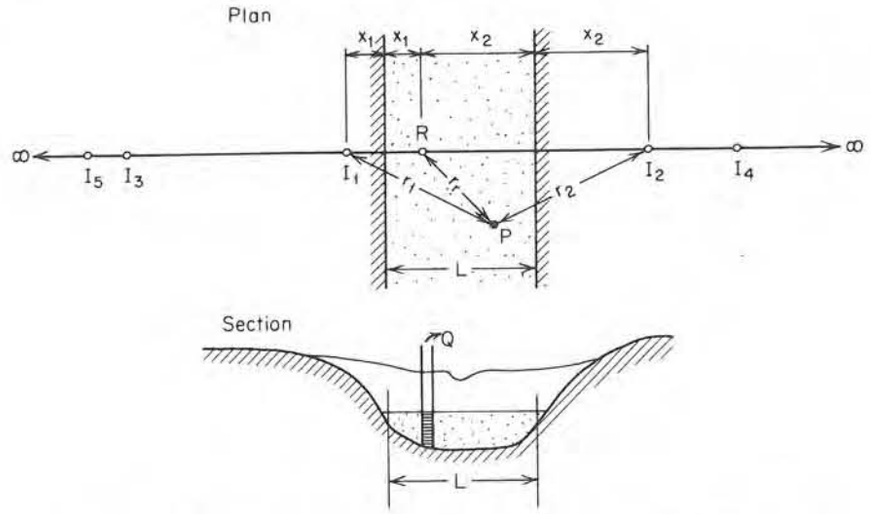

Figure 8.16 Image-well system for pumpage from a confined aquifer in a river valley bounded by impermeable boundaries.

The Response of Ideal Aquitards

The most common geological occurrence of exploitable confined aquifers is in sedimentary systems of interbedded aquifers and aquitards. In many cases the aquitards are much thicker than the aquifers and although their permeabilities are low, their storage capacities can be very high. In the very early pumping history of a production well, most of the water comes from the depressurization of the aquifer in which the well is completed. As time proceeds the leakage properties of the aquitards are brought into play and at later times the majority of the water being produced by the well is aquitard leakage. In many aquifer-aquitard systems, the *aquitards provide* the water and the *aquifers transmit* it to the wells. It is thus of considerable interest to be able to predict the response of aquitards as well as aquifers.

In the earlier discussion of leaky aquifers, two theories were introduced: the Hantush-Jacob theory, which utilizes the $W(u, r/B)$ curves of Figure 8.8, and the Neuman-Witherspoon theory, which utilizes the $W(u, r/B_{11}, r/B_{21}, \beta_{11}, \beta_{21})$ curves of Figure 8.9. In that the Hantush-Jacob theory does not include the storage properties of the aquitard, it is not suitable for the prediction of aquitard response. The Neuman-Witherspoon solution, in the form of Eq. (8.11) can be used to predict the hydraulic head $h(r, z, t)$ at any elevation z in the aquitard (Figure 8.7) at any time t, at any radial distance r, from the well. In many cases, however, it may be quite satisfactory to use a simpler approach. If the hydraulic conductivity of the aquitards is at least 2 orders of magnitude less than the hydraulic conductivity in the aquifers, it can be assumed that flow in the aquifers is horizontal and leakage in the aquitards is vertical. If one can predict, or has measurements of, $h(r, t)$ at some point in an aquifer, one can often predict the hydraulic head $h(z, t)$

at an overlying point in the aquitard by the application of a one-dimensional flow theory, developed by Karl Terzaghi, the founder of modern soil mechanics.

Consider an aquitard of thickness b' (Figure 8.17) sandwiched between two producing aquifers. If the initial condition is a constant hydraulic head $h = h_0$ in the aquitard, and if the drawdowns in hydraulic head in the adjacent aquifers can be represented as an instantaneous step function Δh, the system can be represented by the following one-dimensional boundary-value problem.

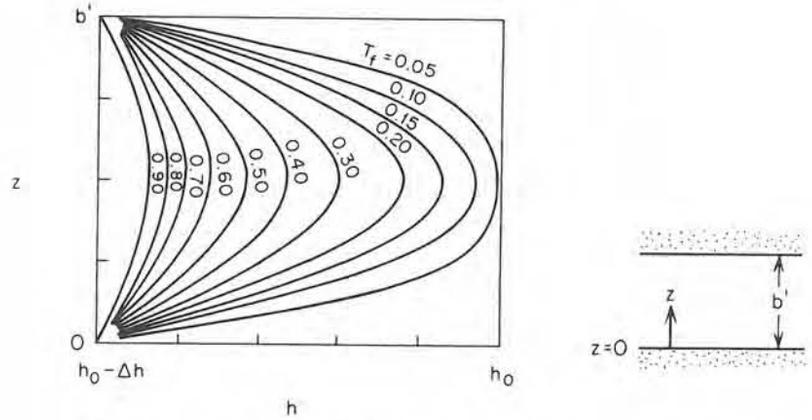

Figure 8.17 Response of an ideal aquitard to a step drawdown in head in the two adjacent aquifers.

From Eq. (2.76), the one-dimensional form of the flow equation is

$$\frac{\partial^2 h}{\partial z^2} = \frac{\rho g(\alpha' + n'\beta)}{K'} \frac{\partial h}{\partial t} \tag{8.21}$$

where the primed parameters are the aquitard properties. The initial condition is

$$h(z, 0) = h_0$$

and the boundary conditions are

$$h(0, t) = h_0 - \Delta h$$

$$h(b', t) = h_0 - \Delta h$$

Terzaghi (1925) provided an analytical solution to this boundary-value problem. He noted that for clays $n'\beta \ll \alpha'$ in Eq. (8.21). He grouped the remaining aquitard parameters into a single parameter c_v, known as the *coefficient of consolidation* and defined as

$$c_v = \frac{K'}{\rho g \alpha'} \tag{8.22}$$

He further defined the dimensionless time factor, T_f, as

$$T_f = \frac{4c_v t}{(b')^2} \tag{8.23}$$

Given the aquitard parameter c_v and the geometric parameter b', one can calculate T_f for any time t.

Figure 8.17 is a graphical presentation of Terzaghi's solution $h(z, T_f)$. It allows the prediction of the hydraulic head at any elevation z at any time t in an aquitard sandwiched between two producing aquifers, as long as the drop in hydraulic head Δh can be estimated in the aquifers. It is also possible to interpret this solution for an aquitard that drains to only one aquifer. For example, if the lower boundary of the aquitard on the inset to Figure 8.17 is impermeable, only the upper half of the curves shown in the figure are used for the prediction of $h(z, t)$. The $z = 0$ line passes through the center of the figure, and the parameters c_v and T_f are defined as above. Wolff (1970) has described a case history that utilizes the concepts of one-dimensional aquitard response.

Predictions of aquitard response, and the inverse application of this theory to determine aquitard parameters, as discussed in Section 8.6, are also important in assessing contaminant migration (Chapter 9) and land subsidence (Section 8.12).

The Real World

Each of the analytical solutions presented in this section describes the response to pumping in a very idealized representation of actual aquifer configurations. In the real world, aquifers are heterogeneous and anisotropic; they usually vary in thickness; and they certainly do not extend to infinity. Where they are bounded, it is not by straight-line boundaries that provide perfect confinement. In the real world, aquifers are created by complex geologic processes that lead to irregular stratigraphy, interfingering of strata, and pinchouts and trendouts of both aquifers and aquitards. The predictions that can be carried out with the analytical expressions presented in this section must be viewed as best estimates. They have greater worth the more closely the actual hydrogeological environment approaches the idealized configuration.

In general, well-hydraulics equations are most applicable when the unit of study is a well or well field. They are less applicable on a larger scale, where the unit of study is an entire aquifer or a complete groundwater basin. Short-term yields around wells are very dependent on aquifer properties and well-field geometry, both of which are emphasized in the well-hydraulics equations. Long-term yields on an aquifer scale are more often controlled by the nature of the boundaries. Aquifer studies on the larger scale are usually carried out with the aid of models based on numerical simulation or electric-analog techniques. These approaches are discussed in Sections 8.8 and 8.9.

The predictive formulas developed in this section and the simulation techniques described in later sections allow one to calculate the drawdowns in hydraulic

head that will occur in an aquifer in response to groundwater development through wells. They require as input either the three basic hydrogeological parameters: hydraulic conductivity, K, porosity, n, and compressibility, α; or the two derived aquifer parameters: transmissivity, T, and storativity, S. There is a wide variety of techniques that can be used to measure these parameters. In the next section, we will discuss *laboratory tests*; in Section 8.5, *piezometer tests*; and in Section 8.6, *pumping tests*. In Section 8.7, we will examine some *estimation techniques*, and in Section 8.8, the determination of aquifer parameters by *inverse simulation*. The formulas presented in this section are the basis for the pumping-test approach that is described in Section 8.6.

8.4 Measurement of Parameters: Laboratory Tests

The laboratory tests described in this section can be considered as providing point values of the basic hydrogeologic parameters. They are carried out on small samples that are collected during test-drilling programs or during the mapping of surficial deposits. If the samples are undisturbed core samples, the measured values should be representative of the *in situ* point values. For sands and gravels, even disturbed samples may yield useful values. We will describe testing methods for the determination of hydraulic conductivity, porosity, and compressibility in the saturated state; and we will provide references for the determination of the characteristic curves relating moisture content, pressure head, and hydraulic conductivity in the unsaturated state. We will emphasize principles; for a more complete description of each testing apparatus and more detailed directions on laboratory procedures, the reader is directed to the soil-testing manual by Lambe (1951), the permeability handbook of the American Society of Testing Materials (1967), or the pertinent articles in the compendium of soil analysis methods edited by Black (1965). Our discussions relate more to soils than to rocks, but the principles of measurement are the same. The rock mechanics text by Jaeger (1972) discusses rock-testing procedures.

Hydraulic Conductivity

The hydraulic conductivity, K, was defined in Section 2.1, and its relationship to the permeability, k, was explored in Section 2.3. The saturated hydraulic conductivity of a soil sample can be measured with two types of laboratory apparatus. The first type, known as a *constant-head permeameter*, is shown in Figure 8.18(a); the second type, a *falling-head permeameter*, is shown in Figure 8.18(b).

In a constant-head test, a soil sample of length L and cross-sectional area A is enclosed between two porous plates in a cylindrical tube, and a constant-head differential H is set up across the sample. A simple application of Darcy's law leads to the expression

$$K = \frac{QL}{AH} \tag{8.24}$$

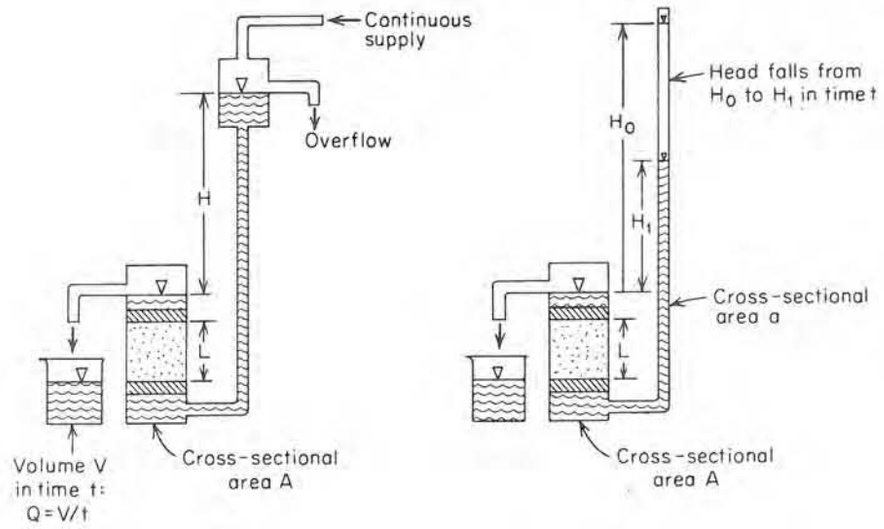

Figure 8.18 (a) Constant-head permeameter; (b) falling-head permeameter (after Todd, 1959).

where Q is the steady volumetric discharge through the system. It is important that no air become entrapped in the system, and for this reason it is wise to use deaired water. If disturbed samples are being tested in the permeameter, they should be carefully saturated from below as they are emplaced.

In a falling-head test [Figure 8.18(b)], the head, as measured in a tube of cross-sectional area a, is allowed to fall from H_0 to H_1 during time t. The hydraulic conductivity is calculated from

$$K = \frac{aL}{At} \ln\left(\frac{H_0}{H_1}\right) \tag{8.25}$$

This equation can be derived (Todd, 1959) from the simple boundary-value problem that describes one-dimensional transient flow across the soil sample. In order that the head decline be easily measurable in a finite time period, it is necessary to choose the standpipe diameter with regard to the soil being tested. Lambe (1951) suggests that for a coarse sand a standpipe whose diameter is approximately equal to that of the permeameter is usually satisfactory, whereas a fine silt may necessitate a standpipe whose diameter is one-tenth the permeameter diameter. Lambe also suggests that the point $\sqrt{H_0H_1}$ be marked on the standpipe. If the time required for the head decline from H_0 to $\sqrt{H_0H_1}$ is not equal to that for the decline from $\sqrt{H_0H_1}$ to H_1, the test has not functioned correctly and a check should be made for leaks or entrapped air.

Klute (1965a) notes that the constant-head system is best suited to samples with conductivities greater than 0.01 cm/min while the falling-head system is best suited to samples with lower conductivity. He also notes that elaborate, painstaking

measurements are not generally required for conductivity determinations on field samples. The variability among samples is usually large enough that precise determination of the conductivity of a given sample is not warranted.

For clayey materials the hydraulic conductivity is commonly determined from a consolidation test, which is described in the subsection on compressibility below.

Porosity

In principle, the porosity, n, as defined in Section 2.5, would be most easily measured by saturating a sample, measuring its volume, V_T, weighing it and then oven drying it to constant weight at 105°C. The weight of water removed could be converted to a volume, knowing the density of water. This volume is equivalent to the volume of the void space, V_v; and the porosity could be calculated from $n = V_v/V_T$.

In practice, it is quite difficult to exactly and completely saturate a sample of given volume. It is more usual (Vomocil, 1965) to make use of the relationship

$$n = 1 - \frac{\rho_b}{\rho_s} \tag{8.26}$$

which can be developed by simple arithmetic manipulation of the basic definition of porosity. In Eq. (8.26), ρ_b is the *bulk mass density* of the sample and ρ_s is the *particle mass density*. The bulk density is the oven-dried mass of the sample divided by its field volume. The particle density is the oven-dried mass divided by the volume of the solid particles, as determined by a water-displacement test. In cases where great accuracy is not required, $\rho_s = 2.65\ \text{g/cm}^3$ can be assumed for most mineral soils.

Compressibility

The compressibility of a porous medium was defined in Section 2.9 with the aid of Figure 2.19. It is a measure of the relative volumetric reduction that will take place in a soil under an increased effective stress. Compressibility is measured in a consolidation apparatus of the kind commonly used by soils engineers. In this test, a soil sample is placed in a loading cell of the type shown schematically in Figure 2.19(a). A load L is applied to the cell, creating a stress σ, where $\sigma = L/A$, A being the cross-sectional area of the sample. If the soil sample is saturated and the fluid pressure on the boundaries of the sample is atmospheric (i.e., the sample is free-draining), the effective stress, σ_e, which leads to consolidation of the sample, is equal to the applied stress, σ.

The reduction in sample thickness, b, is measured after equilibrium is achieved at each of several loading increments, and the results are converted into a graph of void ratio, e, versus effective stress, σ_e, as shown in Figure 2.19(b). The compressibility, α, is determined from the slope of such a plot by

$$\alpha = -\frac{de/(1 + e_0)}{d\sigma_e} \tag{8.27}$$

where e_0 is the initial void ratio prior to loading. As noted in Section 2.9, α is a function of the applied stress and it is dependent on the previous loading history.

Lambe (1951) describes the details of the testing procedure. The most common loading method is a lever system on which weights of known magnitude are hung. There are two types of loading cell in common use. In the *fixed-ring* container [Figure 8.19(a)], all the sample movement relative to the container is downward. In the *floating-ring* container [Figure 8.19(b)], compression occurs toward the middle from both top and bottom. In the floating-ring container, the effect of friction between the container wall and the soil specimen is smaller than in the fixed-ring container. In practice, it is difficult to determine the magnitude of the friction in any case, and because its effect is thought to be minor, it is normally neglected. Cohesionless sands are usually tested as disturbed samples. Cohesive clays must be carefully trimmed to fit the consolidometer ring.

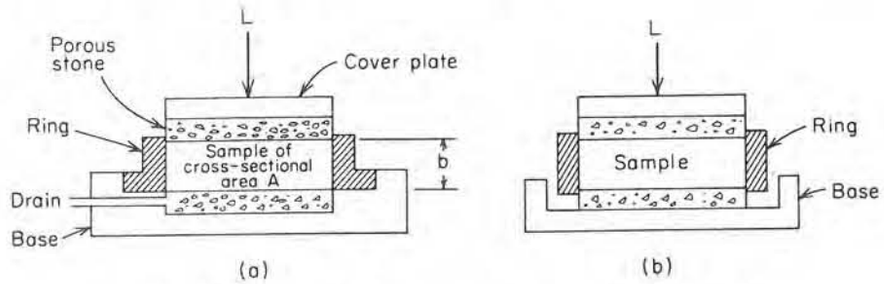

Figure 8.19 (a) Fixed-ring consolidometer; (b) floating-ring consolidometer (after Lambe, 1951).

In soil mechanics terminology, the slope of the $e - \sigma_e$ curve is called the *coefficient of compressibility*, a_v. The relationship between a_v and α is easily seen to be

$$a_v = \frac{-de}{d\sigma_e} = (1 + e_0)\alpha \tag{8.28}$$

More commonly, soils engineers plot the void ratio, e, against the logarithm of σ_e. When plotted in this manner, there is usually a significant portion of the curve that is a straight line. The slope of this line is called the *compression index*, C_c, where

$$C_c = \frac{-de}{d(\log \sigma_e)} \tag{8.29}$$

In most civil engineering applications the *rate* of consolidation is just as important as the *amount* of consolidation. This rate is dependent both on the compressibility, α, and the hydraulic conductivity, K. As noted in connection with Eq. (8.22), soils engineers utilize a grouped parameter known as the *coefficient of consolidation*, c_v, which is defined as

$$c_v = \frac{K}{\rho g \alpha} \tag{8.30}$$

At each loading level in a consolidation test, the sample undergoes a transient drainage process (fast for sands, slow for clays) that controls the rate of consolidation of the sample. If the rate of decline in sample thickness is recorded for each loading increment, such measurements can be used in the manner described by Lambe (1951) to determine the coefficient of consolidation, c_v, and the hydraulic conductivity, K, of the soil.

In Section 8.12, we will further examine the mechanism of one-dimensional consolidation in connection with the analysis of land subsidence.

Unsaturated Characteristic Curves

The characteristic curves, $K(\psi)$ and $\theta(\psi)$, that relate the moisture content, θ, and the hydraulic conductivity, K, to the pressure head, ψ, in unsaturated soils were described in Section 2.6. Figure 2.13 provided a visual example of the hysteretic relationships that are commonly observed. The methods used for the laboratory determination of these curves have been developed exclusively by soil scientists. It is not within the scope of this text to outline the wide variety of sophisticated laboratory instrumentation that is available. Rather, the reader is directed to the soil science literature, in particular to the review articles by L. A. Richards (1965), Klute (1965b), Klute (1965c), and Bouwer and Jackson (1974).

8.5 Measurement of Parameters: Piezometer Tests

It is possible to determine *in situ* hydraulic conductivity values by means of tests carried out in a single piezometer. We will look at two such tests, one suitable for point piezometers that are open only over a short interval at their base, and one suitable for screened or slotted piezometers that are open over the entire thickness of a confined aquifer. Both tests are initiated by causing an instantaneous change in the water level in a piezometer through a sudden introduction or removal of a known volume of water. The recovery of the water level with time is then observed. When water is removed, the tests are often called *bail tests*; when it is added, they are known as *slug tests*. It is also possible to create the same effect by suddenly introducing or removing a solid cylinder of known volume.

The method of interpreting the water level versus time data that arise from bail tests or slug tests depends on which of the two test configurations is felt to be most representative. The method of Hvorslev (1951) is for a point piezometer, while that of Cooper et al. (1967) is for a confined aquifer. We will now describe each in turn.

The simplest interpretation of piezometer-recovery data is that of Hvorslev (1951). His initial analysis assumed a homogeneous, isotropic, infinite medium in which both soil and water are incompressible. With reference to the bail test of Figure 8.20(a), Hvorslev reasoned that the rate of inflow, q, at the piezometer tip at any time t is proportional to the hydraulic conductivity, K, of the soil and to the unrecovered head difference, $H - h$, so that

$$q(t) = \pi r^2 \frac{dh}{dt} = FK(H - h) \tag{8.31}$$

where F is a factor that depends on the shape and dimensions of the piezometer intake. If $q = q_0$ at $t = 0$, it is clear that $q(t)$ will decrease asymptotically toward zero as time goes on.

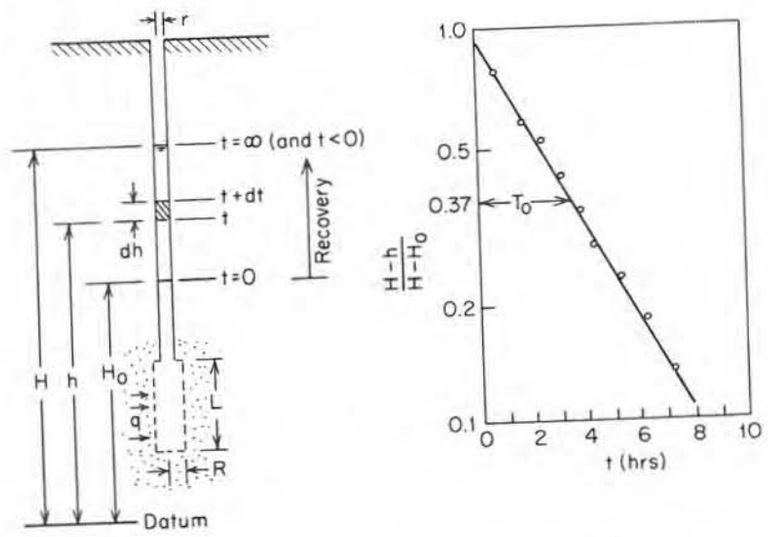

Figure 8.20 Hvorslev piezometer test. (a) Geometry; (b) method of analysis.

Hvorslev defined the *basic time lag*, T_0, as

$$T_0 = \frac{\pi r^2}{FK} \tag{8.32}$$

When this parameter is substituted in Eq. (8.31), the solution to the resulting ordinary differential equation, with the initial condition, $h = H_0$ at $t = 0$, is

$$\frac{H - h}{H - H_0} = e^{-t/T_0} \tag{8.33}$$

A plot of field recovery data, $H - h$ versus t, should therefore show an exponential decline in recovery rate with time. If, as shown on Figure 8.20(b), the recovery is normalized to $H - H_0$ and plotted on a logarithmic scale, a straight-line plot results. Note that for $H - h/H - H_0 = 0.37$, $\ln(H - h/H - H_0) = -1$, and from Eq. (8.33), $T_0 = t$. The basic time lag, T_0, can be defined by this relation; or if a more physical definition is desired, it can be seen, by multiplying both top and bottom of Eq. (8.32) by $H - H_0$, that T_0 is the time that would be required for the complete equalization of the head difference if the original rate of inflow were maintained. That is, $T_0 = V/q_0$, where V is the volume of water removed or added.

To interpret a set of field recovery data, the data are plotted in the form of Figure 8.20(b). The value of T_0 is measured graphically, and K is determined from Eq. (8.32). For a piezometer intake of length L and radius R [Figure 8.20(a)], with $L/R > 8$, Hvorslev (1951) has evaluated the shape factor, F. The resulting expression for K is

$$K = \frac{r^2 \ln(L/R)}{2LT_0} \tag{8.34}$$

Hvorslev also presents formulas for anisotropic conditions and for a wide variety of shape factors that treat such cases as a piezometer open only at its basal cross section and a piezometer that just encounters a permeable formation underlying an impermeable one. Cedergren (1967) also lists these formulas.

In the field of agricultural hydrology, several *in situ* techniques, similar in principle to the Hvorslev method but differing in detail, have been developed for the measurement of saturated hydraulic conductivity. Boersma (1965) and Bouwer and Jackson (1974) review those methods that involve auger holes and piezometers.

For bail tests of slug tests run in piezometers that are open over the entire thickness of a confined aquifer, Cooper et al. (1967) and Papadopoulos et al. (1973) have evolved a test-interpretation procedure. Their analysis is subject to the same assumptions as the Theis solution for pumpage from a confined aquifer. Contrary to the Hvorslev method of analysis, it includes consideration of both formation and water compressibilities. It utilizes a curve-matching procedure to determine the aquifer coefficients T and S. The hydraulic conductivity K can then be determined on the basis of the relation, $K = T/b$. Like the Theis solution, the method is based on the solution to a boundary-value problem that involves the transient equation of groundwater flow, Eq. (2.77). The mathematics will not be described here.

For the bail-test geometry shown in Figure 8.21(a), the method involves the preparation of a plot of recovery data in the form $H - h/H - H_0$ versus t. The plot is prepared on semilogarithmic paper with the reverse format to that of the Hvorslev test; the $H - h/H - H_0$ scale is linear, while the t scale is logarithmic. The field curve is then superimposed on the type curves shown in Figure 8.21(b). With the axes coincident, the data plot is translated horizontally into a position where the data best fit one of the type curves. A matchpoint is chosen (or rather, a vertical axis is matched) and values of t and W are read off the horizontal scales

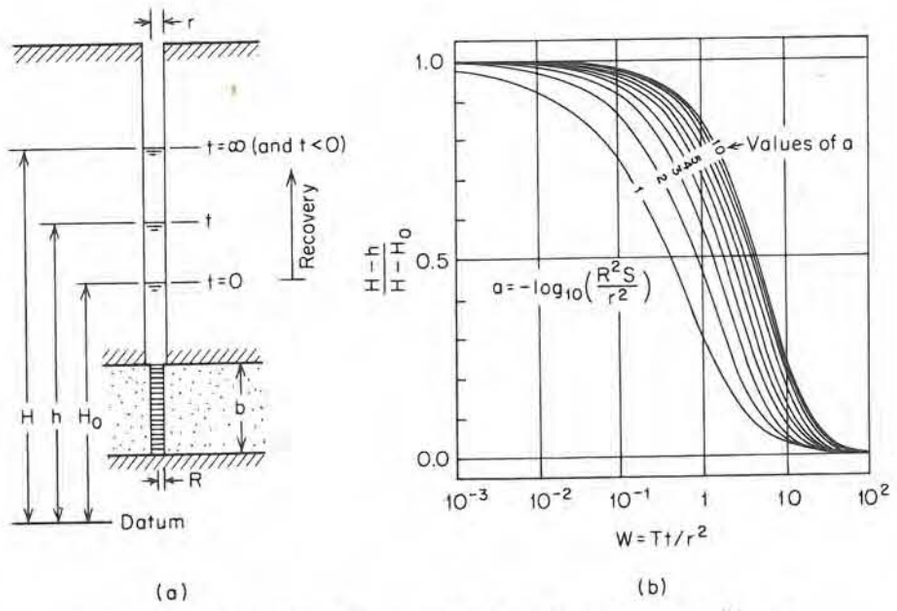

Figure 8.21 Piezometer test in a confined aquifer. (a) Geometry; (b) type curves (after Papadopoulos et al., 1973).

at the matched axis of the field plot and the type plot, respectively. For ease of calculation it is common to choose a matched axis at $W = 1.0$. The transmissivity T is then given by

$$T = \frac{Wr^2}{t} \tag{8.35}$$

where the parameters are expressed in any consistent set of units.

In principle, the storativity, S, can be determined from the a value of the matched curve and the expression shown on Figure 8.21(b). In practice, since the slopes of the various a lines are very similar, the determination of S by this method is unreliable.

The main limitation on slug tests and bail tests is that they are heavily dependent on a high-quality piezometer intake. If the wellpoint or screen is corroded or clogged, measured values may be highly inaccurate. On the other hand, if a piezometer is developed by surging or backwashing prior to testing, the measured values may reflect the increased conductivities in the artificially induced gravel pack around the intake.

It is also possible to determine hydraulic conductivity in a piezometer or single well by the introduction of a tracer into the well bore. The tracer concentration decreases with time under the influence of the natural hydraulic gradient that exists in the vicinity of the well. This approach is known as the *borehole dilution method*, and it is described more fully in Section 9.4.

8.6 Measurement of Parameters: Pumping Tests

In this section, a method of parameter measurement that is specifically suited to the determination of transmissivity and storativity in confined and unconfined aquifers will be described. Whereas laboratory tests provide point values of the hydrogeological parameters, and piezometer tests provide *in situ* values representative of a small volume of porous media in the immediate vicinity of a piezometer tip, pumping tests provide *in situ* measurements that are averaged over a large aquifer volume.

The determination of T and S from a pumping test involves a direct application of the formulas developed in Section 8.3. There, it was shown that for a given pumping rate, if T and S are known, it is possible to calculate the time rate of drawdown, $h_0 - h$ versus t, at any point in an aquifer. Since this response depends solely on the values of T and S, it should be possible to take measurements of $h_0 - h$ versus t at some observational point in an aquifer and work backward through the equations to determine the values of T and S.

The usual course of events during the initial exploitation of an aquifer involves (1) the drilling of a test well with one or more observational piezometers, (2) a short-term pumping test to determine the values of T and S, and (3) application of the predictive formulas of Section 8.3, using the T and S values determined in the pumping test, to design a production well or wells that will fulfill the pumpage requirements of the project without leading to excessive long-term drawdowns. The question of what constitutes an "excessive" drawdown and how drawdowns and well yields are related to groundwater recharge rates and the natural hydrologic cycle are discussed in Section 8.10.

Let us now examine the methodology of pumping-test interpretation in more detail. There are two methods that are in common usage for calulating aquifer coefficients from time-drawdown data. Both approaches are graphical. The first involves curve matching on a log-log plot (the *Theis method*), and the second involves interpretations with a semilog plot (the *Jacob method*).

Log-Log Type-Curve Matching

Let us first consider data taken from an aquifer in which the geometry approaches that of the idealized Theis configuration. As was explained in connection with Figure 8.5, the time-drawdown response in an observational piezometer in such an aquifer will always have the shape of the Theis curve, regardless of the values of T and S in the aquifer. However, for high T a measurable drawdown will reach the observation point faster than for low T, and the drawdown data will begin to march up the Theis curve sooner. Theis (1935) suggested the following graphical procedure to exploit this curve-matching property:

1. Plot the function $W(u)$ versus $1/u$ on log-log paper. (Such a plot of dimensionless theoretical response is known as a *type curve*.)

2. Plot the measured time-drawdown values, $h_0 - h$ versus t, on log-log paper of the same size and scale as the $W(u)$ versus $1/u$ curve.
3. Superimpose the field curve on the type curve keeping the coordinate axes parallel. Adjust the curves until most of the observed data points fall on the type curve.
4. Select an arbitrary match point and read off the paired values of $W(u)$, $1/u$, $h_0 - h$, and t at the match point. Calculate u from $1/u$.
5. Using these values, together with the pumping rate Q and the radial distance r from well to piezometer, calculate T from the relationship

$$T = \frac{QW(u)}{4\pi(h_0 - h)} \tag{8.36}$$

6. Calculate S from the relationship

$$S = \frac{4uTt}{r^2} \tag{8.37}$$

Equations (8.36) and (8.37) follow directly from Eqs. (8.7) and (8.6). They are valid for any consistent system of units. Some authors prefer to present the equations in the form

$$T = \frac{AQW(u)}{h_0 - h} \tag{8.38}$$

$$S = \frac{uTt}{Br^2} \tag{8.39}$$

where the coefficients A and B are dependent on the units used for the various parameters. For SI units, with $h_0 - h$ and r measured in meters, t in seconds, Q in m^3/s, and T in m^2/s, $A = 0.08$ and $B = 0.25$. For the inconsistent set of practical units widely used in North America, with $h_0 - h$ and r measured in feet, t in days, Q in U.S. gal/min, and T in U.S. gal/day/ft, $A = 114.6$ and $B = 1.87$. For Q and T in terms of Imperial gallons, A remains unchanged and $B = 1.56$.

Figure 8.22 illustrates the curve-matching procedure and calculations for a set of field data. The alert reader will recognize these data as being identical to the calculated data originally presented in Figure 8.5(b). It would probably be intuitively clearer if the match point were taken at some point on the coincident portions of the superimposed curves. However, a few quick calculations should convince doubters that it is equally valid to take the matchpoint anywhere on the overlapping fields once they have been fixed in their correct relative positions. For ease of calculation, the matchpoint is often taken at $W(u) = 1.0$, $u = 1.0$.

The log-log curve-matching technique can also be used for leaky aquifers (Walton, 1962) and unconfined aquifers (Prickett, 1965; Neuman, 1975a). Figure 8.23 provides a comparative review of the geometry of these systems and the types of $h_0 - h$ versus t data that should be expected in an observational piezometer

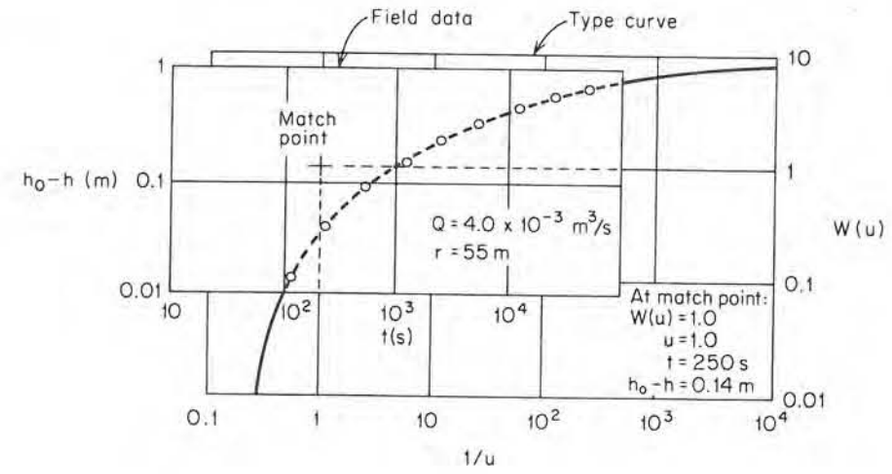

$$T = \frac{QW(u)}{4\pi(h_0-h)} = \frac{(4.0 \times 10^{-3})(1.0)}{(4.0)(3.14)(0.14)} = 0.0023\ m^2/s \quad (15{,}700\ U.S.\ gal/day/ft)$$

$$S = \frac{4uTt}{r^2} = \frac{(4.0)(1.0)(0.0023)(250)}{(55.0)^2} = 7.5 \times 10^{-4}$$

Figure 8.22 Determination of T and S from $h_0 - h$ versus t data using the log-log curve-matching procedure and the $W(u)$ versus $1/u$-type curve.

in each case. Sometimes time-drawdown data unexpectedly display one of these forms, thus indicating a geological configuration that has gone unrecognized during the exploration stage of aquifer evaluation.

For leaky aquifers the time-drawdown data can be matched against the leaky type curves of Figure 8.8. The r/B value of the matched curve, together with the matchpoint values of $W(u, r/B)$, u, $h_0 - h$, and t, can be substituted into Eqs. (8.6), (8.8), and (8.9) to yield the aquifer coefficients T and S. Because the development of the r/B solutions does not include consideration of aquitard storativity, an r/B curve matching approach is not suitable for the determination of the aquitard conductivity K'. As noted in the earlier subsection on aquitard response, there are many aquifer-aquitard configurations where the leakage properties of the aquitards are more important in determining long-term aquifer yields than the aquifer parameters themselves. In such cases it is necessary to design a pumping-test configuration with observational piezometers that bottom in the aquitards as well as in the aquifers. One can then use the pumping-test procedure outlined by Neuman and Witherspoon (1972), which utilizes their more general leaky-aquifer solution embodied in Eqs. (8.6), (8.10), and (8.11). They present a ratio method that obviates the necessity of matching field data to type curves as complex as

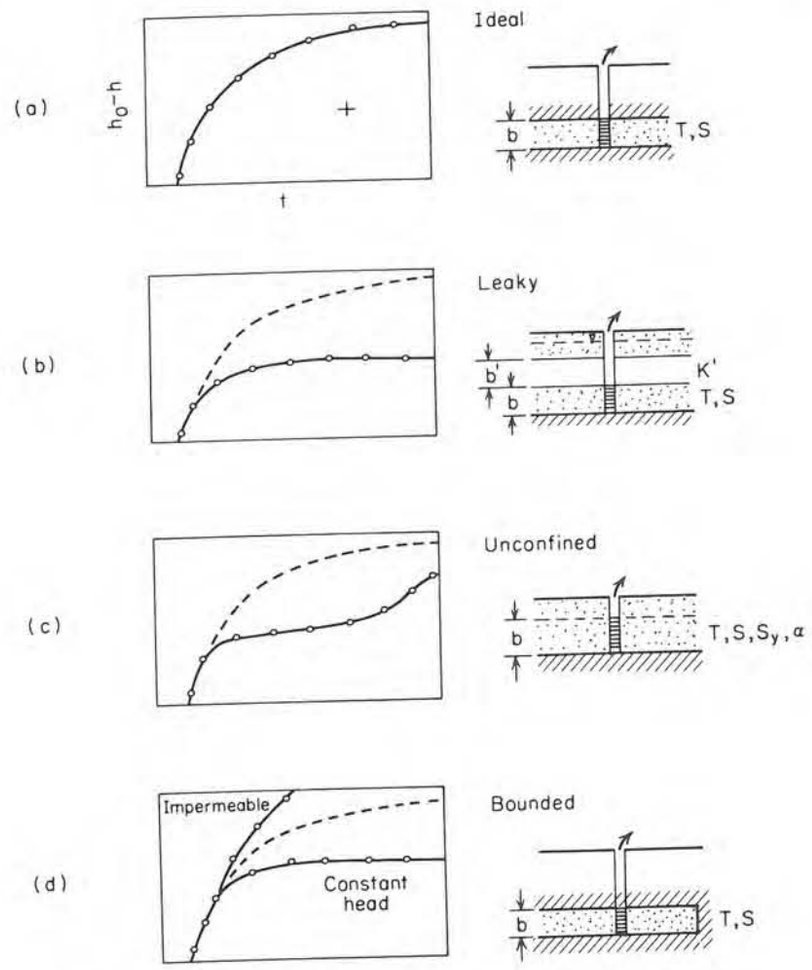

Figure 8.23 Comparison of log-log $h_0 - h$ versus t data for ideal, leaky, unconfined, and bounded systems.

those of Figure 8.9. The method only requires matching against the Theis curve, and calculations are relatively easy to carry out.

As an alternative approach (Wolff, 1970), one can simply read off a T_f value from Figure 8.17 given a hydraulic head value h measured in an aquitard piezometer at elevation z at time t. Knowing the aquitard thickness, b', one can solve Eq. (8.23) for c_v. If an α value can be estimated, Eq. (8.22) can be solved for K'.

For unconfined aquifers the time-drawdown data should be matched against the unconfined type curves of Figure 8.12. The η value of the matched curve, together with the match-point values of $W(u_A, u_B, \eta)$, $u_A, u_B, h_0 - h$, and t can be substituted into Eqs. (8.13) through (8.15) to yield the aquifer coefficients T, S, and S_y. Moench and Prickett (1972) discuss the interpretation of data at sites

where lowered water levels cause a conversion from confined to unconfined conditions.

Figure 8.23(d) shows the type of log-log response that would be expected in the vicinity of an impermeable or constant-head boundary. However, bounded systems are more easily analyzed with the semilog approach that will now be described.

Semilog Plots

The semilog method of pump-test interpretation rests on the fact that the exponential integral, $W(u)$, in Eqs. (8.5) and (8.7) can be represented by an infinite series. The Theis solution then becomes

$$h_0 - h = \frac{Q}{4\pi T}\left(-0.5772 - \ln u + u - \frac{u^2}{2\cdot 2!} + \frac{u^3}{3\cdot 3!} + \cdots\right) \tag{8.40}$$

Cooper and Jacob (1946) noted that for small u the sum of the series beyond ln u becomes negligible, so that

$$h_0 - h = \frac{Q}{4\pi T}(-0.5772 - \ln u) \tag{8.41}$$

Substituting Eq. (8.6) for u, and noting that $\ln u = 2.3 \log u$, that $-\ln u = \ln 1/u$, and that $\ln 1.78 = 0.5772$, Eq. (8.41) becomes

$$h_0 - h = \frac{2.3Q}{4\pi T} \log \frac{2.25Tt}{r^2 S} \tag{8.42}$$

Since Q, r, T, and S are constants, it is clear that $h_0 - h$ versus log t should plot as a straight line.

Figure 8.24(a) shows the time-drawdown data of Figure 8.22 plotted on a semilog graph. If Δh is the drawdown for one log cycle of time and t_0 is the time intercept where the drawdown line intercepts the zero drawdown axis, it follows from further manipulation with Eq. (8.42) that the values of T and S, in consistent units, are given by

$$T = \frac{2.3Q}{4\pi\,\Delta h} \tag{8.43}$$

$$S = \frac{2.25Tt_0}{r^2} \tag{8.44}$$

As with the log-log methods, these equations can be reshaped as

$$T = \frac{CQ}{\Delta h} \tag{8.45}$$

$$S = \frac{DTt_0}{r^2} \tag{8.46}$$

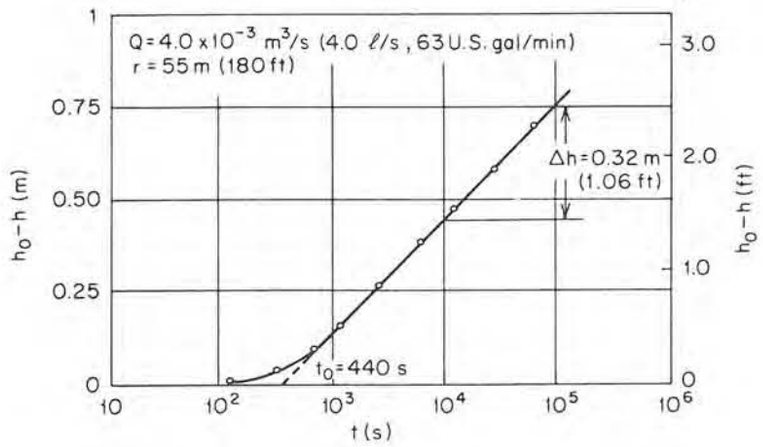

$$T = \frac{2.3Q}{4\pi\Delta h} = \frac{(2.3)(4.0 \times 10^{-3})}{(4)(3.14)(0.32)} = 0.0023 \text{ m}^2/\text{s}$$

$$S = \frac{2.25Tt_0}{r^2} = \frac{(2.25)(0.0023)(440)}{(55)^2} = 7.5 \times 10^{-4}$$

(a)

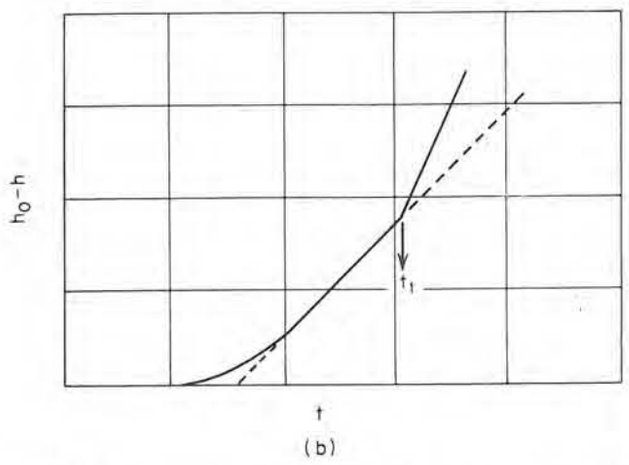

(b)

Figure 8.24 (a) Determination of T and S from $h_0 - h$ versus t data using the semilog method; (b) semilog plot in the vicinity of an impermeable boundary.

where C and D are coefficients that depend on the units used. For Δh and r in meters, t in seconds, Q in m^3/s, and T in m^2/s, $C = 0.18$ and $D = 2.25$. For Δh and r in feet, t in days, Q in U.S. gal/min, and T in U.S. gal/day/ft, $C = 264$ and $D = 0.3$. For Q and T in terms of Imperial gallons, $C = 264$ and $D = 0.36$.

Todd (1959) states that the semilog method is valid for $u < 0.01$. Examination of the definition of u [Eq. (8.6)] shows that this condition is most likely to be satisfied for piezometers at small r and large t.

The semilog method is very well suited to the analysis of bounded confined aquifers. As we have seen, the influence of a boundary is equivalent to that of a recharging or discharging image well. For the case of an impermeable boundary, for example, the effect of the additional imaginary pumping well is to double the slope of the $h_0 - h$ versus log t plot [Figure 8.24(b)]. The aquifer coefficients S and T should be calculated from Eqs. (8.43) and (8.44) on the earliest limb of the plot (before the influence of the boundary is felt). The time, t_1, at which the break in slope takes place can be used together with Eqs. (8.19) to calculate r_i, the distance from piezometer to image well [Figure 8.15(c)]. It takes records from three piezometers to unequivocally locate the position of the boundary if it is not known from geological evidence.

Advantages and Disadvantages of Pumping Tests

The determination of aquifer constants through pumping tests has become a standard step in the evaluation of groundwater resource potential. In practice, there is much art to successful pump testing and the interested reader is directed to Kruseman and de Ridder (1970) and Stallman (1971) for detailed advice on the design of pumping-test geometries, and to Walton's (1970) many case histories.

The advantages of the method are probably self-evident. A pumping test provides *in situ* parameter values, and these values are, in effect, averaged over a large and representative aquifer volume. One obtains information on both conductivity (through the relation $K = T/b$) and storage properties from a single test. In aquifer-aquitard systems it is possible to obtain information on the very important leakage properties of the system if observations are made in the aquitards as well as the aquifers.

There are two disadvantages, one scientific and one practical. The scientific limitation relates to the nonuniqueness of pumping-test interpretation. A perusal of Figure 8.23(b),(c), and (d) indicates the similarity in time-drawdown response that can arise from leaky, unconfined, and bounded systems. Unless there is very clear geologic evidence to direct groundwater hydrologists in their interpretation, there will be difficulties in providing a unique prediction of the effects of any proposed pumping scheme. The fact that a theoretical curve can be matched by pumping test data in no way proves that the aquifer fits the assumptions on which the curve is based.

The practical disadvantage of the method lies in its expense. The installation of test wells and observational piezometers to obtain aquifer coefficients is probably only justified in cases where exploitation of the aquifer by wells at the test site is contemplated. In most such cases, the test well can be utilized as a production well in the subsequent pumping program. In geotechnical applications, in contamination studies, in regional flow-net analysis, or in any flow-net approach that requires hydraulic conductivity data but is not involved with well development,

the use of the pumping-test approach is usually inappropriate. It is our opinion that the method is widely overused. Piezometer tests are simpler and cheaper, and they can provide adequate data in many cases where pumping tests are not justified.

8.7 Estimation of Saturated Hydraulic Conductivity

It has long been recognized that hydraulic conductivity is related to the grain-size distribution of granular porous media. In the early stages of aquifer exploration or in regional studies where direct permeability data are sparse, this interrelationship can prove useful for the estimation of conductivity values. In this section, we will examine estimation techniques based on grain-size analyses and porosity determinations. These types of data are often widely available in geological reports, agricultural soil surveys, or reports of soil mechanics testing at engineering sites.

The determination of a relation between conductivity and soil texture requires the choice of a representative grain-size diameter. A simple and apparently durable empirical relation, due to Hazen in the latter part of the last century, relies on the effective grain size, d_{10}, and predicts a power-law relation with K:

$$K = Ad_{10}^2 \tag{8.47}$$

The d_{10} value can be taken directly from a grain-size gradation curve as determined by sieve analysis. It is the grain-size diameter at which 10% by weight of the soil particles are finer and 90% are coarser. For K in cm/s and d_{10} in mm, the coefficient A in Eq. (8.47) is equal to 1.0. Hazen's approximation was originally determined for uniformly graded sands, but it can provide rough but useful estimates for most soils in the fine sand to gravel range.

Textural determination of hydraulic conductivity becomes more powerful when some measure of the spread of the gradation curve is taken into account. When this is done, the *median grain size*, d_{50}, is usually taken as the representative diameter. Masch and Denny (1966) recommend plotting the gradation curve [Figure 8.25(a)] using Krumbein's ϕ units, where $\phi = -\log_2 d$, d being the grain-size diameter (in mm). As a measure of spread, they use the *inclusive standard deviation*, σ_I, where

$$\sigma_I = \frac{d_{16} - d_{84}}{4} + \frac{d_5 - d_{95}}{6.6} \tag{8.48}$$

For the example shown in Figure 8.25(a), $d_{50} = 2.0$ and $\sigma_I = 0.8$. The curves shown in Figure 8.25(b) were developed experimentally in the laboratory on prepared samples of unconsolidated sand. From them, one can determine K, knowing d_{50} and σ_I.

For a fluid of density, ρ, and viscosity, μ, we have seen in Section 2.3 [Eq. (2.26)] that the hydraulic conductivity of a porous medium consisting of uniform

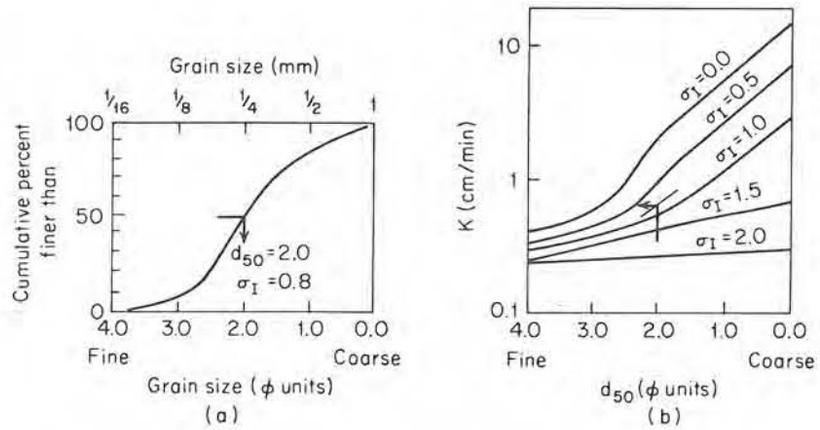

Figure 8.25 Determination of saturated hydraulic conductivity from grain-size gradation curves for unconsolidated sands (after Masch and Denny, 1966).

spherical grains of diameter, d, is given by

$$K = \left(\frac{\rho g}{\mu}\right) C d^2 \tag{8.49}$$

For a nonuniform soil, we might expect the d in Eq. (8.49) to become d_m, where d_m is some representative grain size, and we would expect the coefficient C to be dependent on the shape and packing of the soil grains. The fact that the porosity, n, represents an integrated measure of the packing arrangement has led many investigators to carry out experimental studies of the relationship between C and n. The best known of the resulting predictive equations for hydraulic conductivity is the *Kozeny-Carmen equation* (Bear, 1972), which takes the form

$$K = \left(\frac{\rho g}{\mu}\right)\left[\frac{n^3}{(1-n)^2}\right]\left(\frac{d_m^2}{180}\right) \tag{8.50}$$

In most formulas of this type, the porosity term is identical to the central element of Eq. (8.50), but the grain-size term can take many forms. For example, the *Fair-Hatch equation*, as reported by Todd (1959), take the form

$$K = \left(\frac{\rho g}{\mu}\right)\left[\frac{n^3}{(1-n)^2}\right]\left[\frac{1}{m\left(\frac{\theta}{100}\sum\frac{P}{d_m}\right)^2}\right] \tag{8.51}$$

where m is a packing factor, found experimentally to be about 5; θ is a sand shape factor, varying from 6.0 for spherical grains to 7.7 for angular grains; P is the

percentage of sand held between adjacent sieves; and d_m is the geometric mean of the rated sizes of adjacent sieves.

Both Eqs. (8.50) and (8.51) are dimensionally correct. They are suitable for application with any consistent set of units.

8.8 Prediction of Aquifer Yield by Numerical Simulation

The analytical methods that were presented in Section 8.3 for the prediction of drawdown in multiple-well systems are not sophisticated enough to handle the heterogeneous aquifers of irregular shape that are often encountered in the field. The analysis and prediction of aquifer performance in such situations is normally carried out by numerical simulation on a digital computer.

There are two basic approaches: those that involve a *finite-difference* formulation, and those that involve a *finite-element* formulation. We will look at finite-difference methods in moderate detail, but our treatment of finite-element methods will be very brief.

Finite-Difference Methods

As with the steady-state finite-difference methods that were described in Section 5.3, transient simulation requires a discretization of the continuum that makes up the region of flow. Consider a two-dimensional, horizontal, confined aquifer of constant thickness, b; and let it be discretized into a finite number of blocks, each with its own hydrogeologic properties, and each having a node at the center at which the hydraulic head is defined for the entire block. As shown in Figure 8.26(a), some of these blocks may be the site of pumping wells that are removing water from the aquifer.

Let us now examine the flow regime in one of the interior nodal blocks and its four surrounding neighbors. The equation of continuity for transient, saturated flow states that the net rate of flow into any nodal block must be equal to the time rate of change of storage within the nodal block. With reference to Figure 8.26(b), and following the developments of Section 2.11, we have

$$Q_{15} + Q_{25} + Q_{35} + Q_{45} = S_{s_5}\,\Delta x\,\Delta y\,b\,\frac{\partial h_5}{\partial t} \tag{8.52}$$

where S_{s_5} is the specific storage of nodal block 5. From Darcy's law,

$$Q_{15} = K_{15}\frac{h_1 - h_5}{\Delta y}\,\Delta x\,b \tag{8.53}$$

where K_{15} is a representative hydraulic conductivity between nodes 1 and 5. Similar expressions can be written for Q_{25}, Q_{35}, and Q_{45}.

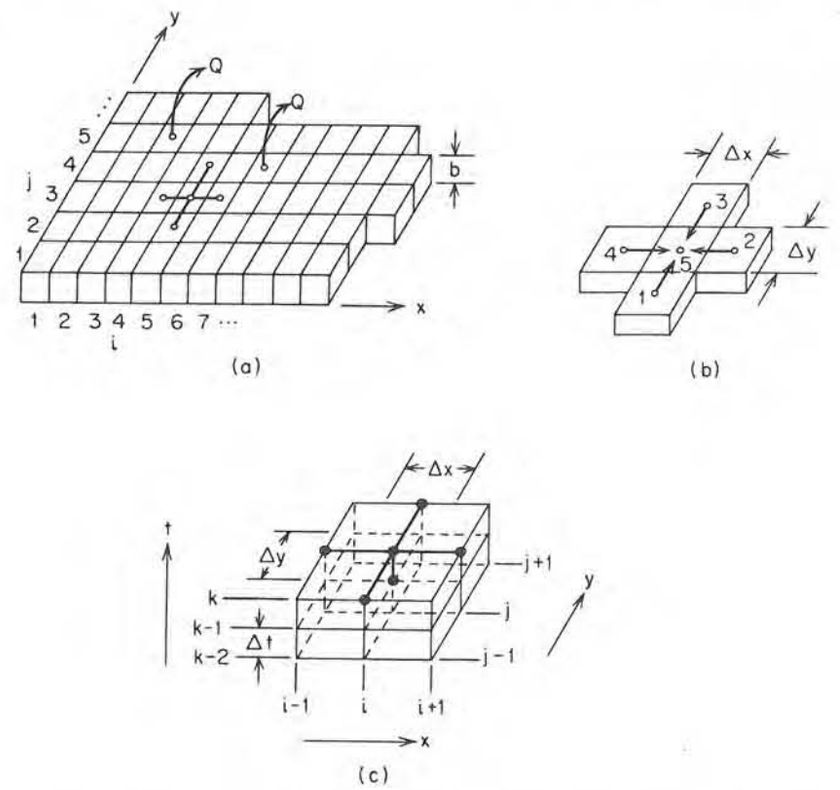

Figure 8.26 Discretization of a two-dimensional, horizontal, confined aquifer.

Let us first consider the case of a homogeneous, isotropic medium for which $K_{15} = K_{25} = K_{35} = K_{45} = K$ and $S_{s_1} = S_{s_2} = S_{s_3} = S_{s_4} = S_s$. If we arbitrarily select a square nodal grid with $\Delta x = \Delta y$, and note that $T = Kb$ and $S = S_s b$, substitution of expressions such as that of Eq. (8.53) into Eq. (8.52) leads to

$$T(h_1 + h_2 + h_3 + h_4 - 4h_5) = S\,\Delta x^2\,\frac{\partial h_5}{\partial t} \tag{8.54}$$

The time derivative on the right-hand side can be approximated by

$$\frac{\partial h_5}{\partial t} = \frac{h_5(t) - h_5(t - \Delta t)}{\Delta t} \tag{8.55}$$

where Δt is the time step that is used to discretize the numerical model in a time-wise sense. If we now convert to the *ijk* notation indicated on Figure 8.26(c), where the subscript (i, j) refers to the nodal position and the superscript $k = 0, 1, 2, \ldots$

indicates the time step, we have

$$h^k_{i,j-1} + h^k_{i+1,j} + h^k_{i-1,j} + h^k_{i,j+1} - 4h^k_{i,j} = \frac{S\,\Delta x^2}{T\,\Delta t}(h^k_{i,j} - h^{k-1}_{i,j}) \tag{8.56}$$

In a more general form,

$$Ah^k_{i,j} = Bh^k_{i,j-1} + Ch^k_{i+1,j} + Dh^k_{i,j+1} + Eh^k_{i-1,j} + F \tag{8.57}$$

where

$$A = \frac{S\,\Delta x^2}{T\,\Delta t} + 4 \tag{8.58}$$

$$B = C = D = E = 1 \tag{8.59}$$

$$F = \frac{S\,\Delta x^2}{T\,\Delta t} \cdot h^{k-1}_{i,j} \tag{8.60}$$

Equation (8.57) is the *finite-difference* equation for an internal node (i, j) in a homogeneous, isotropic, confined aquifer. Each of the parameters S, T, Δx, and Δt that appear in the definitions of the coefficients are known, as is the value of the hydraulic head, $h_{i,j}$, at the previous time step, $k - 1$. In a similar fashion, it is possible to develop finite-difference equations for boundary nodes and corner nodes, and for nodes from which pumping takes place. In each case, the finite-difference equation is similar in form to Eq. (8.57), but the expressions for the coefficients will differ. For boundary nodes, some of the coefficients will be zero. For an internal pumping node, the coefficients A, B, C, D, and E are as given in Eqs. (8.58) and (8.59), but

$$F = \frac{\Delta x^2}{T}\left(\frac{S}{\Delta t} \cdot h^{k-1}_{i,j} + W_{i,j}\right) \tag{8.61}$$

where $W_{i,j}$ is a sink term with units $[L/T]$. W is related to the pumping rate, Q $[L^3/T]$, by

$$W_{i,j} = \frac{Q_{i,j}}{\Delta x^2} \tag{8.62}$$

Sometimes W is given a more general definition,

$$W_{i,j} = \frac{Q_{i,j}}{\Delta x^2} - R_{i,j} \tag{8.63}$$

where $R_{i,j}$ is a source term with units $[L/T]$ that represents vertical leakage into the aquifer from overlying aquitards. In this case Eq. (8.61) is used for all nodes in the system and $W_{i,j}$ is specified for every node. It will be negative for nodes accepting leakage and positive for nodes undergoing pumping.

It is possible to develop Eq. (8.57) in a more rigorous way, starting with the

partial differential equation that describes transient flow in a horizontal confined aquifer. In Appendix IX, the rigorous approach is used to determine the values for the coefficients A, B, C, D, E, and F, in the general finite-difference equation for an internal node in a heterogeneous, anisotropic aquifer. In such a system each node (i, j) may be assigned its own specific values of $S_{i,j}$, $(T_x)_{i,j}$, and $(T_y)_{i,j}$, where T_x and T_y are the principal components of the transmissivity tensor in the x and y coordinate directions. The derivation of Appendix IX is carried out for a rectangular nodal grid in which $\Delta x \neq \Delta y$. A further sophistication, which is not considered there, would allow an irregular nodal grid in which the Δx and Δy values are themselves a function of nodal position. Irregular nodal spacings are often required in the vicinity of pumping wells where hydraulic gradients tend to be large. The concepts that underlie the development of these more complex finite-difference formulations is identical to that which led to Eq. (8.57). The more complex the finite-difference equations embodied in the computer program, the more versatile is that program as a numerical simulator of aquifer performance.

It is possible, then, to develop a finite-difference equation, at some degree of sophistication, for every node in the nodal grid. If there are N nodes, there are N finite-difference equations. At each time step, there are also N unknowns: namely, the N values of $h_{i,j}$ at the N nodes. At each time step, we have N linear, algebraic equations in N unknowns. This set of equations must be solved simultaneously at each time step, starting from a set of initial conditions wherein $h_{i,j}$ is known for all (i, j), and proceeding through the time steps, $k = 1, 2, \ldots$. Many methods are available for the solution of the system of equations, and numerical aquifer models are often classified on the basis of the approach that is used. For example, the method of *successive overrelaxation* that was described in Section 5.3 for the numerical simulation of steady-state flow nets is equally applicable to the system of equations that arises at each time step of a transient aquifer model. More commonly a method known as the *alternating-direction implicit procedure* is used. Remson et al. (1971) and Pinder and Gray (1977) provide a systematic and detailed presentation of these various methods as they pertain to aquifer simulation. Advanced mathematical treatment of the methods is available in the textbook by Forsythe and Wasow (1960). The original development of most numerical-simulation techniques took place in the petroleum engineering field, where the primary application is in the simulation of oil-reservoir behavior. Pinder and Bredehoeft (1968) adapted the powerful alternating-direction implicit procedure to the needs of groundwater hydrologists.

There are two aquifer-simulation programs that have been completely documented and widely applied in North America. One is the U.S. Geological Survey model, which is an outgrowth of Pinder and Bredehoeft's original work. Trescott et al. (1976) provide an updated manual for the most recent version of the computer program. The other is the Illinois State Water Survey model, which is fully documented by Prickett and Lonnquist (1971). Bredehoeft and Pinder (1970) have also shown how a sequence of two-dimensional aquifer models can be coupled together to form a quasi-three-dimensional model of an aquifer-aquitard system.

As a practical example, we will consider the analysis carried out by Pinder and Bredehoeft (1968) for an aquifer at Musquoduboit Harbour, Nova Scotia. The aquifer there is a glaciofluvial deposit of limited areal extent. Figure 8.27(a) shows the initial estimate of the areal distribution of transmissivity for the aquifer as determined from the rather sparse hydrogeological data that were available. Simulations with this transmissivity matrix failed to reproduce the drawdown patterns observed during a pumping test that was run near the center of the aquifer. The aquifer parameters were then adjusted and readjusted over several computer runs until a reasonable duplication was achieved between the measured time-drawdown data and the results of the digital model. Additional test-well logs tended to support the adjusted parameters at several points. The final transmissivity distribution is shown in Figure 8.27(b). The model was then put into prediction mode; Figure 8.27(c) is a plot of the predicted drawdown pattern 206.65 days after the start of exploitation by a proposed production well pumping at a rate of $Q = 0.963\ \text{ft}^3/\text{s}$.

Render (1971, 1972) and Huntoon (1974) provide additional case histories of interest.

Finite-Element Methods

The finite-element method, first noted in Section 5.3 in connection with the simulation of steady-state flow nets, can also be used for the simulation of transient aquifer performance. As in the finite-difference approach, the finite-element approach leads to a set of N algebraic equations in N unknowns at each time step, where the N unknowns are the values of the hydraulic heads at a set of nodal points distributed through the aquifer. The fundamental difference lies in the nature of the nodal grid. The finite-element method allows the design of an irregular mesh that can be hand-tailored to any specific application. The number of nodes can often be significantly reduced from the number required for a finite-difference simulation. The finite-element approach also has some advantages in the way it treats boundary conditions and in the simulation of anisotropic media.

The development of the finite-element equations for each node requires an understanding of both partial differential equations and the calculus of variations. Remson, Hornberger, and Molz (1971) provide an introductory treatment of the method as it applies to aquifer simulation. Pinder and Gray (1977) provide an advanced treatment. Zienkiewicz (1967) and Desai and Abel (1972) are the most widely quoted general reference texts. The finite-element method was introduced into the groundwater literature by Javandel and Witherspoon (1969). Pinder and Frind (1972) were among the first to utilize the method for the prediction of regional aquifer performance. Gupta and Tanji (1976) have reported an application of a three-dimensional finite-element model for the simulation of flow in an aquifer-aquitard system in the Sutter Basin, California.

Model Calibration and the Inverse Problem

If measurements of aquifer transmissivity and storativity were available at every nodal position in an aquifer-simulation model, the prediction of drawdown patterns would be a very straightforward matter. In practice, the data base on which models

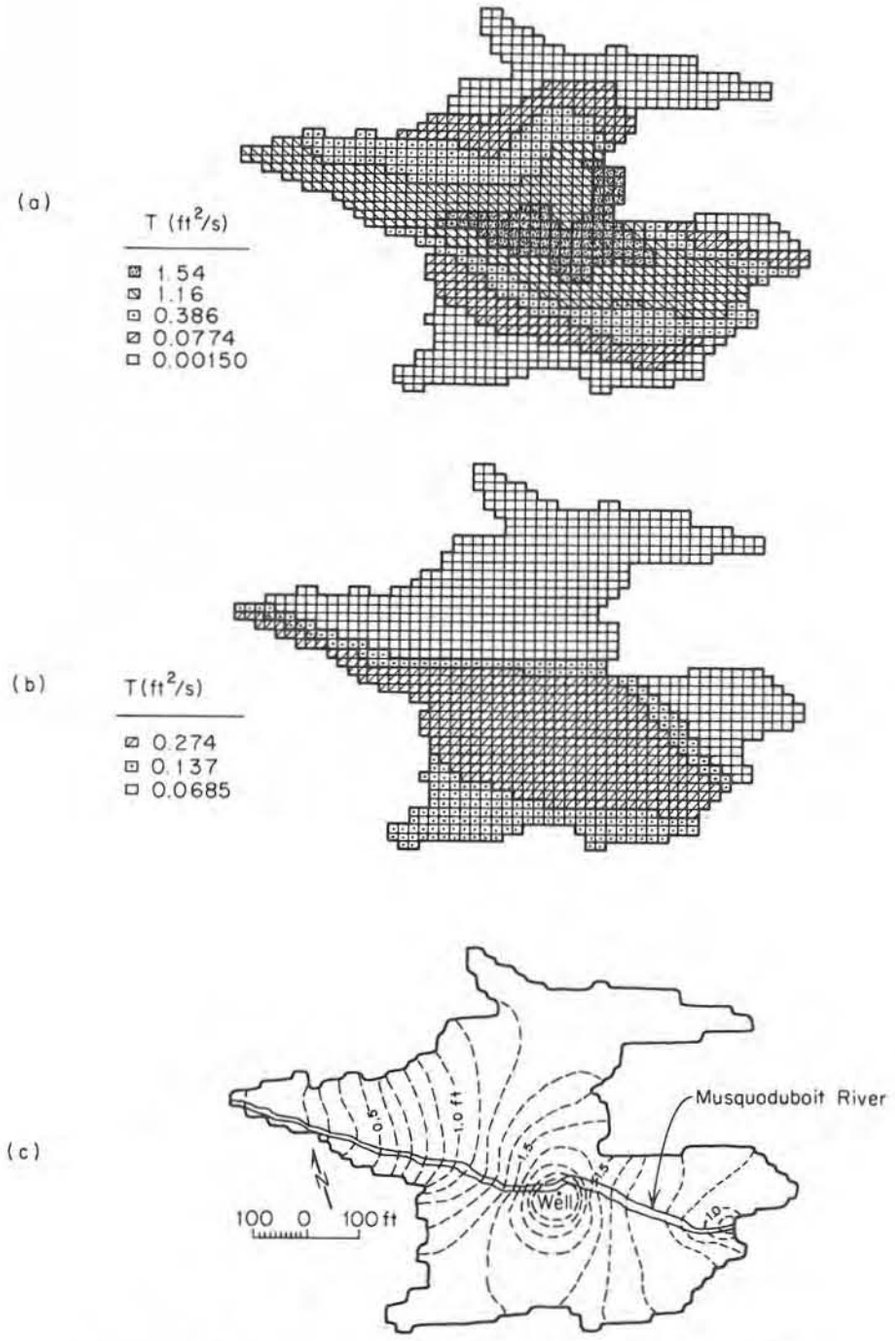

Figure 8.27 Numerical simulation of aquifer performance at Musquoduboit Harbour, Nova Scotia (after Pinder and Bredehoeft, 1968).

must be designed is often very sparse, and it is almost always necessary to calibrate the model against historical records of pumping rates and drawdown patterns. The parameter adjustment procedure that was described in connection with Figure 8.27 represents the calibration phase of the modeling procedure for that particular example. In general, a model should be calibrated against one period of the historical record, then verified against another period of record. The application of a simulation model for a particular aquifer then becomes a three-step process of *calibration*, *verification*, and *prediction*.

Figure 8.28 is a flowchart that clarifies the steps involved in the repetitive trial-and-error approach to calibration. Parameter correction may be carried out on the basis of purely empirical criteria or with a performance analyzer that embodies formal optimization procedures. The contribution by Neuman (1973a) includes a good review and a lengthy reference list. The role of subjective information in establishing the constraints for optimization was treated by Lovell et al. (1972). Gates and Kisiel (1974) considered the question of the worth of additional data. They analyzed the trade-off between the cost of additional measurements and the value they have in improving the calibration of the model.

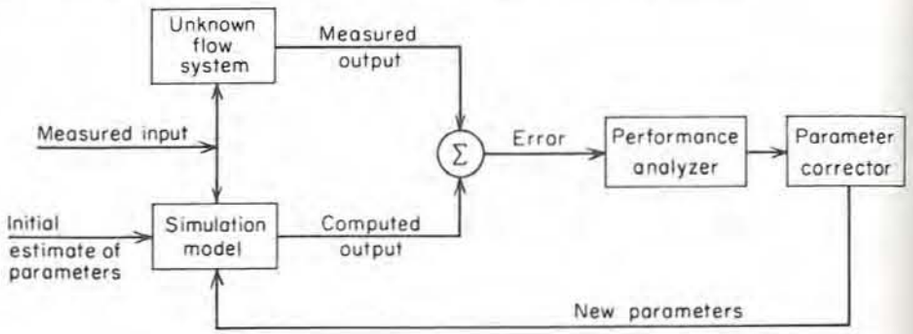

Figure 8.28 Flowchart of the trial-and-error calibration process (after Neuman, 1973a).

The term *calibration* usually refers to the trial-and-error adjustment of aquifer parameters as outlined in Figure 8.28. This approach involves the repetitive application of the aquifer model in its usual mode. In each simulation the boundary-value problem is set up in the usual way with the transmissivity, $T(x, y)$, storativity, $S(x, y)$, leakage, $R(x, y, t)$, and pumpage, $Q(x, y, t)$, known, and the hydraulic head, $h(x, y, t)$, unknown. It is possible to carry out the calibration process more directly by utilizing an aquifer simulation model in the inverse mode. In this case only a single application of the model is required, but the model must be set up as an inverse boundary-value problem where $h(x, y, t)$ and $Q(x, y, t)$ are known and $T(x, y)$, $S(x, y)$, and $R(x, y, t)$ are unknown. When posed in this fashion, the calibration process is known as the *inverse problem*.

In much of the literature, the term *parameter identification* is used to encompass all facets of the problem at hand. What we have called *calibration* is often called

the *indirect* approach to the parameter identification problem, and what we have called the *inverse problem* is called the *direct* approach.

The solution of the inverse formulation is not, in general, unique. In the first place there may be too many unknowns; and in the second place, $h(x, y, t)$ and $Q(x, y, t)$ are not known for all (x, y). In practice, pumpage takes place at a finite number of points, and the historical records of head are available at only a finite number of points. Even if $R(x, y, t)$ is assumed constant or known, the problem remains ill-posed mathematically. Emsellem and de Marsily (1971) have shown, however, that the problem can be made tractable by using a "flatness criteria" that limits the allowable spatial variations in T and S. The mathematics of their approach is not simple, but their paper remains the classic discussion of the inverse problem. Neuman (1973a, 1975b) suggests using available measurements of T and S to impose constraints on the structure of $T(x, y)$ and $S(x, y)$ distributions. The contributions of Yeh (1975) and Sagar (1975) include reviews of more recent developments.

There is another approach to inverse simulation that is simpler in concept but apparently open to question as to its validity (Neuman, 1975b). It is based on the assumption of steady-state conditions in the flow system. As first recognized by Stallman (1956), the steady-state hydraulic head pattern, $h(x, y, z)$ in a three-dimensional system can be interpreted inversely in terms of the hydraulic conductivity distribution, $K(x, y, z)$. In a two-dimensional, unpumped aquifer, $h(x, y)$ can be used to determine $T(x, y)$. Nelson (1968) showed that the necessary condition for the existence and uniqueness of a solution to the steady-state inverse problem is that, in addition to the hydraulic heads, the hydraulic conductivity or transmissivity must be known along a surface crossed by all streamlines in the system. Frind and Pinder (1973) have pointed out that, since transmissivity and flux are related by Darcy's law, this criterion can be stated alternatively in terms of the flux that crosses a surface. If water is being removed from an aquifer at a steady pumping rate, the surface to which Nelson refers occurs around the circumference of the well and the well discharge alone provides a sufficient boundary condition for a unique solution. Frind and Pinder (1973) utilized a finite-element model to solve the steady-state inverse problem. Research is continuing on the question of what errors are introduced into the inverse solution when a steady-state approach is used for model calibration for an aquifer that has undergone a transient historical development.

8.9 Prediction of Aquifer Yield by Analog Simulation

Numerical simulation of aquifer performance requires a moderately large computer and relatively sophisticated programming expertise. Electric-analog simulation provides an alternative approach that circumvents these requirements at the expense of a certain degree of versatility.

Analogy Between Electrical Flow and Groundwater Flow

The principles underlying the physical and mathematical analogy between electrical flow and groundwater flow were introduced in Section 5.2. The application under discussion was the simulation of steady-state flow nets in two-dimensional vertical cross sections. One of the methods described there utilized a *resistance-network* analog that was capable of handling heterogeneous systems of irregular shape. In this section, we will pursue analog methods further, by considering the application of two-dimensional *resistance-capacitance networks* for the prediction of transient hydraulic-head declines in heterogeneous, confined aquifers of irregular shape.

Consider a horizontal confined aquifer of thickness b. If it is overlaid with a square grid of spacing, Δx_A [as in Figure 8.26(a)], any small homogeneous portion of the discretized aquifer [Figure 8.29(a)] can be modeled by a scaled-down array of electrical resistors and capacitors on a square grid of spacing, Δx_M [Figure 8.29(b)]. The analogy between electrical flow in the resistance-capacitance network and groundwater flow in the horizontal confined aquifer can be revealed by examining the finite-difference form of the equations of flow for each system. For groundwater flow, from Eq. (8.54),

$$T(h_1 + h_2 + h_3 + h_4 - 4h_5) = S\,\Delta x_A^2 \frac{\partial h_5}{\partial t_A} \tag{8.64}$$

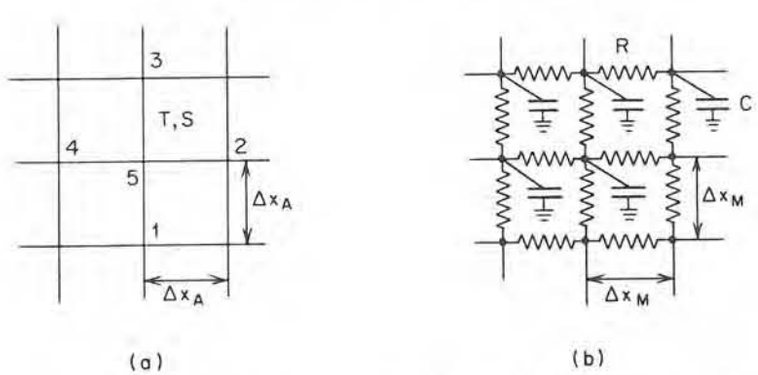

Figure 8.29 Small homogeneous portion of discretized aquifer and analogous resistor-capacitor network (after Prickett, 1975).

For the electrical circuit, from Kirchhoff's laws:

$$\frac{1}{R}(V_1 + V_2 + V_3 + V_4 - 4V_5) = C\frac{\partial V_5}{\partial t_M} \tag{8.65}$$

Comparison of Eqs. (8.64) and (8.65) leads to the analogous quantities:

1. Hydraulic head, h; and voltage, V.
2. Transmissivity, T; and the reciprocal of the resistance, R, of the resistors.

3. The product of the storativity, S, times the nodal block area, Δx_A^2; and the capacitance, C, of the capacitors.
4. Aquifer coordinates, x_A and y_A (as determined by the spacing, Δx_A); and model coordinates, x_M and y_M (as determined by the spacing, Δx_M).
5. Real time, t_A; and model time, t_M.

In addition, if pumpage is considered, there is an analogy between:

6. Pumping rate, Q, at a well; and current strength, I, at an electrical source.

Resistance-Capacitance Network

The network of resistors and capacitors that constitutes the analog model is usually mounted on a Masonite pegboard perforated with holes on approximately 1-inch centers. There are four resistors and one capacitor connected to each terminal. The resistor network is often mounted on the front of the board, and the capacitor network, with each capacitor connected to a common ground, on the back. The boundary of the network is designed in a stepwise fashion to approximate the shape of the actual boundary of the aquifer.

The design of the components of the analog requires the choice of a set of scale factors, F_1, F_2, F_3, and F_4, such that

$$F_1 = \frac{h}{V} \tag{8.66}$$

$$F_2 = \frac{\Delta x_A}{\Delta x_M} \tag{8.67}$$

$$F_3 = \frac{t_A}{t_M} \tag{8.68}$$

$$F_4 = \frac{Q}{I} \tag{8.69}$$

Heterogeneous and transversely anisotropic aquifers can be simulated by choosing resistors and capacitors that match the transmissivity and storativity at each point in the aquifer. Comparison of the hydraulic flow through an aquifer section and the electrical flow through an analogous resistor [Figure 8.30(a)] leads to the relation

$$R = \frac{F_4}{F_1 T} \tag{8.70}$$

Comparison of the storage in an aquifer section and the electrical capacitance of an analogous capacitor [Figure 8.30(b)] leads to the relation

$$C = \frac{F_1 S\,\Delta x_A^2}{F_4 F_3} \tag{8.71}$$

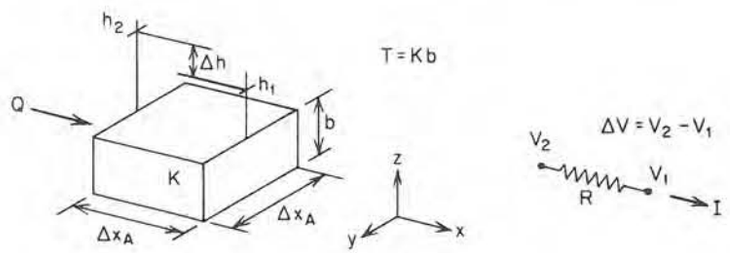

(a)

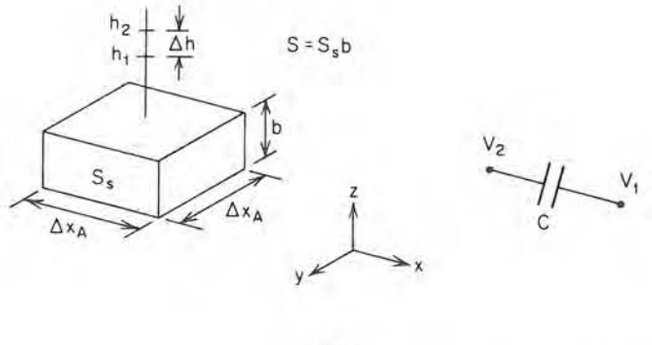

(b)

Figure 8.30 Aquifer nodal block and analogous (a) resistor and (b) capacitor (after Prickett, 1975).

The resistors and capacitors that make up the network are chosen on the basis of Eqs. (8.70) and (8.71). The scale factors, F_1, F_2, F_3, and F_4, must be selected in such a way that (1) the resistors and capacitors fall within the range of inexpensive, commercially available components; (2) the size of the model is practical; and (3) the response times of the model are within the range of available excitation-response equipment.

Figure 8.31 is a schematic diagram that shows the arrangement of excitation-response apparatus necessary for electric-analog simulation using a resistance-capacitance network. The pulse generator, in tandem with a waveform generator, produces a rectangular pulse of specific duration and amplitude. This input pulse is displayed on channel 1 of a dual-channel oscilloscope as it is fed through a resistance box to the specific terminal of the resistance-capacitance network that represents the pumped well. The second channel on the oscilloscope is used to display the time-voltage response obtained by probing various observation points in the network. The input pulse is analogous to a step-function increase in pumping rate; the time-voltage graph is analogous to a time-drawdown record at an observational piezometer. The numerical value of the head drawdown is calculated from the

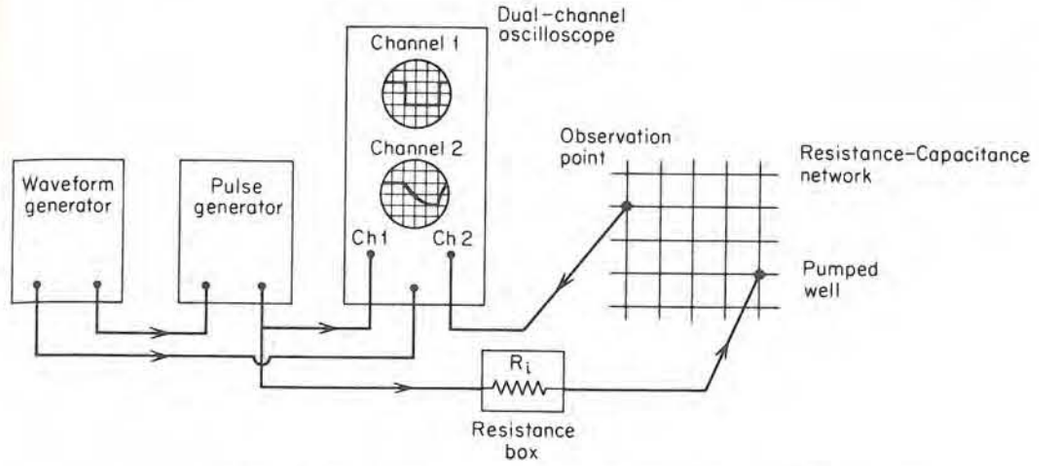

Figure 8.31 Excitation-response apparatus for electrical-analog simulation using a resistance-capacitance network.

voltage drawdown by Eq. (8.66). The time at which any specific drawdown applies is given by Eq. (8.68). Any pumping rate, Q, may be simulated by setting the current strength, I, in Eq. (8.69). This is done by controlling the resistance, R_i, of the resistance box in Figure 8.31. The current strength is given by $I = V_i/R_i$, where V_i is the voltage drop across the resistance box.

Walton (1970) and Prickett (1975) provide detailed coverage of the electric-analog approach to aquifer simulation. Most groundwater treatments owe much to the general discussion of analog simulation by Karplus (1958). Results of analog simulation are usually presented in the form of maps of predicted water-level drawdowns similar to that shown in Figure 8.27(c). Patten (1965), Moore and Wood (1967), Spieker (1968), and Render (1971) provide case histories that document the application of analog simulation to specific aquifers.

Comparison of Analog and Digital Simulation

Prickett and Lonnquist (1968) have discussed the advantages, disadvantages, and similarities between analog and digital techniques of aquifer simulation. They note that both methods use the same basic field data, and the same method of assigning hydrogeologic properties to a discretized representation of the aquifer. Analog simulation requires knowledge of specialized electronic equipment; digital simulation requires expertise in computer programming. Digital simulation is more flexible in its ability to handle irregular boundaries and pumping schemes that vary through time and space. It is also better suited to efficient data readout and display.

The physical construction involved in the preparation of a resistance-capacitance network is both the strength and the weakness of the analog method. The

fact that the variables of the system under study are represented by analogous physical quantities and pieces of equipment is extremely valuable for the purposes of teaching or display, but the cost in time is large. The network, once built, describes only one specific aquifer. In digital modeling, on the other hand, once a general computer program has been prepared, data decks representing a wide variety of aquifers and aquifer conditions can be run with the same program. The effort involved in designing and keypunching a new data deck is much less than that involved in designing and building a new resistance-capacitance network. This flexibility is equally important during the calibration phase of aquifer simulation.

The advantages of digital simulation weigh heavily in its favor, and with the advent of easy accessibility to large computers, the method is rapidly becoming the standard tool for aquifer management. However, analog simulation will undoubtedly continue to play a role for some time, especially in developing countries where computer capacities are not yet large.

8.10 Basin Yield

Safe Yield and Optimal Yield of a Groundwater Basin

Groundwater yield is best viewed in the context of the full three-dimensional hydrogeologic system that constitutes a groundwater basin. On this scale of study we can turn to the well-established concept of *safe yield* or to the more rigorous concept of *optimal yield.*

Todd (1959) defines the *safe yield* of a groundwater basin as the amount of water that can be withdrawn from it annually without producing an undesired result. Any withdrawal in excess of safe yield is an *overdraft.* Domenico (1972) and Kazmann (1972) review the evolution of the term. Domenico notes that the "undesired results" mentioned in the definition are now recognized to include not only the depletion of the groundwater reserves, but also the intrusion of water of undesirable quality, the contravention of existing water rights, and the deterioration of the economic advantages of pumping. One might also include excessive depletion of streamflow by induced infiltration and land subsidence.

Although the concept of safe yield has been widely used in groundwater resource evaluation, there has always been widespread dissatisfaction with it (Thomas, 1951; Kazmann, 1956). Most suggestions for improvement have encouraged consideration of the yield concept in a socioeconomic sense within the overall framework of optimization theory. Domenico (1972) reviews the development of this approach, citing the contributions of Bear and Levin (1967), Buras (1966), Burt (1967), Domenico et al. (1968), and others. From an optimization viewpoint, groundwater has value only by virtue of its use, and the *optimal yield* must be determined by the selection of the optimal groundwater management scheme from a set of possible alternative schemes. The optimal scheme is the one that best meets

a set of economic and/or social objectives associated with the uses to which the water is to be put. In some cases and at some points in time, consideration of the present and future costs and benefits may lead to optimal yields that involve mining groundwater, perhaps even to depletion. In other situations, optimal yields may reflect the need for complete conservation. Most often, the optimal groundwater development lies somewhere between these extremes.

The graphical and mathematical methods of optimization, as they relate to groundwater development, are reviewed by Domenico (1972).

Transient Hydrologic Budgets and Basin Yield

In Section 6.2 we examined the role of the average annual groundwater recharge, R, as a component in the steady-state hydrologic budget for a watershed. The value of R was determined from a quantitative interpretation of the steady-state, regional, groundwater flow net. Some authors have suggested that the safe yield of a groundwater basin be defined as the annual extraction of water that does not exceed the average annual groundwater recharge. This concept is not correct. As pointed out by Bredehoeft and Young (1970), major groundwater development may significantly change the recharge-discharge regime as a function of time. Clearly, the basin yield depends both on the manner in which the effects of withdrawal are transmitted through the aquifers *and* on the changes in rates of groundwater recharge and discharge induced by the withdrawals. In the form of a transient hydrologic budget for the saturated portion of a groundwater basin,

$$Q(t) = R(t) - D(t) + \frac{dS}{dt} \tag{8.72}$$

where $Q(t)$ = total rate of groundwater withdrawal
$R(t)$ = total rate of groundwater recharge to the basin
$D(t)$ = total rate of groundwater discharge from the basin
dS/dt = rate of change of storage in the saturated zone of the basin.

Freeze (1971a) examined the response of $R(t)$ and $D(t)$ to an increase in $Q(t)$ in a hypothetical basin in a humid climate where water tables are near the surface. The response was simulated with the aid of a three-dimensional transient analysis of a complete saturated-unsaturated system such as that of Figure 6.10 with a pumping well added. Figure 8.32 is a schematic representation of his findings. The diagrams show the time-dependent changes that might be expected in the various terms of Eq. (8.72) under increased pumpage. Let us first look at the case shown in Figure 8.32(a), in which withdrawals increase with time but do not become excessive. The initial condition at time t_0 is a steady-state flow system in which the recharge, R_0, equals the discharge, D_0. At times t_1, t_2, t_3, and t_4, new wells begin to tap the system and the pumping rate Q undergoes a set of stepped increases. Each increase is initially balanced by a change in storage, which in an unconfined aquifer takes the form of an immediate water-table decline. At the

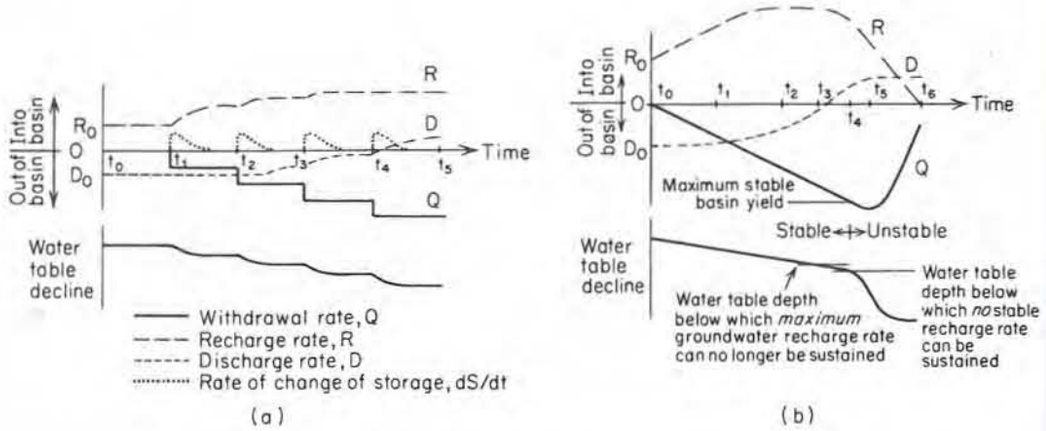

Figure 8.32 Schematic diagram of transient relationships between recharge rates, discharge rates, and withdrawal rates (after Freeze, 1971a).

same time, the basin strives to set up a new equilibrium under conditions of increased recharge, R. The unsaturated zone will now be induced to deliver greater flow rates to the water table under the influence of higher gradients in the saturated zone. Concurrently, the increased pumpage may lead to decreased discharge rates, D. In Figure 8.32(a), after time t_4, all natural discharge ceases and the discharge curve rises above the horizontal axis, implying the presence of induced recharge from a stream that had previously been accepting its baseflow component from the groundwater system. At time t_5, the withdrawal Q is being fed by the recharge, R, and the induced recharge, D; and there has been a significant decline in the water table. Note that the recharge rate attains a maximum between t_3 and t_4. At this rate, the groundwater body is accepting all the infiltration that is available from the unsaturated zone under the lowered water-table conditions.

In Figure 8.32(a), steady-state equilibrium conditions are reached prior to each new increase in withdrawal rate. Figure 8.32(b) shows the same sequence of events under conditions of continuously increasing groundwater development over several years. This diagram also shows that if pumping rates are allowed to increase indefinitely, an unstable situation may arise where the declining water table reaches a depth below which the *maximum* rate of groundwater recharge R can no longer be sustained. After this point in time the same annual precipitation rate no longer provides the same percentage of infiltration to the water table. Evapotranspiration during soil-moisture-redistribution periods now takes more of the infiltrated rainfall before it has a chance to percolate down to the groundwater zone. At t_4 in Figure 8.32(b), the water table reaches a depth below which *no* stable recharge rate can be maintained. At t_5 the maximum available rate of *induced* recharge is attained. From time t_5 on, it is impossible for the basin to supply increased rates of withdrawal. The only source lies in an increased rate of change of storage that manifests itself in rapidly declining water tables. Pumping rates can

no longer be maintained at their original levels. Freeze (1971a) defines the value of Q at which instability occurs as the *maximum stable basin yield*. To develop a basin to its limit of stability would, of course, be foolhardy. One dry year might cause an irrecoverable water-table drop. Production rates must allow for a factor of safety and must therefore be somewhat less than the maximum stable basin yield.

The discussion above emphasizes once again the important interrelationships between groundwater flow and surface runoff. If a groundwater basin were developed up to its maximum yield, the potential yields of surface-water components of the hydrologic cycle in the basin would be reduced. It is now widely recognized that optimal development of the water resources of a watershed depend on the *conjunctive use* of surface water and groundwater. The subject has provided a fertile field for the application of optimization techniques (Maddock, 1974; Yu and Haimes, 1974). Young and Bredehoeft (1972) describe the application of digital computer simulations of the type described in Section 8.8 to the solution of management problems involving conjunctive groundwater and surface-water systems.

8.11 Artificial Recharge and Induced Infiltration

In recent years, particularly in the more populated areas of North America where water resource development has approached or exceeded available yield, there has been considerable effort placed on the management of water resource systems. Optimal development usually involves the conjunctive use of groundwater and surface water and the reclamation and reuse of some portion of the available water resources. In many cases, it involves the importation of surface water from areas of plenty to areas of scarcity, or the conservation of surface water in times of plenty for use in times of scarcity. These two approaches require storage facilities, and there is often advantage to storing water underground where evaporation losses are minimized. Underground storage may also serve to replenish groundwater resources in areas of overdraft.

Any process by which man fosters the transfer of surface water into the groundwater system can be classified as *artificial recharge*. The most common method involves infiltration from spreading basins into high-permeability, unconfined, alluvial aquifers. In many cases, the spreading basins are formed by the construction of dikes in natural channels. The recharge process involves the growth of a *groundwater mound* beneath the spreading basin. The areal extent of the mound and its rate of growth depend on the size and shape of the recharging basin, the duration and rate of recharge, the stratigraphic configuration of subsurface formations, and the saturated and unsaturated hydraulic properties of the geologic materials. Figure 8.33 shows two simple hydrogeological environments and the type of groundwater mound that would be produced in each case beneath a circular spreading basin. In Figure 8.33(a), recharge takes place into a horizontal unconfined aquifer bounded at the base by an impermeable formation. In Figure 8.33(b),

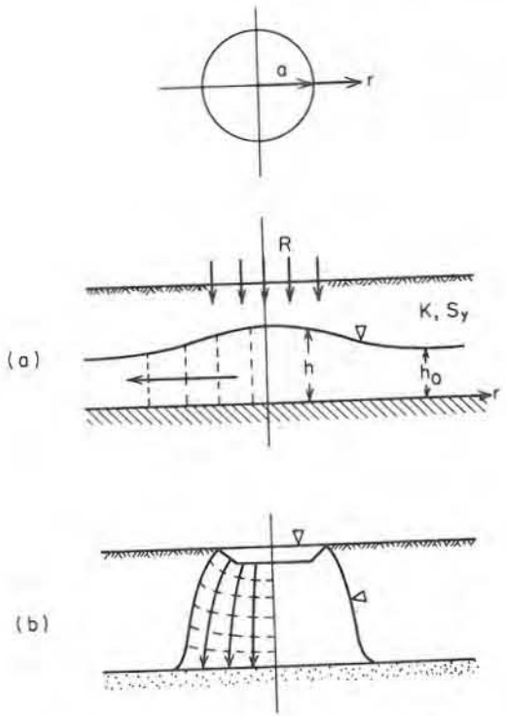

Figure 8.33 Growth of a groundwater mound beneath a circular recharge basin.

recharge takes place through a less-permeable formation toward a high-permeability layer at depth.

Both cases have been the subject of a large number of predictive analyses, not only for circular spreading basins but also for rectangular basins and for recharge from an infinitely long strip. The latter case, with boundary conditions like those shown in Figure 8.33(b), also has application to canal and river seepage. It has been studied in this context by Bouwer (1965), Jeppson (1968), and Jeppson and Nelson (1970). The case shown in Figure 8.33(a), which also has application to the development of mounds beneath waste disposal ponds and sanitary landfills, has been studied in even greater detail. Hantush (1967) provides an analytical solution for the prediction of $h(r, t)$, given the initial water-table height, h_0, the diameter of the spreading basin, a, the recharge rate, R, and the hydraulic conductivity and specific yield, K and S_y, of the unconfined aquifer. His solution is limited to homogeneous, isotropic aquifers and a recharge rate that is constant in time and space. In addition, the solution is limited to a water-table rise that is less than or equal to 50% of the initial depth of saturation, h_0. This requirement implies that $R \ll K$. Bouwer (1962) utilized an electric-analog model to analyze the same problem, and Marino (1975a, 1975b) produced a numerical simulation. All three of these analyses have two additional limitations. First, they neglect unsaturated flow by assuming that the recharge pulse traverses the unsaturated zone vertically and reaches the water table unaffected by soil moisture-conditions above the water table. Second, they utilize the Dupuit-Forchheimer theory of unconfined flow (Section 5.5) which neglects any vertical flow gradients that develop in the saturated zone in the vicinity of the mound. Numerical simulations carried out on the complete saturated-unsaturated system using the approaches of Rubin (1968), Jeppson and Nelson (1970), and Freeze (1971a) would provide a more accurate approach to the problem, but at the expense of added complexity in the calculations.

Practical research on spreading basins has shown that the niceties of predictive analysis are seldom reflected in the real world. Even if water levels in spreading ponds are kept relatively constant, the recharge rate almost invariably declines with time as a result of the buildup of silt and clay on the basin floor and the growth of microbial organisms that clog the soil pores. In addition, air entrapment between the wetting front and the water table retards recharge rates. Todd (1959) notes that alternating wet and dry periods generally furnish a greater total recharge than does continuous spreading. Drying kills the microbial growths, and tilling and scraping of the basin floor during dry periods reopens the soil pores.

There are several excellent case histories that provide an account of specific projects involving artificial recharge from spreading basins. Seaburn (1970) describes hydrologic studies carried out at two of the more than 2000 recharge basins that are used on Long Island, east of New York City, to provide artificial recharge of storm runoff from residential and industrial areas. Bianchi and Haskell (1966, 1968) describe the piezometric monitoring of a complete recharge cycle of mound growth and dissipation. They report relatively good agreement between the field data and analytical predictions based on Dupuit-Forchheimer theory. They note, however, that the anomalous water-level rises that accompany air entrapment (Section 6.8) often make it difficult to accurately monitor the growth of the groundwater mound.

While water spreading is the most ubiquitous form of artificial recharge, it is limited to locations with favorable geologic conditions at the surface. There have also been some attempts made to recharge deeper formations by means of injection wells. Todd (1959) provides several case histories involving such diverse applications as the disposal of storm-runoff water, the recirculation of air-conditioning water, and the buildup of a freshwater barrier to prevent further intrusion of seawater into a confined aquifer. Most of the more recent research on deep-well injection has centered on utilization of the method for the disposal of industrial wastewater and tertiary-treated municipal wastewater (Chapter 9) rather than for the replenishment of groundwater resources.

The oldest and most widely used method of conjunctive use of surface water and groundwater is based on the concept of *induced infiltration*. If a well produces water from alluvial sands and gravels that are in hydraulic connection with a

stream, the stream will act as a constant-head line source in the manner noted in Figures 8.15(d) and 8.23(d). When a new well starts to pump in such a situation, the pumped water is initially derived from the groundwater zone, but once the cone of depression reaches the stream, the source of some of the pumped water will be streamflow that is induced into the groundwater body under the influence of the gradients set up by the well. In due course, steady-state conditions will be reached, after which time the cone of depression and the drawdowns within it remain constant. Under the steady flow system that develops at such times, the source of all the pumped groundwater is streamflow. One of the primary advantages of induced infiltration schemes over direct surface-water utilization lies in the chemical and biological purification afforded by the passage of stream water through the alluvial deposits.

8.12 Land Subsidence

In recent years it has become apparent that the extensive exploitation of groundwater resources in this century has brought with it an undesired environmental side effect. At many localities in the world, groundwater pumpage from unconsolidated aquifer-aquitard systems has been accompanied by significant land subsidence. Poland and Davis (1969) and Poland (1972) provide descriptive summaries of all the well-documented cases of major land subsidence caused by the withdrawal of fluids. They present several case histories where subsidence has been associated with oil and gas production, together with a large number of cases that involve groundwater pumpage. There are three cases–the Wilmington oil field in Long Beach, California, and the groundwater overdrafts in Mexico City, Mexico, and in the San Joaquin valley, California–that have led to rates of subsidence of the land surface of almost 1 m every 3 years over the 35-year period 1935–1970. In the San Joaquin valley, where groundwater pumpage for irrigation purposes is to blame, there are three separate areas with significant subsidence problems. Taken together, there is a total area of 11,000 km² that has subsided more than 0.3 m. At Long Beach, where the subsiding region is adjacent to the ocean, subsidence has resulted in repeated flooding of the harbor area. Failure of surface structures, buckling of pipe lines, and rupturing of oil-well casing have been reported. Remedial costs up to 1962 exeeded $100 million.

Mechanism of Land Subsidence

The depositional environments at the various subsidence sites are varied, but there is one feature that is common to all the groundwater-induced sites. In each case there is a thick sequence of unconsolidated or poorly consolidated sediments forming an interbedded aquifer-aquitard system. Pumpage is from sand and gravel aquifers, but a large percentage of the section consists of high-compressibility clays. In earlier chapters we learned that groundwater pumpage is accompanied by vertical leakage from the adjacent aquitards. It should come as no surprise to find

that the process of aquitard drainage leads to compaction* of the aquitards just as the process of aquifer drainage leads to compaction of the aquifers. There are two fundamental differences, however: (1) since the compressibility of clay is 1–2 orders of magnitude *greater* than the compressibility of sand, the total potential compaction of an aquitard is much greater than that for an aquifer; and (2) since the hydraulic conductivity of clay may be several orders of magnitude *less* than the hydraulic conductivity of sand, the drainage process, and hence the compaction process, is much slower in aquitards than in aquifers.

Consider the vertical cross section shown in Figure 8.34. A well pumping at

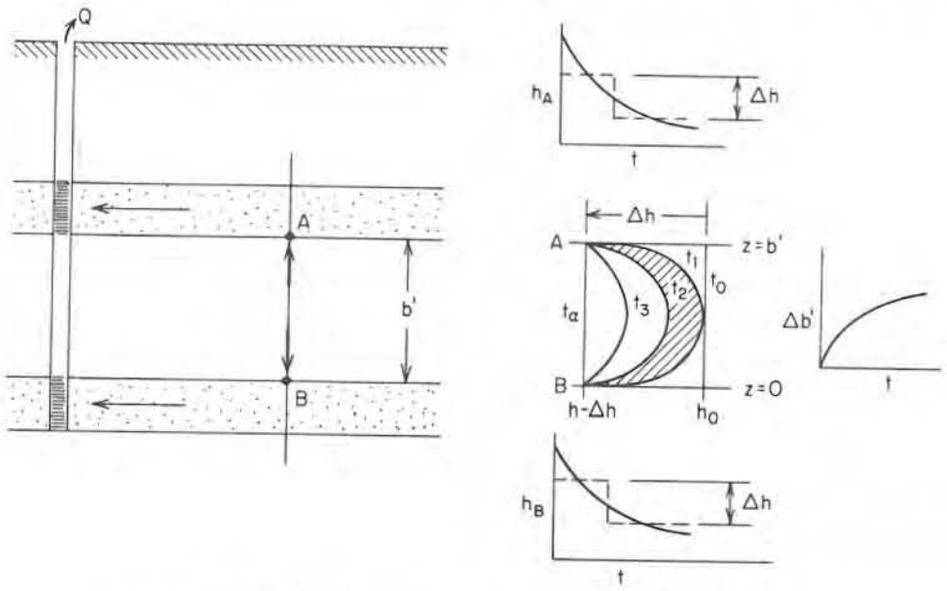

Figure 8.34 One-dimensional consolidation of an aquitard.

a rate Q is fed by two aquifers separated by an aquitard of thickness b. Let us assume that the geometry is radially symmetric and that the transmissivities in the two aquifers are identical. The time-dependent reductions in hydraulic head in the aquifers (which could be predicted from leaky-aquifer theory) will be identical at points A and B. We wish to look at the hydraulic-head reductions in the aquitard along the line AB under the influence of the head reductions in the aquifers at A and B. If $h_A(t)$ and $h_B(t)$ are approximated by step functions with a step Δh (Figure 8.34), the aquitard drainage process can be viewed as the one-dimensional, transient boundary-value problem described in Section 8.3 and presented as Eq. (8.21). The initial condition is $h = h_0$ all along AB, and the boundary conditions are

*Following Poland and Davis (1969), we are using the term "compaction" in its geological sense. In engineering jargon the term is often reserved for the increase in soil density achieved through the use of rollers, vibrators or other heavy machinery.

$h = h_0 - \Delta h$ at A and at B for all $t > 0$. A solution to this boundary-value problem was obtained by Terzaghi (1925) in the form of an analytical expression for $h(z, t)$. An accurate graphical presentation of his solution appears as Figure 8.17. The central diagram on the right-hand side of Figure 8.34 is a schematic plot of his solution; it shows the time-dependent decline in hydraulic head at times $t_0, t_1, \ldots, t_\infty$ along the line AB. To obtain quantitative results for a particular case, one must know the thickness b', the vertical hydraulic conductivity K', the vertical compressibility α', and the porosity n' of the aquitard, together with the head reduction Δh on the boundaries.

In soil mechanics the compaction process associated with the drainage of a clay layer is known as *consolidation*. Geotechnical engineers have long recognized that for most clays $\alpha \gg n\beta$, so the latter term is usually omitted from Eq. (8.21). The remaining parameters are often grouped into a single parameter c_v, defined by

$$c_v = \frac{K'}{\rho g \alpha'} \tag{8.73}$$

The hydraulic head $h(z, t)$ can be calculated from Figure 8.17 with the aid of Eq. (8.23) given c_v, Δh, and b.

In order to calculate the compaction of the aquitard given the hydraulic head declines at each point on AB as a function of time, it is necessary to recall the effective stress law: $\sigma_T = \sigma_e + p$. For $\sigma_T =$ constant, $d\sigma_e = -dp$. In the aquitard, the head reduction at any point z between the times t_1 and t_2 (Figure 8.34) is $dh = h_1(z, t_1) - h_2(z, t_2)$. This head drop creates a fluid pressure reduction: $dp = \rho g\, d\psi = \rho g\, d(h - z) = \rho g\, dh$, and the fluid pressure reduction is reflected by an increase in the effective stress $d\sigma_e = -dp$. It is the change in effective stress, acting through the aquitard compressibility α', that causes the aquitard compaction $\Delta b'$. To calculate $\Delta b'$ along AB between the times t_1 and t_2, it is necessary to divide the aquitard into m slices. Then, from Eq. (2.54),

$$\Delta b'_{t_1 - t_2} = b' \sum_{i=1}^{m} \rho g \alpha'\, dh_i \tag{8.74}$$

where dh_i is the average head decline in the ith slice.

For a multiaquifer system with several pumping wells, the land subsidence as a function of time is the summation of all the aquitard and aquifer compactions. A complete treatment of consolidation theory appears in most soil mechanics texts (Terzaghi and Peck, 1967; Scott, 1963). Domenico and Mifflin (1965) were the first to apply these solutions to cases of land subsidence.

It is reasonable to ask whether land subsidence can be arrested by injecting groundwater back into the system. In principle this should increase the hydraulic heads in the aquifers, drive water back into the aquitards, and cause an expansion of both aquifer and aquitard. In practice, this approach is not particularly effective because aquitard compressibilities in expansion have only about one-tenth the value they have in compression. The most successful documented injection

scheme is the one undertaken at the Wilmington oil field in Long Beach, California (Poland and Davis, 1969). Repressuring of the oil reservoir was initiated in 1958 and by 1963 there had been a modest rebound in a portion of the subsiding region and the rates of subsidence were reduced elsewhere.

Field Measurement of Land Subsidence

If there are any doubts about the aquitard-compaction theory of land subsidence, they should be laid to rest by an examination of the results of the U.S. Geological Survey subsidence research group during the last decade. They have carried out field studies in several subsiding areas in California, and their measurements provide indisputable confirmation of the interrelationships between hydraulic head declines, aquitard compaction, and land subsidence.

Figure 8.35 is a contoured map, based on geodetic measurements, of the land subsidence in the Santa Clara valley during the period 1934–1960. Subsidence is

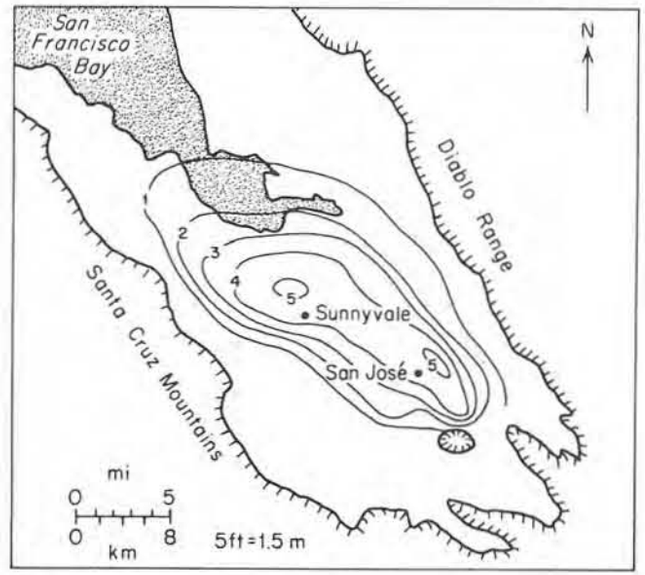

Figure 8.35 Land subsidence in feet, 1934–1960, Santa Clara valley, California (after Poland and Davis, 1969).

confined to the area underlain by unconsolidated deposits of alluvial and shallow-marine origin. The centers of subsidence coincide with the centers of major pumping, and the historical development of the subsidence coincides with the period of settlement in the valley and with the increased utilization of groundwater.

Quantitative confirmation of the theory is provided by results of the type shown in Figure 8.36. An ingeniously simple compaction-recorder installation [Figure 8.36(a)] produces a graph of the time-dependent growth of the total

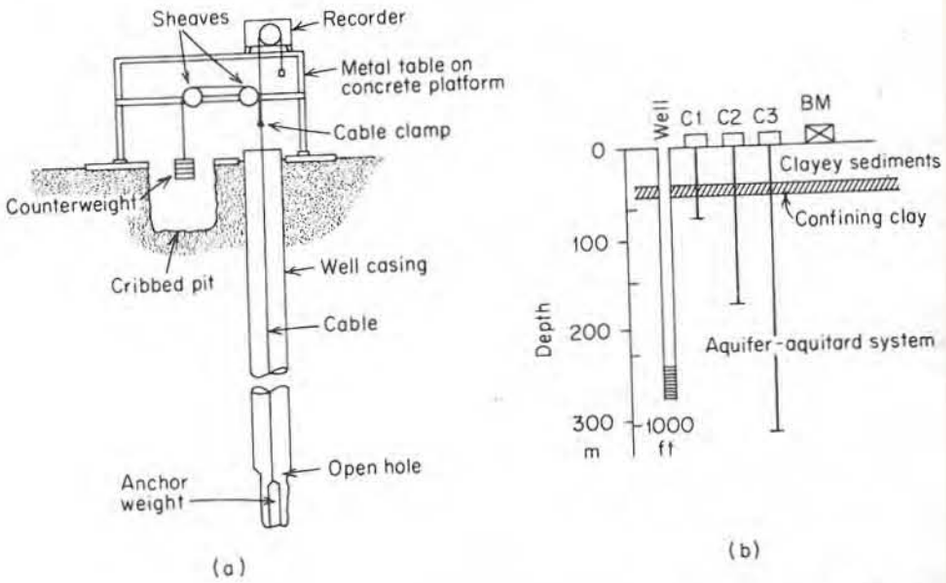

Figure 8.36 (a) Compaction-recorder installation; (b) compaction measurement site near Sunnyvale, California; (c) measured compactions, land subsidence, and hydraulic head variations at the Sunnyvale site, 1960–1962 (after Poland and Davis, 1969).

compaction of all material between the land surface and the bottom of the hole. Near Sunnyvale in the Santa Clara valley, three compaction recorders were established at different depths in the confined aquifer system that exists there [Figure 8.36(b)]. Figure 8.36(c) shows the compaction records together with the total land subsidence as measured at a nearby benchmark, and the hydraulic head for the 250- to 300-m-depth range as measured in an observation well at the measurement site. Decreasing hydraulic heads are accompanied by compaction. Increasing hydraulic heads are accompanied by reductions in the rate of compaction, but there is no evidence of rebound. At this site "the land subsidence is demonstrated to be equal to the compaction of the water-bearing deposits within the depth tapped by water wells, and the decline in artesian head is proved to be the sole cause of the subsidence" (Poland and Davis, 1969, p. 259).

Riley (1969) noted that data of the type shown on Figure 8.36(c) can be viewed as the result of a large-scale field consolidation test. If the reductions in aquitard volume reflected by the land subsidence are plotted against the changes in effective stress created by the hydraulic-head declines, it is often possible to calculate the average compressibility and the average vertical hydraulic conductivity of the aquitards. Helm (1975, 1976) has carried these concepts forward in his numerical models of land subsidence in California.

It is also possible to develop predictive simulation models that can relate possible pumping patterns in an aquifer-aquitard system to the subsidence rates that will result. Gambolati and Freeze (1973) designed a two-step mathematical model for this purpose. In the first step (the hydrologic model), the regional hydraulic-head drawdowns are calculated in an idealized two-dimensional vertical cross section in radial coordinates, using a model that is a boundary-value problem based on the equation of transient groundwater flow. Solutions are obtained with a numerical finite-element technique. In the second step of the modeling procedure (the subsidence model), the hydraulic head declines determined with the hydrologic model for the various aquifers are used as time-dependent boundary conditions in a set of one-dimensional vertical consolidation models applied to a more refined geologic representation of each aquitard. Gambolati et al. (1974a, 1974b) applied the model to subsidence predictions for Venice, Italy. Recent measurements summarized by Carbognin et al. (1976) verify the model's validity.

8.13 Seawater Intrusion

When groundwater is pumped from aquifers that are in hydraulic connection with the sea, the gradients that are set up may induce a flow of salt water from the sea toward the well. This migration of salt water into freshwater aquifers under the influence of groundwater development is known as *seawater intrusion*.

As a first step toward understanding the nature of the processes involved, it is necessary to examine the nature of the saltwater-freshwater interface in coastal aquifers under natural conditions. The earliest analyses were carried out independently by two European scientists (Ghyben, 1888; Herzberg, 1901) around the turn of the century. Their analysis assumed simple hydrostatic conditions in a homogeneous, unconfined coastal aquifer. They showed [Figure 8.37(a)] that the

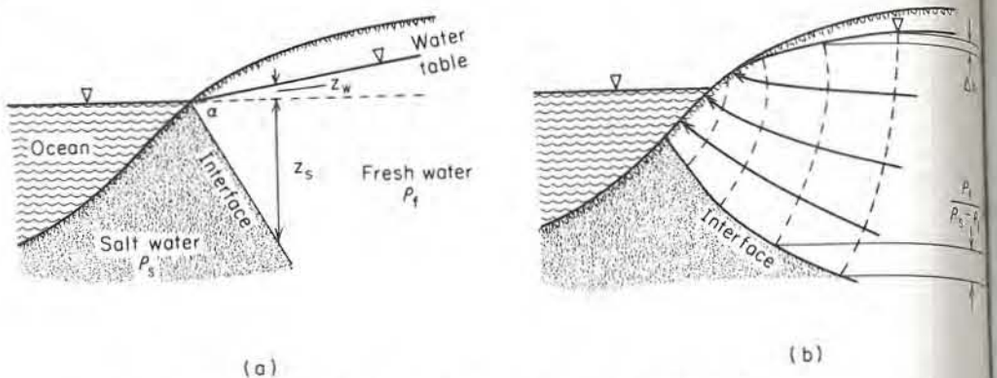

Figure 8.37 Saltwater-freshwater interface in an unconfined coastal aquifer (a) under hydrostatic conditions; (b) under conditions of steady-state seaward flow (after Hubbert, 1940).

interface separating salt water of density ρ_s and fresh water of density ρ_f must project into the aquifer at an angle $\alpha < 90°$. Under hydrostatic conditions, the weight of a unit column of fresh water extending from the water table to the interface is balanced by a unit column of salt water extending from sea level to the same depth as the point on the interface. With reference to Figure 8.37(a), we have

$$\rho_s g z_s = \rho_f g(z_s + z_w) \tag{8.75}$$

or

$$z_s = \frac{\rho_f}{\rho_s - \rho_f} z_w \tag{8.76}$$

For $\rho_f = 1.0$ and $\rho_s = 1.025$,

$$z_s = 40 z_w \tag{8.77}$$

Equation (8.77) is often called the *Ghyben-Herzberg relation.*

If we specify a change in the water-table elevation of Δz_w, then from Eq. (8.77), $\Delta z_s = 40\Delta z_w$. If the water table in an unconfined coastal aquifer is lowered 1 m, the saltwater interface will rise 40 m.

In most real situations, the Ghyben-Herzberg relation underestimates the depth to the saltwater interface. Where freshwater flow to the sea takes place, the hydrostatic assumptions of the Ghyben-Herzberg analysis are not satisfied. A more realistic picture was provided by Hubbert (1940) in the form of Figure 8.37(b) for steady-state outflow to the sea. The exact position of the interface can be determined for any given water-table configuration by graphical flow-net construction, noting the relationships shown on Figure 8.37(b) for the intersection of equipotential lines on the water table and on the interface.

The concepts outlined in Figure 8.37 do not reflect reality in yet another way. Both the hydrostatic analysis and the steady-state analysis assume that the interface

separating fresh water and salt water in a coastal aquifer is a sharp boundary. In reality, there tends to be a mixing of salt water and fresh water in a zone of diffusion around the interface. The size of the zone is controlled by the dispersive characteristics of the geologic strata. Where this zone is narrow, the methods of solution for a sharp interface may provide a satisfactory prediction of the freshwater flow pattern, but an extensive zone of diffusion can alter the flow pattern and the position of the interface, and must be taken into account. Henry (1960) was the first to present a mathematical solution for the steady-state case that includes consideration of dispersion. Cooper et al. (1964) provide a summary of the various analytical solutions.

Seawater intrusion can be induced in both unconfined and confined aquifers. Figure 8.38(a) provides a schematic representation of the saltwater wedge that would exist in a confined aquifer under conditions of natural steady-state outflow. Initiation of pumping [Figure 8.38(b)] sets up a transient flow pattern that leads to declines in the potentiometric surface on the confined aquifer and inland migration of the saltwater interface. Pinder and Cooper (1970) presented a numerical mathematical method for the calculation of the transient position of the saltwater front in a confined aquifer. Their solution includes consideration of dispersion.

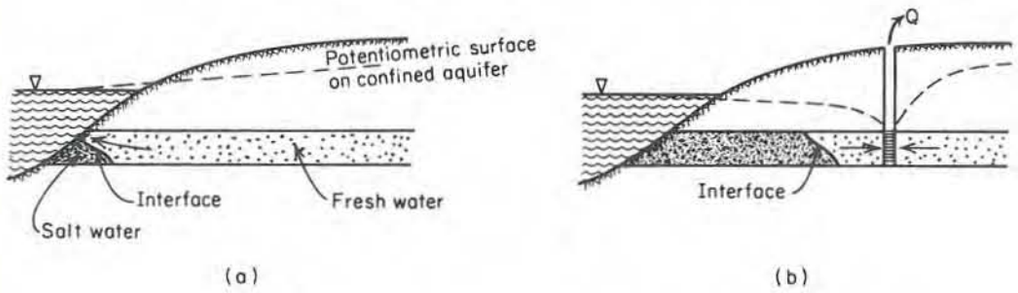

Figure 8.38 (a) Saltwater-freshwater interface in a confined coastal aquifer under conditions of steady-state seaward flow; (b) seawater intrusion due to pumping.

One of the most intensively studied coastal aquifers in North America is the Biscayne aquifer of southeastern Florida (Kohout, 1960a, 1960b). It is an unconfined aquifer of limestone and calcareous sandstone extending to an average depth of 30 m below sea level. Field data indicate that the saltwater front undergoes transient changes in position under the influence of seasonal recharge patterns and the resulting water-table fluctuations. Lee and Cheng (1974) and Segol and Pinder (1976) have simulated transient conditions in the Biscayne aquifer with finite-element numerical models. Both the field evidence and the numerical modeling confirm the necessity of considering dispersion in the steady-state and transient analyses. The nature of dispersion in groundwater flow will be considered more fully in Chapter 9 in the context of groundwater contamination.

Todd (1959) summarizes five methods that have been considered for controlling seawater intrusion: (1) reduction or rearrangement of the pattern of groundwater pumping, (2) artificial recharge of the intruded aquifer from spreading basins or recharge wells, (3) development of a pumping trough adjacent to the coast by means of a line of pumping wells parallel to the coastline, (4) development of a freshwater ridge adjacent to the coast by means of a line of recharge wells parallel to the coastline, and (5) construction of an artificial subsurface barrier. Of these five alternatives, only the first has been proven effective and economic. Both Todd (1959) and Kazmann (1972) describe the application of the freshwater-ridge concept in the Silverado aquifer, an unconsolidated, confined, sand-and-gravel aquifer in the Los Angeles coastal basin of California. Kazmann concludes that the project was technically successful, but he notes that the economics of the project remain a subject of debate.

Suggested Readings

BOUWER, H., and R. D. JACKSON. 1974. Determining soil properties. *Drainage for Agriculture*, ed. J. van Schilfgaarde. American Society of Agronomy, Madison, Wis., pp. 611–672.

COOPER, H. H. JR., F. A. KOHOUT, H. R. HENRY, and R. E. GLOVER. 1964. Sea water in coastal aquifers. *U.S. Geol. Surv. Water-Supply Paper 1613C*, 84 pp.

FERRIS, J. G., D. B. KNOWLES, R. H. BROWNE, and R. W. STALLMAN. 1962. Theory of aquifer tests. *U.S. Geol. Surv. Water-Supply Paper 1536E.*

HANTUSH, M. S. 1964. Hydraulics of wells. *Adv. Hydrosci.*, 1, pp. 281–432.

KRUSEMAN, G. P., and N. A. DE RIDDER. 1970. Analysis and evaluation of pumping test data. *Intern. Inst. for Land Reclamation and Improvement Bull. 11*, Wageningen, The Netherlands.

NEUMAN, S. P., and P. A. WITHERSPOON. 1969. Applicability of current theories of flow in leaky aquifers. *Water Resources Res.*, 5, pp. 817–829.

POLAND, J. F., and G. H. DAVIS. 1969. Land subsidence due to withdrawal of fluids. *Geol. Soc. Amer. Rev. Eng. Geol.*, 2, pp. 187–269.

PRICKETT, T. A. 1975. Modeling techniques for groundwater evaluation. *Adv. Hydrosci.*, 11, pp. 46–66, 91–116.

REMSON, I., G. M. HORNBERGER, and F. J. MOLZ. 1971. *Numerical Methods in Subsurface Hydrology*. Wiley Interscience, New York, pp. 56–122.

STALLMAN, R. W. 1971. Aquifer-test design, observation and data analysis. *Techniques of Water Resources Investigations of the U.S. Geological Survey*, Chapter B1. Government Printing Office, Washington, D.C.

YOUNG, R. A., and J. D. BREDEHOEFT. 1972. Digital computer simulation for solving management problems of conjunctive groundwater and surface-water systems. *Water Resources Res.*, 8, pp. 533–556.

Problems

1. (a) Show by dimensional analysis on Eq. (8.6) that u is dimensionless.
   (b) Show by dimensional analysis on Eq. (8.7) that $W(u)$ is dimensionless.
   (c) Show that the values of the coefficients A and B given in connection with Eqs. (8.38) and (8.39) are correct for the engineering system of units commonly used in North America in which volumes are measured in U.S. gallons.

2. A fully penetrating well pumps water from an infinite, horizontal, confined, homogeneous, isotropic aquifer at a constant rate of 25 ℓ/s. If T is 1.2×10^{-2} m²/s and S is 2.0×10^{-4}, make the following calculations.
   (a) Calculate the drawdown that would occur in an observation well 60 m from the pumping well at times of 1, 5, 10, 50, and 210 min after the start of pumping. Plot these values on a log-log graph of $h_0 - h$ versus t.
   (b) Calculate the drawdown that would occur in a set of observation wells at distances 1 m, 3 m, 15 m, 60 m, and 300 m from the pumping well at a time 210 min after the start of pumping. Plot these values on a semilog graph of $h_0 - h$ versus r.

3. A confined aquifer with $T = 7.0 \times 10^{-3}$ m²/s and $S = 5.0 \times 10^{-4}$ is pumped by two wells 35 m apart. One well is pumped at 7.6 ℓ/s and one at 15.2 ℓ/s. Plot the drawdown $h_0 - h$ as a function of position along the line joining the two wells at a time 4 h after the start of pumping.

4. (a) Why is a 10-day pumping test better than a 10-h pumping text?
   (b) Why are storativities for unconfined aquifers so much larger than those for confined aquifers?
   (c) What kind of pumping-test arrangement would be required to determine the exact location of a straight, vertical impermeable boundary?

5. (a) List the assumptions underlying the Theis solution.
   (b) Sketch two plots that show the approximate shape you would expect for the time drawdown curve from a confined aquifer if:
   (1) The aquifer pinches out to the west.
   (2) The overlying confining formations are impermeable, but the underlying formations are leaky.
   (3) The pumping well is located near a fault that is in hydraulic connection to a surface stream.
   (4) The well is on the shore of a tidal estuary.
   (5) The pump broke down halfway through the test.
   (6) The barometric pressure increased at the pump test site.

6. (a) Plot the values of u versus $W(u)$ given in Table 8.1 on a log-log graph. It is only necessary to plot those values lying in the range $10^{-9} < u < 1$.
   (b) Plot these same values as $1/u$ versus $W(u)$ on a log-log graph.

7. The thickness of a horizontal, confined, homogeneous, isotropic aquifer of infinite areal extent is 30 m. A well fully penetrating the aquifer was continuously pumped at a constant rate of 0.1 m^3/s for a period of 1 day. The drawdowns given in the attached table were observed in a fully penetrating observation well 90 m from the pumping well. Compute the transmissivity and the storativity by using:

(a) The Theis method of log-log matching [using the type curve prepared in Problem 6(b)].

(b) The Jacob method of semilog plotting.

t (min)	$h_0 - h$ (m)	t	$h_0 - h$	t	$h_0 - h$	t	$h_0 - h$
1	0.14	7	0.39	40	0.66	100	0.81
2	0.22	8	0.40	50	0.70	200	0.90
3	0.28	9	0.42	60	0.71	400	0.99
4	0.32	10	0.44	70	0.73	800	1.07
5	0.34	21	0.55	80	0.76	1000	1.10
6	0.37	30	0.62	90	0.79		

8. A homogeneous, isotropic, confined aquifer is 30.5 m thick and infinite in horizontal extent. A fully penetrating production well is pumped at a constant rate of 38 ℓ/s. The drawdown in an observation well 30.5 m from the production well after 200 days is 2.56 m.

(a) Assume a reasonable value for the storativity and then calculate the transmissivity T for the aquifer.

(b) Calculate the hydraulic conductivity and the compressibility of the aquifer. (Assume reasonable values for any unknown parameters.)

9. (a) A well pumps at 15.7 ℓ/s from a horizontal, confined, homogeneous, isotropic aquifer. The attached table lists the drawdown observed in an observation well 30 m from the pumping well. Plot these data on a semilogarithmic graph and use the Jacob method on the early data to calculate T and S.

(b) What kind of boundary is indicated by the break in slope? Measure the slope of the two limbs and note that the second limb has twice the slope of the first limb. In this case, how many image wells must be needed to provide an equivalent aquifer of infinite extent? Draw a sketch showing a possible configuration of pumping well, image well(s), and boundary, and note whether the image wells are pumping wells or recharge wells.

t (min)	$h_0 - h$ (m)	t	$h_0 - h$	t	$h_0 - h$	t	$h_0 - h$
11	2.13	21	2.50	52	3.11	88	3.70
14	2.27	28	2.68	60	3.29	100	3.86
18	2.44	35	2.80	74	3.41	112	4.01
						130	4.14

10. The straight-line portion of a semilog plot of drawdown versus time taken from an observation well 200 ft from a pumping well ($Q = 500$ U.S. gal/min) in a confined aquifer goes through the points ($t = 4 \times 10^{-4}$ day, $h_0 - h = 1.6$ ft) and ($t = 2 \times 10^{-2}$ day, $h_0 - h = 9.4$ ft).

(a) Calculate T and S for the aquifer.

(b) Calculate the drawdown that would occur 400 ft from the pumping well 10 h after the start of pumping.

11. (a) The hydraulic conductivity of a 30-m-thick confined aquifer is known from laboratory testing to have a value of 4.7×10^{-4} m/s. If the straight-line portion of a Jacob semilogarithmic plot goes through the points ($t = 10^{-3}$ day, $h_0 - h = 0.3$ m) and ($t = 10^{-2}$ day, $h_0 - h = 0.6$ m) for an observation well 30 m from a pumping well, calculate the transmissivity and storativity of the aquifer.

(b) Over what range of time values is the Jacob method of analysis valid for this observation well in this aquifer?

12. You are asked to design a pump test for a confined aquifer in which the transmissivity is expected to be about 1.4×10^{-2} m^2/s and the storativity about 1.0×10^{-4}. What pumping rate would you recommend for the test if it is desired that there be an easily measured drawdown of at least 1 m during the first 6 h of the test in an observation well 150 m from the pumping well?

13. (a) Venice, Italy, has subsided 20 cm in 35 years; San Jose, California, has subsided 20 ft in 35 years. List the hydrogeological conditions that these two cities must have in common (in that they have both undergone subsidence), and comment on how these conditions may differ (to account for the large difference in total subsidence).

(b) The following data were obtained from a laboratory consolidation test on a core sample with a cross-sectional area of 100.0 cm^2 taken from a confining clay bed at Venice. Calculate the compressibility of the sample in m^2/N that would apply at an effective stress of 2.0×10^6 N/m^2.

Load (N)	0	2000	5000	10,000	15,000	20,000	30,000
Void ratio	0.98	0.83	0.75	0.68	0.63	0.59	0.56

(c) Calculate the coefficient of compressibility, a_v, and the compression index, C_c, for these data. Choose a K value representative of a clay and calculate the coefficient of consolidation, c_v.

14. It is proposed to construct an unlined, artificial pond near the brink of a cliff. The geological deposits are unconsolidated, interbedded sands and clays. The water table is known to be rather deep.

(a) What are the possible negative impacts of the proposed pond?

(b) List in order, and briefly describe, the methods of exploration you would recommend to clarify the geology and hydrogeology of the site.

(c) List four possible methods that could be used to determine hydraulic conductivities. Which methods would be the most reasonable to use? The least reasonable? Why?

15. An undisturbed cylindrical core sample of soil 10 cm high and 5 cm in diameter weights 350 gm. Calculate the porosity.

16. If the water level in a 5-cm-diameter piezometer standpipe recovers 90% of its bailed drawdown in 20 h, calculate K. The intake is 0.5 m long and the same diameter as the standpipe. Assume that the assumptions underlying the Hvorslev point test are met.

17. Assume that the grain-size curve of Figure 8.25(a) is shifted one ϕ unit to the left. Calculate the hydraulic conductivity for the soil according to both the Hazen relation and the Masch and Denny curves.

18. (a) Develop the transient finite-difference equation for an internal node in a three-dimensional, homogeneous, isotropic nodal grid where $\Delta x = \Delta y = \Delta z$.

(b) Develop the transient finite-difference equation for a node adjacent to an impermeable boundary in a two-dimensional homogeneous, isotropic system with $\Delta x = \Delta y$. Do so:

(1) Using the simple approach of Section 8.8.

(2) The more sophisticated approach of Appendix IX.

19. Assume that resistors in the range 10^4–10^5 Ω and capacitors in the range 10^{-12}–10^{-11} F are commercially available. Choose a set of scale factors for the analog simulation of an aquifer with $T \simeq 10^5$ U.S. gal/day/ft and $S \simeq 3 \times 10^{-3}$. The aquifer is approximately 10 miles square and drawdowns of 10's of feet are expected over 10's of years in response to total pumping rates up to 10^6 U.S. gal/day.

CHAPTER 9

Groundwater Contamination

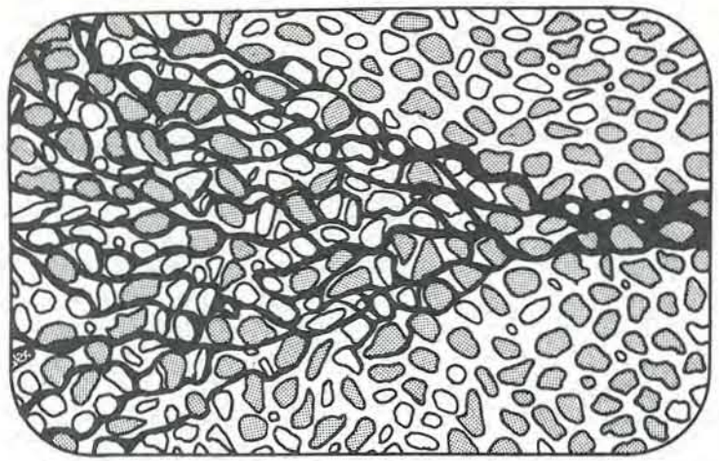

During recent years much of the emphasis in groundwater investigations in industrialized countries has shifted from problems of groundwater supply to considerations of groundwater quality. As a result of our consumptive way of life, the groundwater environment is being assaulted with an ever-increasing number of soluble chemicals. Current data indicate that in the United States there are at least 17 million waste disposal facilities emplacing more than 6.5 billion cubic meters of liquid into the ground each year (U.S. Environmental Protection Agency, 1977). As time goes on, the vast subsurface reservoir of fresh water, which a few decades ago was relatively unblemished by man's activities, is gradually becoming degraded.

The problem of water quality degradation of rivers and lakes has been evident for a long time. In general, solutions to this problem have been found in the implementation of effective legislation for discontinuing contaminant emissions. Already in some parts of the world, effective emission abatement measures have led to great improvements in surface-water quality. Unfortunately, problems of groundwater quality degradation are in many ways more difficult to overcome. Because of the heterogeneities inherent in subsurface systems, zones of degraded groundwater can be very difficult to detect. The U.S. Environmental Protection Agency (1977) has reported that almost every known instance of aquifer contamination has been discovered only after a water-supply well has been affected. Often by the time subsurface pollution is conclusively identified, it is too late to apply remedial measures that would be of much benefit. From a water quality viewpoint, degradation of groundwater often requires long periods of time before the true extent of the problem is readily detectable. Long periods of groundwater flow are often required for pollutants to be flushed from contaminated aquifers. Groundwater pollution often results in aquifers or parts of aquifers being damaged beyond repair.

Whereas the problem of achieving acceptable quality of surface waters focuses mainly on decreasing the known emissions of pollutants to these systems, the problem facing scientists and engineers involved in the protection of groundwater resources is to identify the areas and mechanisms by which pollutants can enter

groundwater flow systems and to develop reliable predictions of the transport of contaminants within the flow systems. This is necessary as a basis for minimizing the impact of existing or proposed industrial, agricultural, or municipal activities on groundwater quality.

The purpose of this chapter is to provide some insight into the physical and chemical factors that influence the subsurface migration of dissolved contaminants. To this end the behavior of nonreactive solutes and of solutes that undergo reactions during subsurface migration will be considered. Following this, more specific contamination problems related to activities such as agriculture, mining, nuclear power development, and disposal of refuse, sewage, and industrial wastes will be briefly reviewed.

Throughout this chapter all solutes introduced into the hydrologic environment as a result of man's activities are referred to as *contaminants*, regardless of whether or not the concentrations reach levels that cause significant degradation of water quality. The term *pollution* is reserved for situations where contaminant concentrations attain levels that are considered to be objectionable.

The emphasis in this chapter is on the occurrence and processes that control the migration of *dissolved* contaminants in groundwater. Groundwater can also be contaminated by oily substances that exist in a liquid state in contact with water in a manner that does not lead to mixing of the oils in a dissolved form. The oily liquid is said to be *immiscible* in the water. The physical processes that control the movement of immiscible fluids in subsurface systems are described by Bear (1972) and are introduced in Section 9.5.

9.1 Water Quality Standards

Before proceeding with discussions of the principles of contaminant behavior in groundwater flow systems and of sources of groundwater contamination, we will briefly examine some of the more important water quality standards. These standards serve as a basis for appraisal of the results of chemical analyses of water in terms of suitability of the water for various intended uses. The most important of these standards are those established for drinking water (Table 9.1). The recommended limits for concentrations of inorganic constituents in drinking water have existed for many years. Limits for organic constutuents such as pesticide residues are a recent addition. There is considerable controversy with regard to the specific organic constituents that should be included in drinking water standards and the concentration limits that should be established for them.

In Table 9.1 the major constituents for which recommended permissible limits are listed are total dissolved solids (TDS), sulfate, and chloride. Consumption by humans of waters with concentrations somewhat above these limits is generally not harmful. In many regions groundwater used for drinking-water supply exceeds the limits of one or more of these parameters. Several hundred milligrams per liter of chloride must be present in order for saltiness to be detected by taste.

Table 9.1 Drinking Water Standards

Constituent	Recommended concentration limit* (mg/ℓ)
Inorganic	
Total dissolved solids	500
Chloride (Cl)	250
Sulfate (SO_4^{2-})	250
Nitrate (NO_3^-)	45†
Iron (Fe)	0.3
Manganese (Mn)	0.05
Copper (Cu)	1.0
Zinc (Zn)	5.0
Boron (B)	1.0
Hydrogen sulfide (H_2S)	0.05
	Maximum permissible concentration‡
Arsenic (As)	0.05
Barium (Ba)	1.0
Cadmium (Cd)	0.01
Chromium (Cr^{VI})	0.05
Selenium	0.01
Antimony (Sb)	0.01
Lead (Pb)	0.05
Mercury (Hg)	0.002
Silver (Ag)	0.05
Fluoride (F)	1.4–2.4§
Organic	
Cyanide	0.05
Endrine	0.0002
Lindane	0.004
Methoxychlor	0.1
Toxaphene	0.005
2,4-D	0.1
2,4,5-TP silvex	0.01
Phenols	0.001
Carbon chloroform extract	0.2
Synthetic detergents	0.5
Radionuclides and radioactivity	Maximum permissible activity (pCi/ℓ)
Radium 226	5
Strontium 90	10
Plutonium	50,000
Gross beta activity	30
Gross alpha activity	3
Bacteriological	
Total coliform bacteria	1 per 100 mℓ

SOURCES: U.S. Environmental Protection Agency, 1975 and World Health Organization, European Standards, 1970.

*Recommended concentration limits for these constituents are mainly to provide acceptable esthetic and taste characteristics.

†Limit for NO_3^- expressed as N is 10 mg/ℓ according to U.S. and Canadian standards; according to WHO European standards, it is 11.3 mg/ℓ as N and 50 mg/ℓ as NO_3^-.

Hardness of water is defined as its content of metallic ions which react with sodium soaps to produce solid soaps or scummy residue and which react with negative ions, when the water is evaporated in boilers, to produce solid boiler scale (Camp, 1963). Hardness is normally expressed as the total concentration of Ca^{2+} and Mg^{2+} as milligrams per liter equivalent $CaCO_3$. It can be determined by substituting the concentration of Ca^{2+} and Mg^{2+}, expressed in milligrams per liter, in the expression

$$\text{total hardness} = 2.5(Ca^{2+}) + 4.1(Mg^{2+}) \tag{9.1}$$

Each concentration is multiplied by the ratio of the formula weight of $CaCO_3$ to the atomic weight of the ion; hence the factors 2.5 and 4.1 are included in the hardness relation. Water with hardness values greater than 150 mg/ℓ is designated as being very hard. Soft water has values less than 60 mg/ℓ. Water softening is common practice in many communities where the water supply has a hardness greater than about 80–100 mg/ℓ. Water used for boiler feed will cause excessive scale formation (carbonate-mineral precipitation) if the hardness is above about 60–80 mg/ℓ.

Of the recommended limits specified for minor and trace inorganic constituents in drinking water, many have been established for reasons other than direct hazard to human health. For example iron and manganese are both essential to the human body. Their intake through drinking water is normally an insignificant part of the body requirement. The recommended limits placed on these metals in the Standards is for the purpose of avoiding, in household water use, problems associated with precipitates and stains that form because oxides of these metals are relatively insoluble (Camp, 1963). The recommended limit for zinc is set at 5 mg/ℓ to avoid taste produced by zinc at higher concentrations. Concentrations as high as 40 mg/ℓ can be tolerated with no apparent deteriment to general health. Zinc concentrations as low as 0.02 mg/ℓ are, however, toxic to fish. Zinc contamination can be regarded as severe pollution in ecological systems where fish are of primary interest but may be only of minor significance if human consumption is the primary use of the water.

The most common identifiable contaminant in groundwater is nitrate (NO_3^-). The recommended limit for nitrate in drinking water is 45 mg/ℓ expressed as NO_3^- or 10 mg/ℓ expressed as N. In Europe the limit recommended by the World Health Organization is 50 mg/ℓ as NO_3^- and 11.3 mg/ℓ as N. Excessive concentrations of NO_3^- have potential to harm infant human beings and livestock if consumed on a regular basis. Adults can tolerate much higher concentrations. The extent to which NO_3^- in water is viewed as a serious pollutant therefore depends on the water use.

The constituents for which *maximum permissible concentration limits* have

‡Maximum permissible limits are set according to health criteria.

§Limit depends on average air temperature of the region; fluoride is toxic at about 5–10 mg/ℓ if water is consumed over a long period of time.

been set in drinking water standards (Table 9.1) are all considered to have significant potential for harm to human health at concentrations above the specified limits. The specified limits are not to be exceeded in public water supplies. If the limits for one or more of the constituents are exceeded, the water is considered to be unfit for human consumption. The limits indicated in Table 9.1 are representative of the current standards in the United States and Canada. The limits are continually being appraised and modifications occur from time to time. As more is learned about the role of trace constituents in human health, the list of constituents for which maximum permissible limits exist may expand, particularly in the case of organic substances.

In many regions the most important uses of groundwater are for agriculture. In these situations it is appropriate to appraise the quality of groundwater relative to criteria or guidelines established for livestock or irrigation. Recommended concentration limits for these uses are listed in Table 9.2. The list of constituents and the concentration limits are not as stringent as for drinking water. These water quality criteria do serve to indicate, however, that concentration increases in a variety of constituents due to man's activities can cause serious degradation of groundwater quality even if the water is not used for human consumption.

Table 9.2 Recommended Concentration Limits for Water Used for Livestock and Irrigation Crop Production

	Livestock: Recommended limits (mg/ℓ)	Irrigation crops: Recommended limits (mg/ℓ)
Total dissolved solids		
Small animals	3000	700
Poultry	5000	
Other animals	7000	
Nitrate	45	—
Arsenic	0.2	0.1
Boron	5	0.75
Cadmium	0.05	0.01
Chromium	1	0.1
Fluoride	2	1
Lead	0.1	5
Mercury	0.01	—
Selenium	0.05	0.02

SOURCE: U.S. Environmental Agency, 1973b.

9.2 Transport Processes

The common starting point in the development of differential equations to describe the transport of solutes in porous materials is to consider the flux of solute into and out of a fixed elemental volume within the flow domain. A conservation of mass

statement for this elemental volume is

$$\begin{bmatrix}\text{net rate of}\\ \text{change of mass}\\ \text{of solute within}\\ \text{the element}\end{bmatrix} = \begin{bmatrix}\text{flux of}\\ \text{solute out}\\ \text{of the}\\ \text{element}\end{bmatrix} - \begin{bmatrix}\text{flux of}\\ \text{solute into}\\ \text{the}\\ \text{element}\end{bmatrix} \pm \begin{bmatrix}\text{loss or gain}\\ \text{of solute mass}\\ \text{due to}\\ \text{reactions}\end{bmatrix} \tag{9.2}$$

The physical processes that control the flux into and out of the elemental volume are *advection* and *hydrodynamic dispersion.* Loss or gain of solute mass in the elemental volume can occur as a result of chemical or biochemical *reactions* or radioactive decay.

Advection is the component of solute movement attributed to transport by the flowing groundwater. The rate of transport is equal to the average linear groundwater velocity, $\bar{v}$, where $\bar{v} = v/n$, v being the specific discharge and n the porosity (Section 2.12). The advection process is sometimes called *convection,* a term that in this text is reserved for use in discussion of thermally driven groundwater flow as described in Chapter 11. The process of hydrodynamic dispersion, which is described in Section 2.13, occurs as a result of mechanical mixing and molecular diffusion.

Mathematical descriptions of dispersion are currently limited to materials that are isotropic with respect to dispersion properties of the medium. The principal differential equation that describes transport of dissolved reactive constituents in saturated isotropic porous media is derived in Appendix X. This equation is known as the *advection-dispersion equation.* Our purpose here is to examine the physical significance of the terms in this equation (advection, dispersion, and reaction). We will start with the physical processes and then turn our attention to the chemical processes.

Nonreactive Constituents in Homogeneous Media

The one-dimensional form of the advection-dispersion equation for nonreactive dissolved constituents in saturated, homogeneous, isotropic, materials under steady-state, uniform flow [Eq. (A10.11), Appendix X] is

$$D_l \frac{\partial^2 C}{\partial l^2} - \bar{v}_l \frac{\partial C}{\partial l} = \frac{\partial C}{\partial t} \tag{9.3}$$

where l is a curvilinear coordinate direction taken along the flowline, $\bar{v}$ is the average linear groundwater velocity, D_l is the coefficient of hydrodynamic dispersion in the longitudinal direction (i.e., along the flow path), and C is the solute concentration. The effects of chemical reactions, biological transformations, and radioactive decay are not included in this form of the transport equation.

The coefficient of hydrodynamic dispersion can be expressed in terms of two components,

$$D_l = \alpha_l \bar{v} + D^* \tag{9.4}$$

where α_l is a characteristic property of the porous medium known as the dynamic dispersivity, or simply as *dispersivity* [L], and D^* is the *coefficient of molecular diffusion* for the solute in the porous medium [L^2/T]. The relation between D^* and the coefficient of diffusion for the solute species in water is described in Section 3.4. Some authors have indicated that a more accurate form of the mechanical component of the dispersion coefficient is $\alpha\bar{v}^m$, where m is an empirically determined constant between 1 and 2. Laboratory studies indicate that for practical purposes m can generally be taken as unity for granular geologic materials.

The classical experiment shown in Figure 9.1(a) is one of the most direct ways of illustrating the physical meaning of the one-dimensional form of the advection-dispersion equation. In this experiment, a nonreactive tracer at concentration C_0 is continuously introduced into a steady-state flow regime at the upstream end of a column packed with a homogeneous granular medium. For illustrative purposes it is assumed that the tracer concentration in the column prior to the introduction of the tracer is zero. It is convenient to express the tracer concentration in the

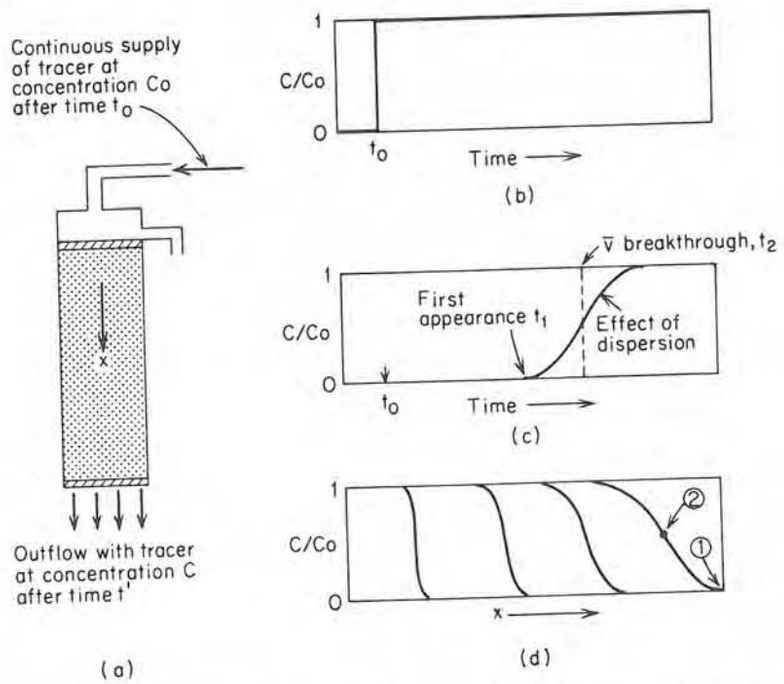

Figure 9.1 Longitudinal dispersion of a tracer passing through a column of porous medium. (a) Column with steady flow and continuous supply of tracer after time t_0; (b) step-function-type tracer input relation; (c) relative tracer concentration in outflow from column (dashed line indicates plug flow condition and solid line illustrates effect of mechanical dispersion and molecular diffusion); (d) concentration profile in the column at various times.

column as a relative concentration, defined as C/C_0, where C is the concentration in the column or in the output. The tracer input can therefore be represented as a step function, as shown in Figure 9.1(b). The concentration versus time relation of the column outflow, known as *the breakthrough curve*, is shown in Figure 9.1(c). If it is assumed that the tracer moves through the column with no mechanical dispersion or molecular diffusion, the tracer front will pass through as a plug and will exit from the column as a step function. This condition is shown as a vertical dashed line in Figure 9.1(c). In real situations, however, mechanical dispersion and molecular diffusion occur and the breakthrough curve spreads out causing the tracer to begin to appear in the outflow from the column (at time t_1) before the arrival of water traveling at the velocity of $\bar{v}$ (time t_2). This is represented in Figure 9.1(c).

Figure 9.1(d) shows instantaneous "pictures" of the dispersion interface inside the column at various times prior to breakthrough. The tracer front is spread out along the flow path. The spread of the profile increases with travel distance. The positions represented by points 1 and 2 in Figures 9.1(d) correspond to times t_1 and t_2 in Figure 9.1(c). Mechanical dispersion and molecular diffusion cause some of the tracer molecules to move faster than the average linear velocity of the water and some to move slower. The average linear velocity of the water in the column is determined by dividing the water input rate (Q) by nA, where A is the cross-sectional area of the column and n is the porosity [Eq. (2.82)].

The boundary conditions represented by the step-function input are described mathematically as

$$C(l, 0) = 0 \qquad l \geq 0$$

$$C(0, t) = C_0 \qquad t \geq 0$$

$$C(\infty, t) = 0 \qquad t \geq 0$$

For these boundary conditions the solution to Eq. (9.3) for a saturated homogeneous porous medium is (Ogata, 1970)

$$\frac{C}{C_0} = \frac{1}{2}\left[\operatorname{erfc}\left(\frac{l - \bar{v}t}{2\sqrt{D_l t}}\right) + \exp\left(\frac{\bar{v}l}{D_l}\right)\operatorname{erfc}\left(\frac{l + \bar{v}t}{2\sqrt{D_l t}}\right)\right] \tag{9.5}$$

where erfc represents the complementary error function, which is tabulated in Appendix V; l is the distance along the flow path; and $\bar{v}$ is the average linear water velocity. For conditions in which the dispersivity of the porous medium is large or when l or t is large, the second term on the right-hand side of the equation is negligible. Equation (9.5) can be used to compute the shapes of the breakthrough curves and concentration profiles illustrated in Figure 9.1(c) and (d). Analytical solutions for Eq. (9.3) with other boundary conditions are described by Rifai et al. (1956), Ebach and White (1958), Ogata and Banks (1961), Ogata (1970), and others.

The spreading out of the concentration profile and breakthrough curve of tracers or contaminants migrating through porous materials is caused by both mechanical dispersion and molecular diffusion. Figure 9.2 shows a concentration profile for the experimental conditions represented in Figure 9.1(a). In this graph

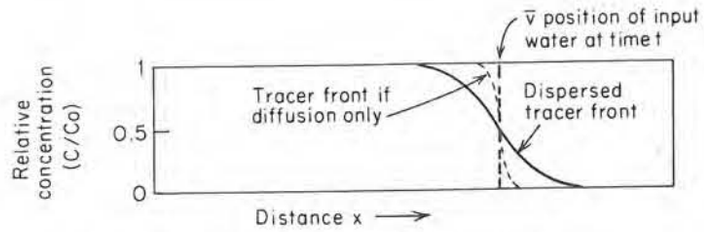

Figure 9.2 Schematic diagram showing the contribution of molecular diffusion and mechanical dispersion to the spread of a concentration front in a column with a step-function input.

the contribution of molecular diffusion to the spread of the curves is indicated schematically. At a low velocity, diffusion is the important contributor to the dispersion, and therefore the coefficient of hydrodynamic dispersion equals the diffusion coefficient ($D_l = D^*$). At a high velocity, mechanical mixing is the dominant dispersive process, in which case $D_l = \alpha_l \bar{v}$. Larger dispersivity of the medium produces greater mixing of the solute front as it advances. Laboratory experiments on tracer migration in saturated homogeneous granular materials have established relations between the influence of diffusion and mechanical dispersion, as illustrated in Figure 9.3. The dimensionless parameter $\bar{v}d/D^*$ is known as the *Peclet number*, where the average particle diameter is denoted by d. The exact shape of the relation between the Peclet number and D_l/D^* depends on the nature of the

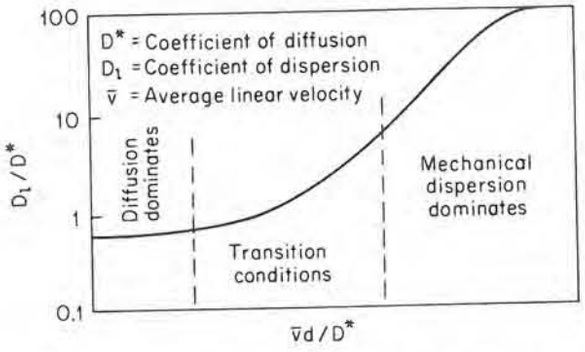

Figure 9.3 Relation between the Peclet number and the ratio of the longitudinal dispersion coefficient and the coefficient of molecular diffusion in a sand of uniform-sized grains (after Perkins and Johnston, 1963).

porous medium and on the fluid used in the experiments. The general shape illustrated in Figure 9.3 has been established by various investigators on the basis of experiments using different media (Bear, 1972).

In situations where the boundary conditions specified for Eq. (9.5) are applicable and where the groundwater velocity is so small that mechanical dispersion is negligible relative to molecular diffusion, Eq. (9.5) reduces to the one-dimensional solution to Fick's second law. This "law" is described in Section 3.4. The rate at which one-dimensional diffusion occurs is expressed graphically in Figure 9.4, which shows, for periods of diffusion of 100 and 10,000 years, diffusion distances as a function of relative concentration. The diffusion distances were obtained using Eq. (3.47) with diffusion coefficient values of 1×10^{-10} and 1×10^{-11} m²/s.

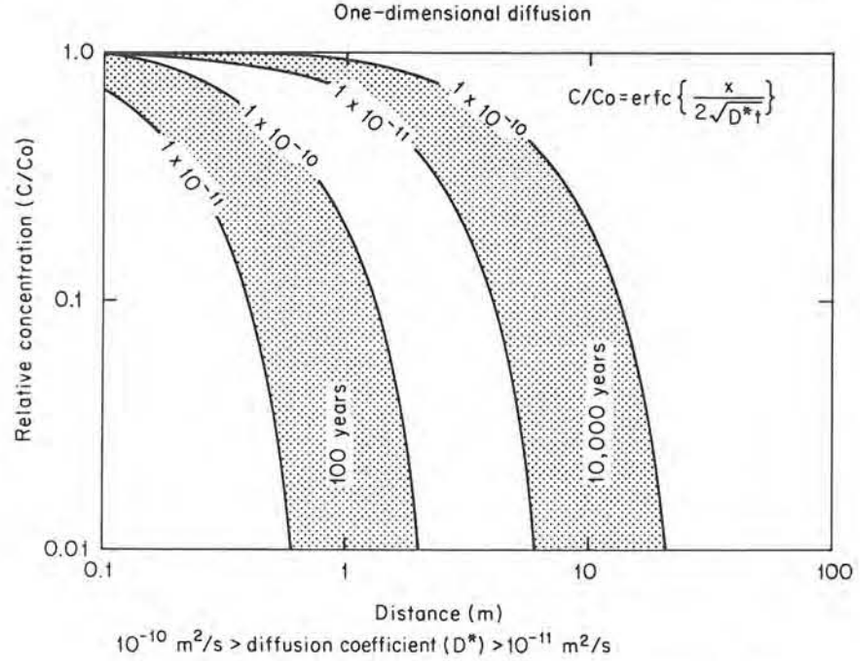

Figure 9.4 Positions of contaminant front migrating by molecular diffusion away from a source where $C = C_0$ at $t > 0$. Migration times are 100 and 10,000 years.

These values are representative of a range typical of nonreactive chemical species in clayey geologic deposits. Values for coarse-grained unconcolidated materials can be somewhat higher than 1×10^{-10} m²/s but are less than the coefficients for the chemical species in water (i.e., $< 2 \times 10^{-9}$ m²/s). Figure 9.4 indicates that over long periods of time, diffusion can cause contaminants to move considerable distances, even through low-permeability materials. Whether contaminant migration on this time scale is important depends on the nature of the problem. In the

case of subsurface disposal of radioactive wastes or highly toxic inorganic or organic compounds, diffusion can be an important process.

One of the characteristic features of the dispersive process is that it causes spreading of the solute, if the opportunity is available, in directions transverse to the flow path as well as in the longitudinal flow direction. This is illustrated schematically for a two-dimensional horizontal flow field in Figure 9.5(a). In this experimental sand box, a nonreactive tracer is introduced as a continuous steady input to the uniform flow field. Dispersion in this two-dimensional flow domain is illustrated in a different manner by the experiment shown in Figure 9.5(b). In this case the tracer is introduced as an instantaneous point source (i.e., a slug of tracer) into the uniform flow regime. As the tracer is transported along the flow path, it spreads in all directions in the horizontal plane. The total mass of the tracer in the flow regime does not change, but the mass occupies an increasing volume of the porous medium. The process of mechanical dispersion is directionally dependent even though the porous medium is isotropic with respect to textural properties and hydraulic conductivity. Figure 9.5(b) shows that the tracer zone develops an elliptical shape as the tracer is transported through the system. This occurs because the *process* of mechanical dispersion is anisotropic. Dispersion is stronger in the direction of flow (the longitudinal dispersion) than in directions normal to the flow line (transverse dispersion).

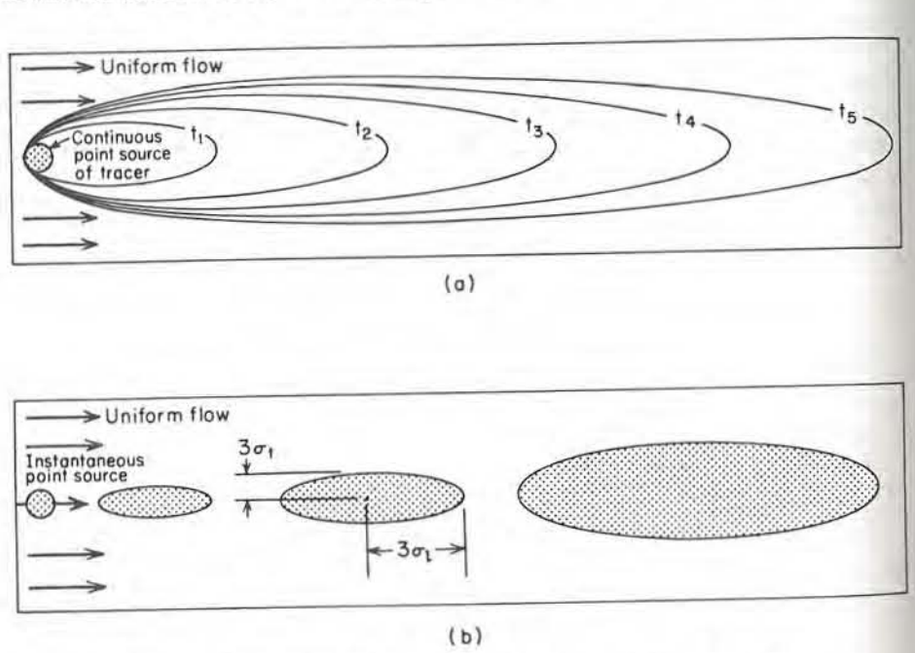

Figure 9.5 Spreading of a tracer in a two-dimensional uniform flow field in an isotropic sand. (a) Continuous tracer feed with step-function initial condition; (b) instantaneous point source.

One-dimensional expressions for the transport of dissolved constituents, such as Eq. (9.5), are useful in the interpretation of laboratory column experiments, but are of limited use in the analysis of field problems because dispersion occurs in the transverse directions as well as in the longitudinal direction. As an example of a solution to the advection-dispersion equation in three-dimensions [Eq. (A10.9), Appendix X], we will follow an approach described by Baetsle (1969). As in Figure 9.5(b), the contaminant is assumed to originate as an instantaneous slug at a point source at $x = 0$, $y = 0$, $z = 0$. The mass of contaminant is then carried away from the source by transport in a steady-state uniform flow field moving in the x-direction in a homogeneous isotropic medium. As the contaminant mass is transported through the flow system, the concentration distribution of the contaminant mass at time t is given by

$$C(x, y, z, t) = \frac{M}{8(\pi t)^{3/2}\sqrt{D_x D_y D_z}} \exp\left(-\frac{X^2}{4D_x t} - \frac{Y^2}{4D_y t} - \frac{Z^2}{4D_z t}\right) \qquad (9.6)$$

where M is the mass of contaminant introduced at the point source, D_x, D_y, and D_z are the coefficients of dispersion in the x, y, z directions and X, Y, and Z are distances in the x, y, z directions from the center of gravity of the contaminant mass. The position of the center of gravity of the contaminant mass at time t will lie along the flow path in the x direction at coordinates (x_t, y_t, z_t), where $y_t = z_t = 0$ and $x_t = \bar{v}t = vt/n$, where $\bar{v}$ is the average linear velocity, v is the specific discharge, and n is the porosity. In Eq. (9.6), $X = x - \bar{v}t$, $Y = y$, and $Z = z$. It is apparent from Eq. (9.6) that the maximum concentration is located at the center of gravity of the contaminant cloud, where $X = 0$, $Y = 0$, and $Z = 0$. The mass of the contaminant introduced at the source equals C_0V_0, where C_0 is the initial concentration and V_0 is the initial volume. In the mathematical formulation of the initial conditions, the contaminant input occurs at a point and therefore has mass but no volume. In practice, however, this is expressed by the quantity C_0V_0.

From Eq. (9.6) it follows that the peak concentration that occurs at the center of gravity of the contaminant cloud is given by

$$C_{\max} = \frac{C_0V_0}{8(\pi t)^{3/2}\sqrt{D_x D_y D_z}} \qquad (9.7)$$

The zone in which 99.7% of the contaminant mass occurs is described by the ellipsoid with dimensions, measured from the center of mass, of $3\sigma_x = \sqrt{2D_x t}$, $3\sigma_y = \sqrt{2D_y t}$, $3\sigma_z = \sqrt{2D_z t}$, where σ is the standard deviation of the concentration distribution. This is illustrated in the xy plane in Figure 9.5(b). At low velocities molecular diffusion is the dominant dispersive mechanism, in which case the migrating contaminant cloud is circular. Because these equations are based on idealized conditions, such as the instantaneous point source and uniform flow, they have limited use in the analysis of most field situations. In simple hydrogeologic settings, however, they can be used to obtain preliminary estimates of the

migration patterns that may arise from small contaminant spills or from leaching of buried wastes (Baetsle, 1969). A variety of other analytical solutions describing the migration of contaminants in two- and three-dimensional space are described by Fried (1975) and Codell and Schreiber (in press).

Mechanical dispersion in the transverse direction is a much weaker process than dispersion in the longitudinal direction, but at low velocities where molecular diffusion is the dominant dispersive mechanism, the coefficients of longitudinal and transverse dispersion are nearly equal. This is illustrated by the experimental results shown in Figure 9.6, which indicates small dispersion coefficients over a range of low velocities. Because mechanical dispersion in the transverse direction is much weaker than in the longitudinal direction, the transverse dispersion coefficient remains diffusion-controlled until the flow velocity is quite high.

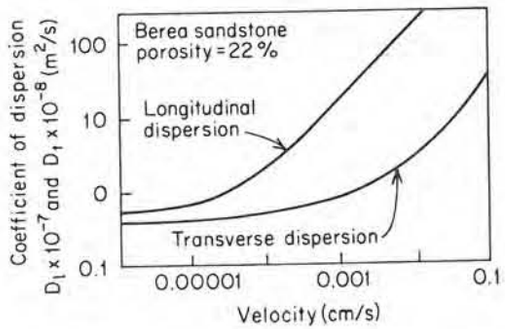

Figure 9.6 Coefficients of longitudinal and transverse dispersion for transport in a homogeneous sandstone at various flow rates (after Crane and Gardner, 1961).

The forms of the transport equation described above are based on the assumption that there is no significant density contrast between the contaminant or tracer fluid and the groundwater in the surrounding flow domain. Equations that make allowance for density contrasts are more complex. As a qualitative example of the effect of density contrasts, consider the sinking contaminant plume in an initially uniform flow field, as illustrated in Figure 9.7. If the contaminant solution

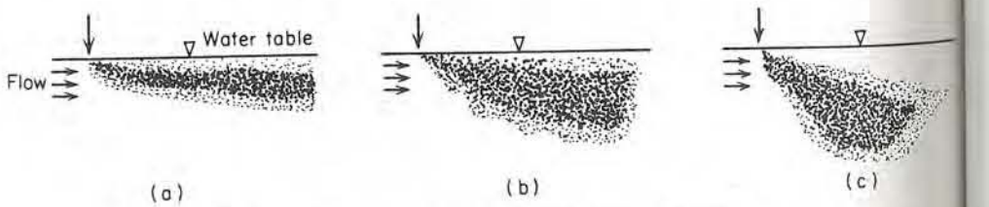

Figure 9.7 Effect of density on migration of contaminant solution in uniform flow field. (a) Slightly more dense than groundwater; (b) and (c) larger density contrasts.

entering this flow regime has the same density as the groundwater, the contaminant plume will spread in a shallow zone close to the water table. If the contaminant solution is considerably more dense than the groundwater, the plume will sink steeply downward into the groundwater flow system. Prediction of contaminant migration patterns requires accurate knowledge of the density of the contaminant solution as well as that of the groundwater.

Nonreactive Constituents in Heterogeneous Media

If it were not for the effects of heterogeneities in natural geological materials, the problem of prediction and detection of contaminant behavior in groundwater flow systems would be easily solved. Advection is the process whereby solutes are transported by the bulk mass of the flowing fluid. Advection is normally considered on the macroscopic scale in terms of the patterns of groundwater flow. These patterns are defined by the spatial and temporal distributions of the average linear velocity of the fluid. Flow patterns and flow nets have been described extensively in Chapters 5 and 6. Our purpose here is to consider in more detail the effects on flow lines and velocities exerted by various types of heterogeneities.

To illustrate the effect of simple layered heterogeneities on transport patterns, the cross-section flow-domain illustrated in Figure 9.8(a) is used. It is assumed that steady-state groundwater flow occurs through the cross section and that the

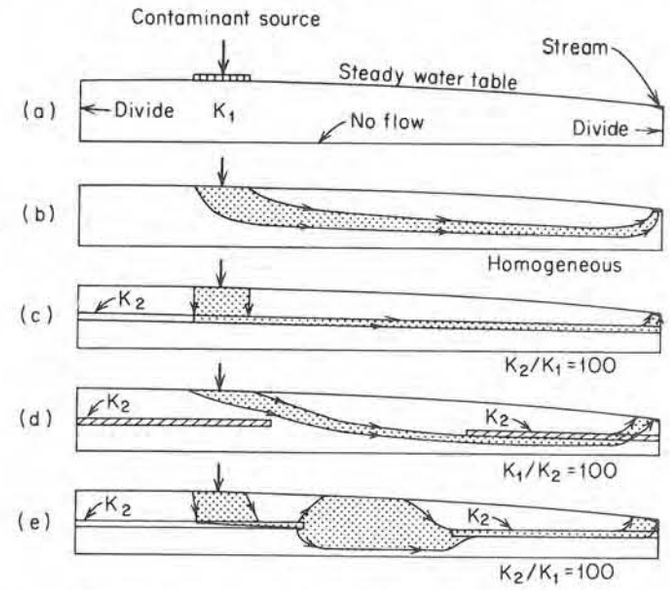

Figure 9.8 Effect of layers and lenses on flow paths in shallow steady-state groundwater flow systems. (a) Boundary conditions; (b) homogeneous case; (c) single higher-conductivity layer; (d) two lower-conductivity lenses; (e) two higher-conductivity lenses.

flow domain is isotropic with respect to hydraulic conductivity. To illustrate the effect of stratigraphic variations on the transport pattern of contaminants entering the system in a recharge area, a contaminant input zone is located on the cross section. In field situations this could represent seepage from a waste lagoon, sanitary landfill, or some other surface or near-surface source. Figure 9.8(b), (c), (d), and (e) shows the patterns of contaminant transport that would occur with various hypothetical stratigraphic configurations. The contaminant is assumed to be nonreactive and the effect of dispersion is neglected. The flow lines that depict the limits of the contaminant migration patterns were obtained by solution of the two-dimensional form of the steady-state groundwater flow equation [Eq. (2.69)], using the finite-element method in the manner described by Pickens and Lennox (1976). Figure 9.8(b) indicates that in situations where the flow domain is homogeneous, the contaminant migration pattern would be simple and relatively easy to monitor. The conditions for the flow system shown in Figure 9.8(c) are similar to the previous case, with the exception of the inclusion of a thin, higher-conductivity horizontal layer that extends across the flow domain. This would cause the contaminants to move through the flow system almost entirely in this thin layer. The total travel time would be one-fifth of the nonstratified case illustrated in Figure 9.8(b). The thin higher conductivity bed has a conductivity 100 times larger than the rest of the system and exerts a very strong influence on the migration patterns and velocity distribution. If the lower-K medium (K_1) represents a very fine-grained sand, the higher-K bed (K_2) could represent a medium- or coarse-grained sand. In stratigraphic studies of waste disposal sites, a thin medium-grained sand bed in an otherwise fine-grained sand deposit could easily be unnoticed unless careful drilling and sampling techniques are used.

In Figure 9.8(d) a discontinuous layer of low-conductivity material exists in the cross section. The contaminant migration zone moves over the first lense and under the second one. To reach the discharge area, it passes through the second lense near the end of its flow path.

Figure 9.8(e) shows the contaminant migration pattern that would exist if a thin higher-conductivity bed is discontinuous through the central part of the cross section. The discontinuity causes a large distortion in the contaminant migration pattern in the middle of the cross section. The contaminated zone spreads out in the central part of the flow system and extends to the water-table zone. In situations where contaminants can be transferred through the unsaturated zone by advection, diffusion, or vegetative uptake, this condition could lead to spread of the contaminants in the biosphere. Figure 9.8(e) also illustrates some of the difficulties that can arise in monitoring contaminated flow systems. If little information were available on the stratigraphy of the system, there would be no reason to suspect that the type of distortions shown in Figure 9.8(e) would occur. Lack of this information could result in inadequate monitoring of the system. In nature, geologic cross sections typically include many stratigraphic units with different hydraulic conductivities. Large conductivity contrasts across sharp discontinuities are common. Relative to real situations, the effects of stratification illustrated in Figure 9.8 are very simple.

In the discussion above, layered heterogeneities on the scale that could, if necessary, be identified and mapped by careful drilling, sampling, and geophysical logging were considered. Heterogeneities in another category also exist in most geologic settings. These are known as small-scale heterogeneities. They cannot be identified individually by conventional methods of field testing. Even if identification is possible using special coring techniques, these heterogeneities usually cannot be correlated from borehole to borehole. In granular aquifers, heterogeneities of this type are ubiquitous. Hydraulic conductivity contrasts as large as an order of magnitude or more can occur as a result of almost unrecognizable variations in grain-size characteristics. For example, a change of silt or clay content of only a few percent in a sandy zone can have a large effect on the hydraulic conductivity.

Figure 9.9 illustrates the effect of two types of small-scale heterogeneities on the pattern of migration of a tracer or contaminant in granular porous media. In Figure 9.9(a) the pattern of dispersion is regular and predictable using the methods described above. In Figure 9.9(b) the lense-type heterogeneities cause the

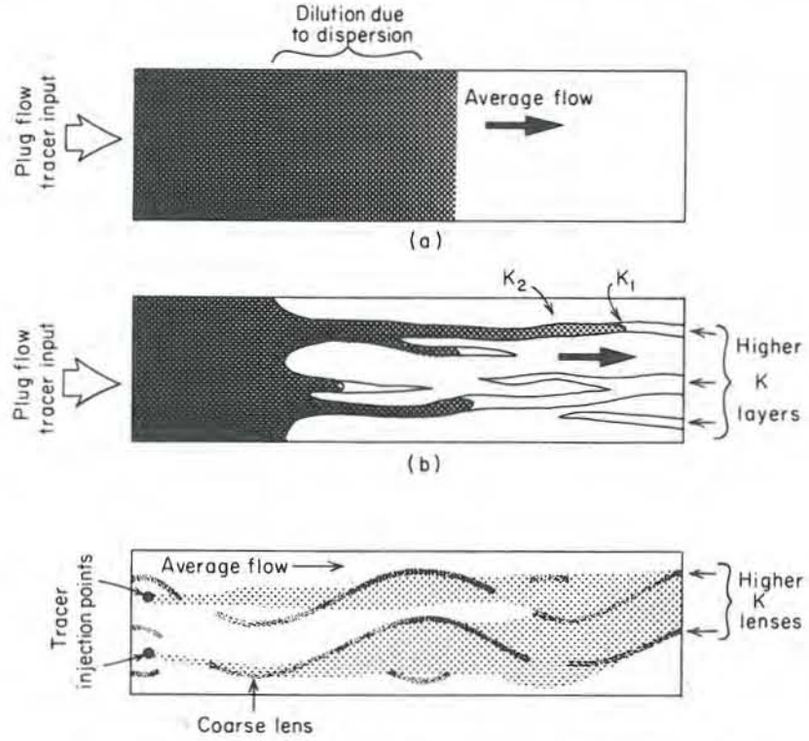

Figure 9.9 Comparison of advance of contaminant zones influenced by hydrodynamic dispersion. (a) Homogeneous granular medium; (b) fingering caused by layered beds and lenses; (c) spreading caused by irregular lenses.

tracer front to advance in a pattern commonly referred to as *fingering*. In this case the contaminant is transported more rapidly in the lenses or beds of higher hydraulic conductivity. Figure 9.9(c) illustrates results obtained by Skibitzke and Robertson (1963) using dye tracers in a box model packed with fine sand and long sinuous lenses of coarser sand. These authors observed that a large angle of refraction at the boundary between sand of contrasting permeability caused accelerated spreading of the tracer zone.

In one of the very few detailed three-dimensional studies of contaminant movement in sandy deposits, Childs et al. (1974) observed that "plumes migrate along zones . . . that, although they are texturally similar, show subtle differences in fabric that result in slight variations in permeability. Bifurcations indicate that detection of a shallow plume does not negate the existence of the other plumes of the same constituent at depth" (p. 369).

Nearly all studies of dispersion reported in the literature have involved relatively homogeneous sandy materials under controlled conditions in the laboratory. These studies have indicated that the dispersivity of these materials is small. Values of longitudinal dispersivity are typically in the range of 0.1 to 10 mm, with transverse dispersivity values normally lower by a factor of 5–20. Whether or not these values are at all indicative of dispersivities in field systems is subject to considerable controversy at the present time. Many investigators have concluded that values of longitudinal and transverse dispersivities in field systems are significantly larger than values obtained in laboratory experiments on homogeneous materials or on materials with simple heterogeneities. Values of longitudinal dispersivity as large as 100 m and lateral dispersivity values as large as 50 m have been used in mathematical simulation studies of the migration of large contaminant plumes in sandy aquifers (Pinder, 1973; Konikow and Bredehoeft, 1974; Robertson, 1974).

To illustrate the effect of large dispersivities on the migration of contaminants in a hypothetical groundwater flow system, a cross-sectional flow domain similar to that shown in Figure 9.8(a) and (b) will be used. Figure 9.10 shows the effect of dispersivity on the spreading of a contaminant plume that emanates from a source in the recharge area of the flow system. Although the cross sections shown in Figure 9.10 are homogeneous, dispersivities for the system are assumed to be large as a result of small-scale heterogeneities. With assigned values of dispersivity the patterns of contaminant distribution can be simulated using a finite-element approximation to the transport equation expressed in two-dimensional form for saturated heterogeneous isotropic media [Eq. (A10.13), Appendix X]:

$$\frac{\partial}{\partial s_l}\left(D_l \frac{\partial C}{\partial s_l}\right) + \frac{\partial}{\partial s_t}\left(D_t \frac{\partial C}{\partial s_t}\right) - \frac{\partial}{\partial s_l}(\bar{v}_l C) = \frac{\partial C}{\partial t} \tag{9.8}$$

where s_l and s_t are the directions of the groundwater flowlines and the normals to these lines, respectively. The finite-element model used to obtain the contaminant distributions shown in Figure 9.10 is described by Pickens and Lennox (1976).

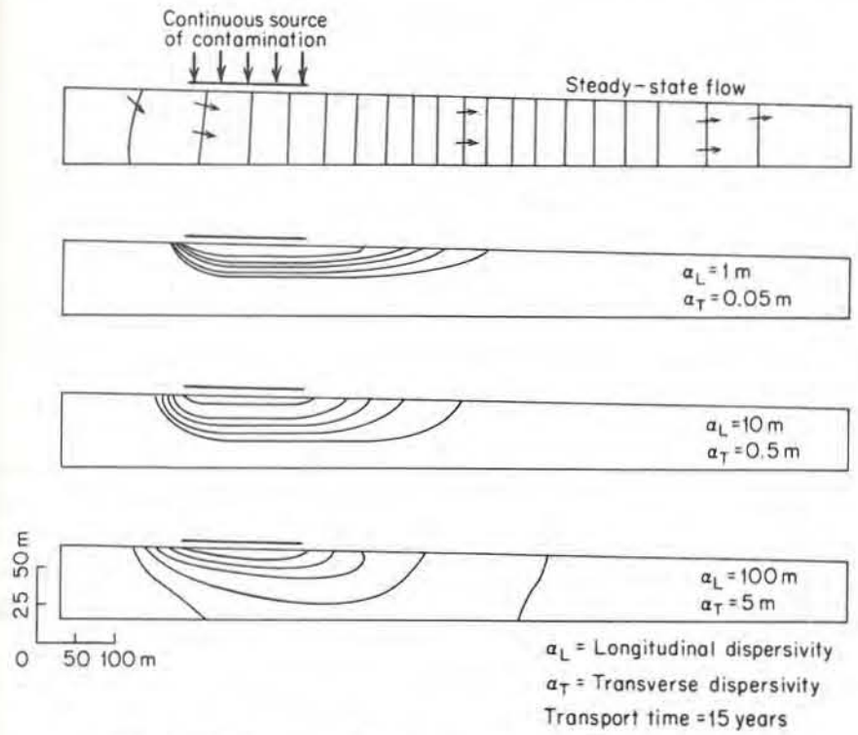

Figure 9.10 Dispersion of a contaminant during transport in a shallow groundwater flow system. Porosity 30%; hydraulic conductivity 0.5 m/day; $\alpha_l/\alpha_t = 20$; transport time 15 years; concentration contours at $C/C_0 = 0.9, 0.7, 0.5, 0.3$, and 0.1 (after Pickens and Lennox, 1976).

Other numerical models have been developed by Reddell and Sunada (1970), Bredehoeft and Pinder (1973), Pinder (1973), and Schwartz (1975). The simulations presented in Figure 9.10 indicate that if dispersivity is large, contaminants can spread to occupy a portion of the flow system many times larger than would be the case in the presence of advection alone. If the transverse dispersivity is very large as indicated in Figure 9.10, contaminants transported along relatively horizontal flow paths can migrate deep into the flow system. The longitudinal and transverse dispersivities represented in the simulated contaminant transport patterns shown in Figure 9.10 indicate that if dispersivity values are orders of magnitude larger than the values obtained from laboratory experiments, dispersion will exert a strong influence on contaminant transport. Whether or not dispersivities in nonfractured geologic materials under field conditions have magnitudes that are this large remains to be established by detailed field experiments. This topic is discussed further in Section 9.4.

Transport of Reactive Constituents

In this section we will consider the transport of solutes that behave as those described above, but with the added influence of chemical reactions. Changes in concentration can occur because of chemical reactions that take place entirely within the aqueous phase or because of the transfer of the solute to or from other phases such as the solid matrix of the porous medium or the gas phase in the unsaturated zone. The myriad of chemical and biochemical reactions that can alter contaminant concentrations in groundwater flow systems can be grouped in six categories: adsorption-desorption reactions, acid-base reactions, solution-precipitation reactions, oxidation-reduction reactions, ion pairing or complexation, and microbial cell synthesis. Radioactive contaminants are influenced by radioactive decay in addition to the nonradiogenic processes. In the following discussion we will focus on adsorption as a concentration-altering mechanism. In Section 9.3 other types of reactions are considered.

For homogeneous saturated media with steady-state flow, the one-dimensional form of the advection-dispersion equation expressed in a manner that includes the influence of adsorption [Eq. (A10.14), Appendix X] is

$$D_l \frac{\partial^2 C}{\partial l^2} - \bar{v}_l \frac{\partial C}{\partial l} + \frac{\rho_b}{n} \frac{\partial S}{\partial t} = \frac{\partial C}{\partial t} \tag{9.9}$$

where ρ_b is the bulk mass density of the porous medium, n is the porosity, and S is the mass of the chemical constituent adsorbed on the solid part of the porous medium per unit mass of solids. $\partial S/\partial t$ represents the rate at which the constituent is adsorbed $[M/MT]$, and $(\rho_b/n)(\partial S/\partial t)$ represents the change in concentration in the fluid caused by adsorption or desorption

$$\frac{M}{L^3}\frac{M}{MT} = \frac{M}{L^3}\frac{1}{T}$$

Adsorption reactions for contaminants in groundwater are normally viewed as being very rapid relative to the flow velocity. The amount of the contaminant that is adsorbed by the solids (i.e., the degree of adsorption) is commonly a function of the concentration in solution, $S = f(C)$. It follows that

$$-\frac{\partial S}{\partial t} = \frac{\partial S}{\partial C} \cdot \frac{\partial C}{\partial t} \tag{9.10}$$

and

$$-\frac{\rho_b}{n} \cdot \frac{\partial S}{\partial t} = \frac{\rho_b}{n} \cdot \frac{\partial S}{\partial C} \cdot \frac{\partial C}{\partial t} \tag{9.11}$$

in which the term $\partial S/\partial C$ represents the partitioning of the contaminant between the solution and the solids.

The partitioning of solutes between liquid and solid phases in a porous medium as determined by laboratory experiments is commonly expressed in two-ordinate graphical form where mass adsorbed per unit mass of dry solids is plotted against the concentration of the constituent in solution. These graphical relations of S versus C and their equivalent mathematical expressions are known as isotherms. This term derives from the fact that adsorption experiments are normally conducted at constant temperature.

Results of adsorption experiments are commonly plotted on double-logarithmic graph paper. For solute species at low or moderate concentrations, straight-line graphical relations are commonly obtained over large ranges of concentration. This condition can be expressed as

$$\log S = b \log C + \log K_d$$

or

$$S = K_d C^b \tag{9.12}$$

where S is the mass of the solute species adsorbed or precipitated on the solids per unit bulk dry mass of the porous medium, C is the solute concentration, and K_d and b are coefficients that depend on the solute species, nature of the porous medium, and other conditions of the system. Equation (9.12) is known as the *Freundlich isotherm*. The slope of the log-log adsorption relation is represented by the term b in Eq. (9.12). If $b = 1$ (i.e., if the straight-line relationship between S and C on a log-log plot has a slope of 45°), then the S versus C data will also plot as a straight line on an arithmetic plot. Such an isotherm is termed *linear*, and from Eq. (9.12) with $b = 1$,

$$\frac{dS}{dC} = K_d \tag{9.13}$$

where K_d is known as the *distribution coefficient*. This parameter is widely used in studies of groundwater contamination. K_d is a valid representation of the partitioning between liquid and solids only if the reactions that cause the partitioning are fast and reversible and only if the isotherm is linear. Fortunately, many contaminants of interest in groundwater studies meet these requirements. A comprehensive treatment of adsorption isotherms is presented by Helfferich (1962), who provides detailed information on many important types of isotherms in addition to the Freundlich isotherm.

The transfer by adsorption or other chemical processes of contaminant mass from the pore water to the solid part of the porous medium, while flow occurs, causes the advance rate of the contaminant front to be retarded. To illustrate this concept, the classical column experiment shown in Figure 9.1(a) will again be considered. It is assumed that two tracers are added to the water passing through the column. One tracer is not adsorbed and therefore moves with the water. The other tracer undergoes adsorption, and as it travels through the column part of

its mass is taken up by the porous medium. The two tracers are added instantaneously to the water at the column input [step-function input as shown in Figure 9.1(b)]. As transport occurs, the two tracers are distributed in the column in the manner represented schematically in Figure 9.11. The transporting water mass represented by the nonreactive tracer moves ahead of the reactive tracer. The concentration profile for the nonadsorbed tracer spreads out as a result of dispersion. The concentration profile of the front of the reactive tracer also spreads out but travels behind the front of the nonreactive tracer. The adsorbed tracer is therefore said to be *retarded.*

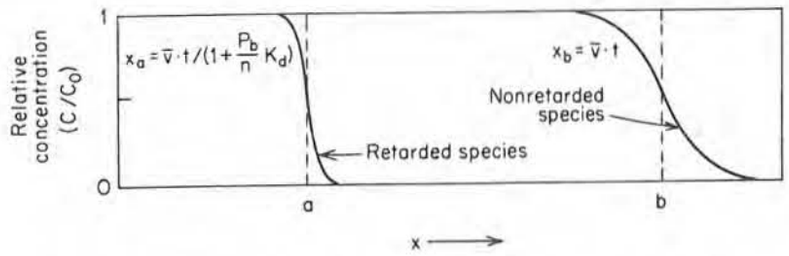

Figure 9.11 Advance of adsorbed and nonadsorbed solutes through a column of porous materials. Partitioning of adsorbed species is described by K_d. Relative velocity = $1/[1 + (\rho_b/n)K_d]$. Solute inputs are at concentration C_0 at $t > 0$.

For cases where the partitioning of the contaminant can be adequately described by the distribution coefficient (i.e., fast reversible adsorption, with linear isotherm), the retardation of the front relative to the bulk mass of water is described by the relation

$$\frac{\bar{v}}{\bar{v}_c} = 1 + \frac{\rho_b}{n} \cdot K_d \tag{9.14}$$

where $\bar{v}$ is the average linear velocity of the groundwater and $\bar{v}_c$ is the velocity of the $C/C_0 = 0.5$ point on the concentration profile of the retarded constituent. Equation (9.14) is commonly known as the *retardation equation.* The term $1 + (\rho_b/n) \cdot K_d$ is referred to as the *retardation factor.* The reciprocal of the retardation factor is known as the relative velocity ($\bar{v}_c/\bar{v}$). Equation (9.14) was originally developed on an empirical basis for use in chemical engineering by Vermeulen and Hiester (1952). It was first applied to groundwater problems by Higgins (1959) and Baetsle (1967, 1969). Baetsle indicated that it can be used to determine the retardation of the center of mass of a contaminant moving from a point source while undergoing adsorption.

To gain a more quantitative appreciation for the effects of chemical retardation on contaminant migration, some representative parameter values will be used in conjunction with Eq. (9.14). For unconsolidated granular deposits, porosity,

expressed as a fraction, is commonly in the range 0.2–0.4. The average mass density of minerals that constitute unconsolidated deposits is approximately 2.65. The range of bulk mass densities, ρ_b, that correspond to the porosity range above is 1.6–2.1 g/cm³. For these ranges of porosity and bulk mass density, ρ_b/n values range from 4 to 10 g/cm³. An approximation to Eq. (9.14) is therefore

$$\frac{\bar{v}}{\bar{v}_c} = (1 + 4K_d) \text{ to } (1 + 10K_d) \tag{9.15}$$

The only major unknown in Eq. (9.15) is the distribution coefficient K_d. The distribution coefficient can be expressed as

$$K_d = \frac{\text{mass of solute on the solid phase per unit mass of solid phase}}{\text{concentration of solute in solution}}$$

The dimensions for this expression reduce to L^3/M. Measured K_d values are normally reported as milliliters per gram (mℓ/g).

Distribution coefficients for reactive solutes range from values near zero to 10^3 mℓ/g or greater. From Eq. (9.15) it is apparent that if $K_d = 1$ mℓ/g, the midconcentration point of the solute would be retarded relative to the bulk groundwater flow by a factor between 5 and 11. For K_d values that are orders of magnitude larger than 1, the solute is essentially immobile.

To further illustrate the effect of liquid- to solid-phase partitioning, a cross-sectional flow domain similar to the one represented in Figures 9.8 and 9.10 is used. The pattern of contamination in this cross section caused by an influx of water with contaminant species of different distribution coefficients is shown in Figure 9.12. The patterns were obtained by Pickens and Lennox (1976) using a finite-element solution to the transport equation with the reaction term described by Eq. (9.11). The case in which $K_d = 0$ shows the zone occupied by a contaminant species that is not affected by chemical reactions. Under this condition the processes of advection and dispersion cause the contaminant to gradually occupy a large part of the flow domain. The transport pattern is controlled by the contaminant input history, by the velocity distribution, and by dispersion. Contaminant species with K_d values greater than zero occupy a much smaller portion of the flow domain. If $K_d = 10$ mℓ/g, most of the contaminant mass migrates only a very short distance from the input zone during the specified migration period. This situation can be anticipated from consideration of the magnitude of this K_d value in Eq. (9.15). There is an extensive zone beyond the $C/C_0 = 0.1$ contours shown in Figure 9.12 in which the contaminant occurs at very low concentrations. If the contaminant is harmful at low concentrations, this zone can be extremely important, even though it includes only a small portion of the total contaminant mass in the flow system.

When a mixture of reactive contaminants enters the groundwater zone, each species will travel at a rate depending on its relative velocity, $\bar{v}_c/\bar{v}$. After a given time t, the original contaminant cloud will have segregated into different zones,

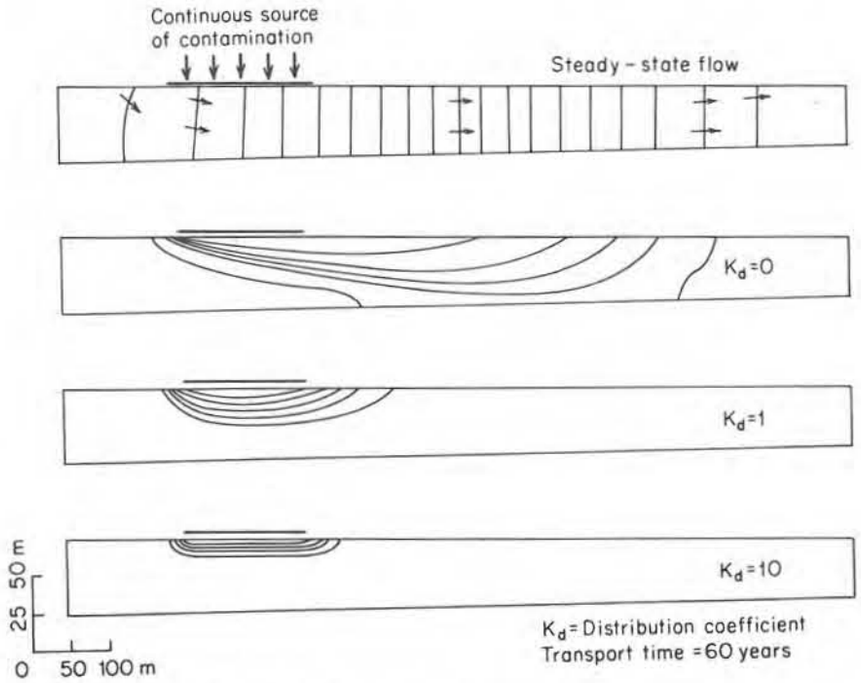

Figure 9.12 Effect of the distribution coefficient on contaminant retardation during transport in a shallow groundwater flow system. Porosity 0.3; hydraulic conductivity 0.5 m/day; α_l = 10 m; α_t = 0.5 m; transport time 60 years; concentration contours at C/C_0 = 0.9, 0.7, 0.5, 0.3, and 0.1 (after Pickens and Lennox, 1976).

each advancing in the same direction at different velocities. Considering the instantaneous point-source example described by Eqs. (9.6) and (9.7), the position of the center of mass of the migrating cloud is obtained from the relative velocity defined by the reciprocal of $\bar{v}/\bar{v}_c$ calculated from Eq. (9.14). Equation (9.6) can be used to calculate the concentration distribution of the dissolved reactive species, with substitution of τ for t, where $\tau = t(\bar{v}_c/\bar{v})$. Since the total standard deviation of a given distribution is a function of time as well as distance traveled, both parameters influence the dispersion pattern of each retarded species (Baetsle, 1969).

The distribution coefficient approach to the representation of chemical partitioning of contaminants in groundwater flow systems is based on the assumption that the reactions that partition the contaminants between the liquid and solid phases are completely reversible. As a contaminant plume advances along flow paths, the front is retarded as a result of transfer of part of the contaminant mass to the solid phase. If the input of contaminant mass to the system is discontinued, contaminants will be transferred back to the liquid phase as lower-concentration water flushes through the previously contaminated zone. In this situation the contaminant moves as a cloud or enclave through the flow system. This is illustrated

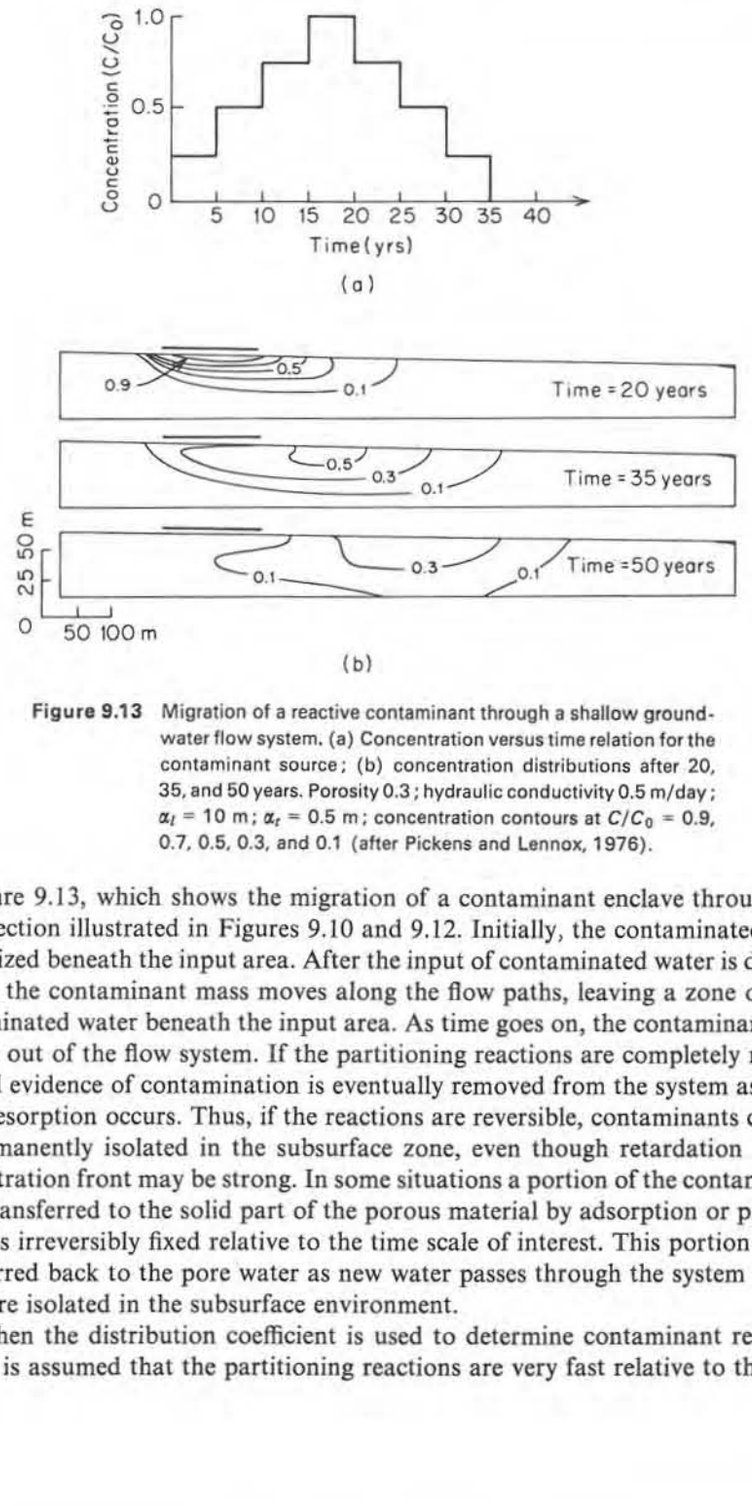

Figure 9.13 Migration of a reactive contaminant through a shallow groundwater flow system. (a) Concentration versus time relation for the contaminant source; (b) concentration distributions after 20, 35, and 50 years. Porosity 0.3; hydraulic conductivity 0.5 m/day; α_l = 10 m; α_t = 0.5 m; concentration contours at C/C_0 = 0.9, 0.7, 0.5, 0.3, and 0.1 (after Pickens and Lennox, 1976).

in Figure 9.13, which shows the migration of a contaminant enclave through the cross section illustrated in Figures 9.10 and 9.12. Initially, the contaminated zone is localized beneath the input area. After the input of contaminated water is discontinued, the contaminant mass moves along the flow paths, leaving a zone of less-contaminated water beneath the input area. As time goes on, the contaminants are flushed out of the flow system. If the partitioning reactions are completely reversible, all evidence of contamination is eventually removed from the system as complete desorption occurs. Thus, if the reactions are reversible, contaminants cannot be permanently isolated in the subsurface zone, even though retardation of the concentration front may be strong. In some situations a portion of the contaminant mass transferred to the solid part of the porous material by adsorption or precipitation is irreversibly fixed relative to the time scale of interest. This portion is not transferred back to the pore water as new water passes through the system and is therefore isolated in the subsurface environment.

When the distribution coefficient is used to determine contaminant retardation, it is assumed that the partitioning reactions are very fast relative to the rate

of groundwater movement. Many substances, however, do not react sufficiently fast with the porous medium for this assumption to be valid. When contaminants of this type move through porous media, they advance more rapidly than would be the case if the reactions produce K_d type partitioning relations. This is illustrated in Figure 9.14, which shows the nonequilibrium front in a position between the front of a nonretarded tracer and the front of a retarded tracer described by the K_d relation. Analysis of the movement of contaminants that undergo partitioning in a manner that cannot be described by equilibrium relations requires information on the rates of reaction between the contaminant and the porous medium. This information is difficult to obtain. In field studies the retardation equation described above is often used because of its simplicity or because there is a lack of information on reaction rates. This can lead to serious errors in prediction of rates of contaminant migration in systems where kinetic factors are important.

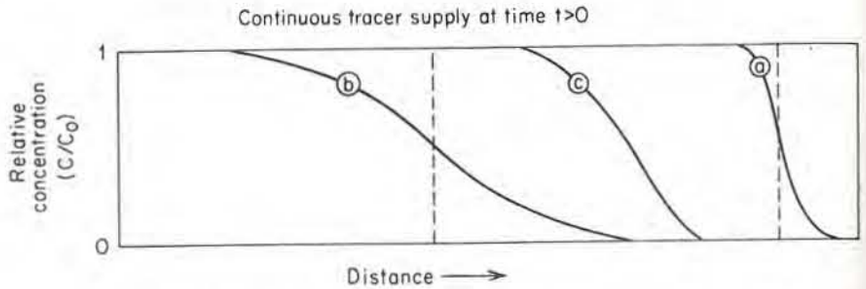

Figure 9.14 Advance of reactive and nonreactive contaminants through a column. (a) Dispersed front of nonretarded solute; (b) front of solute that undergoes equilibrium partitioning between liquid and solids; (c) front of solute that undergoes slower rate of transfer to the solids.

Transport in Fractured Media

Although contaminant transport in fractured geologic materials is governed by the same processes as in granular media—namely, advection, mechanical dispersion, molecular diffusion, and chemical reactions—the effects in fractured media can be quite different. The effective fracture porosity of fractured rocks and of consolidated cohesive materials that are fractured, such as jointed till, silt, or clay, is normally very small. Values in the order of 1–0.001%, or 10^{-2}–10^{-5} expressed as a fraction, are not unusual. Although the porosities are small, the groundwater velocities can be large. The reason for this can be deduced from the modified Darcy relation (Section 2.12)

$$\bar{v} = -\frac{K}{n_f}\frac{dh}{dl} \tag{9.16}$$

where $\bar{v}$ is the average linear velocity of water in the fractures, K the bulk hydraulic conductivity of the fractured medium, n_f the bulk fracture porosity, and dh/dl the hydraulic gradient. This relation treats the fractured medium as an equivalent porous medium. The parameters in the equations relate to a volume segment of the medium that is sufficiently large to be described by hydraulic conductivity and porosity averaged over the bulk mass. In this approach each fracture opening is considered to be very small relative to the bulk volume of the domain over which K is measured. The number of fractures in this domain therefore must be large.

For illustrative purposes we will consider a medium that has a bulk hydraulic conductivity of 10^{-8} m/s and a fracture porosity of 10^{-4}. These values could represent conditions in a slightly fractured granite. Using a hydraulic gradient of 10^{-2}, which is within the range commonly observed in field situations, the groundwater velocity computed from Eq. (9.16) is 10 m/yr. Compared to velocities in fine-grained unfractured granular materials, this velocity is very large. For example, an unfractured granular medium, such as a silt deposit, with this hydraulic conductivity and gradient and an intergranular porosity of 0.3 would have a groundwater velocity of about 0.003 m/yr. The flux of water (volume of water per unit time passing through a specified cross-sectional area) in these two cases is the same and is extremely small. Although Eq. (9.16) can be used to compute average velocities in fractured media, it provides no indication of the velocities in individual fractures. Depending on the fracture aperture and wall roughness, the velocity of groundwater may deviate from the average by orders of magnitude.

It was indicated above that in the mathematical analysis of mechanical dispersion in granular media, the media are assumed to be isotropic with respect to dispersivity. That is, longitudinal dispersivity at a point in the medium has a single value regardless of the direction of the velocity vector. Each of the transverse dispersivities has a single value relative to the longitudinal dispersivity. The differences between longitudinal and transverse dispersivities are related to the mechanism of dispersion rather than to directional properties of the medium. Fractured geologic materials, however, are notoriously anisotropic with respect to the orientation and frequency of fractures. It can be expected that the dispersion of solutes during transport through many types of fractured rocks cannot be described by the equations developed for homogeneous granular materials. Little is known about dispersion in fractured media. A common approach in field investigations of contaminant migration in fractured rock is to treat the problem in the same manner mathematically as for granular porous media. The scale at which this approach becomes valid in the analysis of field situations is not known. As a concluding comment on this topic, the statement by Castillo et al. (1972) is appropriate:

> Although the basic theoretical aspects of . . . (dispersion) . . . have been treated at length for the case where the permeable stratum is composed of granular materials, the classical concept of flow through a porous medium is generally inadequate to describe the flow behaviour in jointed rock, and it becomes increasingly unsuitable for the analysis of dispersion. Despite these limitations, little work has been directed toward extending these ideas to handle flow through jointed rock formations (p. 778).

A modification in approach is necessary for the distribution coefficient or isotherm concept to be applicable in the analysis of the migration of reactive contaminants through fractured media. For granular materials the amount of solute adsorbed on the solid part of the porous media is expressed per unit mass of the bulk medium in a dry state. For convenience the unit mass of the porous medium is used as a reference quantity. A more mechanistic but less convenient approach would be to use a unit surface area of the porous medium as the reference quantity. This would be a reasonable approach because adsorption reactions are much more closely related to the surface area of the solid medium than to the mass of the medium. Nevertheless, for granular materials such as sands, silts, and clays, the use of mass density in the definition of the distribution coefficient normally produces acceptable results. With this approach, measurements of effective surface area are not necessary.

In the case of contaminant migration through fractured materials, it is more appropriate, as suggested by Burkholder (1976), to express the distribution coefficient K_a on a per-unit-surface-area basis.

It is therefore defined as

$$K_a = \frac{\text{mass of solute on the solid phase per unit area of solid phase}}{\text{concentration of solute in solution}}$$

The dimensions for this expression are $[M/L^2 \cdot L^3/M]$ or $[L]$. The units that are commonly used are milliliters per square centimeter.

The retardation equation therefore becomes

$$\frac{\bar{v}}{\bar{v}_c} = 1 + AK_a \tag{9.17}$$

where A is the surface area to void-space (volume) ratio $[1/L]$ for the fracture opening through which the solute is being transported. It is apparent from this relation that fractures with smaller apertures produce greater retardation of reactive solutes. The distribution coefficient in this retardation expression has the same inherent assumptions as Eq. (9.14), namely: the partitioning reactions are reversible and fast relative to the flow velocity.

Equation (9.17) is simple in conceptual terms, but it is difficult to apply to natural systems. If information can be obtained on the aperture of a fracture and if the fracture surface is assumed to be planar, $A = 2/b$, where b is the aperture width (Section 2.12). Fracture surfaces usually have small-scale irregularities and therefore can have much larger surface areas than planar surfaces. In the determination of the adsorption isotherm or distribution coefficient for the fracture, the partitioning of the contaminant between fluid in contact with the fracture and the fracture surface is measured. If the fracture surface is irregular or contains a coating of weathered material or chemical precipitates, the actual surface area with which the contaminant reacts is unknown. Without an elaborate experimental effort, it is indeterminant. A practical approach is to express the K_a relative

to the area of an assumed planar fracture surface, in which case the retardation relation becomes

$$\frac{\bar{v}}{\bar{v}_c} = 1 + \frac{2K_a}{b} \tag{9.18}$$

It should be kept in mind that Eq. (9.17) is only valid for fractured materials in which the porosity of the solid mass between fractures is insignificant. When contaminants occur in fractures, there is a gradient of contaminant concentration between the fracture fluid and the fluid in the unfractured material adjacent to the fracture. If the solid matrix is porous, a portion of the contaminant mass will move by molecular diffusion from the fracture into the matrix. This mass is therefore removed, at least temporarily, from the flow regime in the open fracture.

Figure 9.15 illustrates the effect of matrix diffusion on the concentration distribution of nonreactive and reactive contaminants migrating through a fracture in a medium with a porous matrix. For illustrative purposes it is assumed that dispersion within the fracture is insignificant. Comparison of Figure 9.15(a) and (b) indicates that diffusion into the matrix causes the concentration in the fracture to diminish gradually toward the front of the advancing contaminant zone. The bulk mass of the advancing contaminant zone in the fracture appears to be retarded

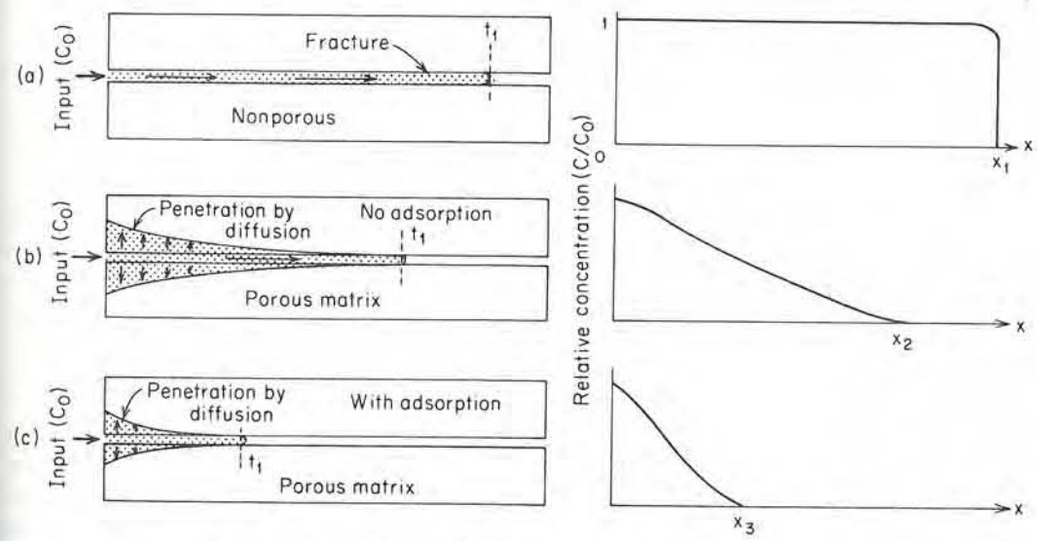

Figure 9.15 Effect of diffusion on contaminant migration in porous fractured medium. (a) Unidirectional hydraulic transport in a fracture in a nonporous medium; (b) unidirectional hydraulic transport with migration into matrix as a result of molecular diffusion; (c) unidirectional hydraulic transport with molecular diffusion and adsorption (profiles of relative concentration of reactive contaminant within fracture shown at time t_1).

because part of the contaminant mass is transferred to the matrix. The general shape of the longitudinal profile is somewhat similar to that produced by longitudinal dispersion in granular materials. If the contaminant undergoes adsorption, the effect of diffusion is to cause adsorption to occur on a much larger surface area than would be the case if the contaminant mass remained entirely within the fracture. A portion of the contaminant is adsorbed on the surface of the fracture and as diffusion occurs a portion is adsorbed in the matrix. The combined effect of adsorption on the fracture surface and adsorption in the matrix is to cause the contaminant mass in the fracture to be retarded relative to the advance that would occur in the absence of adsorption [Figure 9.15(c)].

The contaminant distribution in a porous fractured aquifer receiving waste from a surface source is illustrated schematically in Figure 9.16. As time goes on, the zone of contamination will diffuse farther into the porous matrix. If the source of contamination is discontinued, the contaminant mass in the porous matrix will eventually diffuse back to the fracture openings as fresh water flushes through the fracture network.

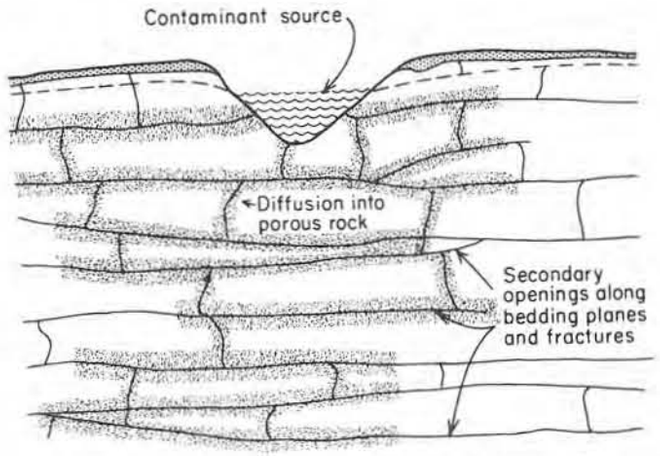

Figure 9.16 Schematic representation of contaminant migration from a surface source through fractured porous limestone.

Molecular diffusion is a process that occurs at a sufficiently rapid rate to exert a strong influence on contaminant behavior in many types of fractured materials. Even granite has appreciable primary porosity and permeability, with porosity values commonly as large as 0.05–1.0% and hydraulic conductivity in the order of 10^{-12} m/s. In the main limestone aquifer in Britain, detailed studies show that subsurface distributions of tritium and nitrate in the limestone are strongly influenced by diffusion of these constituents from the fractures, where rapid flow occurs, into the porous rock matrix (Foster, 1975). In the Plains Region of North America, deposits of glacial till and glaciolacustrine clay are commonly fractured (Section 4.4). Grisak et al. (1976) indicate that although the fractures are generally a major avenue of groundwater flow, the chemical evolution of groundwater is controlled by diffusion of dissolved reaction products from the clayey matrix into the fracture network.

9.3 Hydrochemical Behavior of Contaminants

In this section, the hydrochemical behavior of groundwater contaminants will be discussed. It is not feasible for all the hydrochemical processes that affect contaminants in groundwater to be considered in this text. Our purpose is to illustrate some of the most important processes that control the behavior of several groups of contaminants with different hydrochemical properties. The origin and causes of groundwater contamination are discussed in Section 9.4.

Nitrogen

The most common contaminant identified in groundwater is dissolved nitrogen in the form of nitrate (NO_3^-). This contaminant is becoming increasingly widespread because of agricultural activities and disposal of sewage on or beneath the land surface. Its presence in undesirable concentrations is threatening large aquifer systems in many parts of the world. Although NO_3^- is the main form in which nitrogen occurs in groundwater, dissolved nitrogen also occurs in the form of ammonium (NH_4^+), ammonia (NH_3), nitrite (NO_2^-), nitrogen (N_2), nitrous oxide (N_2O), and organic nitrogen. Organic nitrogen is nitrogen that is incorporated in organic substances.

Nitrate in groundwater generally originates from nitrate sources on the land surface, in the soil zone, or in shallow subsoil zones where nitrogen-rich wastes are buried (Figure 9.17). In some situations NO_3^- that enters the groundwater system originates as NO_3^- in wastes or fertilizers applied to the land surface. These are designated as direct nitrate sources in Figure 9.18. In other cases, NO_3^- originates by conversion of organic nitrogen or NH_4^-, which occur naturally or are introduced to the soil zone by man's activities. The processes of conversion of organic nitrogen to NH_4^- is known as *ammonification*. Through the process of *nitrification*, NH_4^+ is converted to NO_3^- by oxidation. Ammonification and nitrification are processes that normally occur above the water table, generally in the soil zone, where organic matter and oxygen are abundant. Thus, in Figure 9.18 these processes are represented as NO_3^- producers outside the boundaries of the groundwater flow system.

Concentrations of NO_3^- in the range commonly reported for groundwater are not limited by solubility constraints. Because of this and because of its anionic form, NO_3^- is very mobile in groundwater. In groundwater that is strongly oxidizing, NO_3^- is the stable form of dissolved nitrogen. It moves with the groundwater with no transformation and little or no retardation. Very shallow groundwater in highly permeable sediment or fractured rock commonly contains considerable

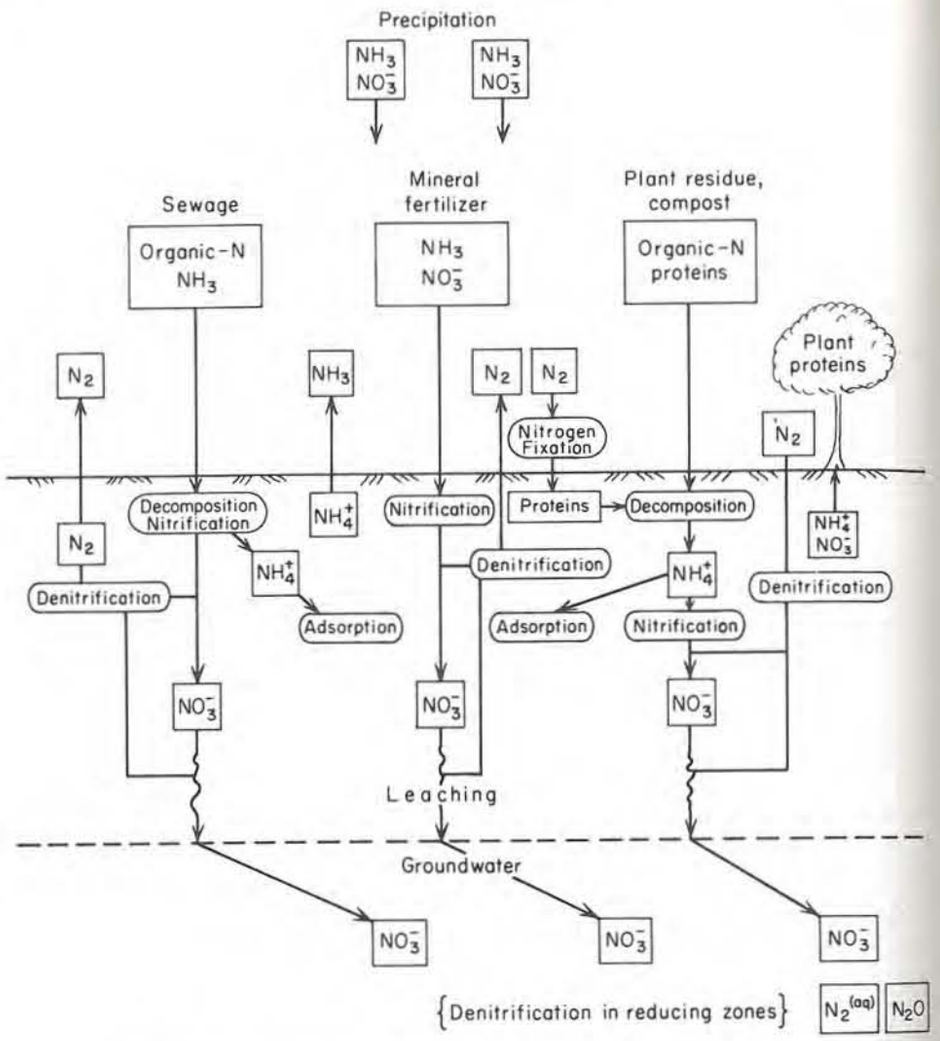

Figure 9.17 Sources and pathways of nitrogen in the subsurface environment.

dissolved O_2. It is in these hydrogeologic environments where NO_3^- commonly migrates large distances from input areas.

A decline in the redox potential of the groundwater can, in some situations, cause denitrification, a process in which NO_3^- is reduced to N_2O or N_2 (Figure 9.17). This process is represented chemically in Table 3.11. In an ideal system, which can be described by reversible thermodynamics, denitrification would occur at a redox potential of about 4.2 as pE (or +250 mv as Eh) in water at pH 7 and

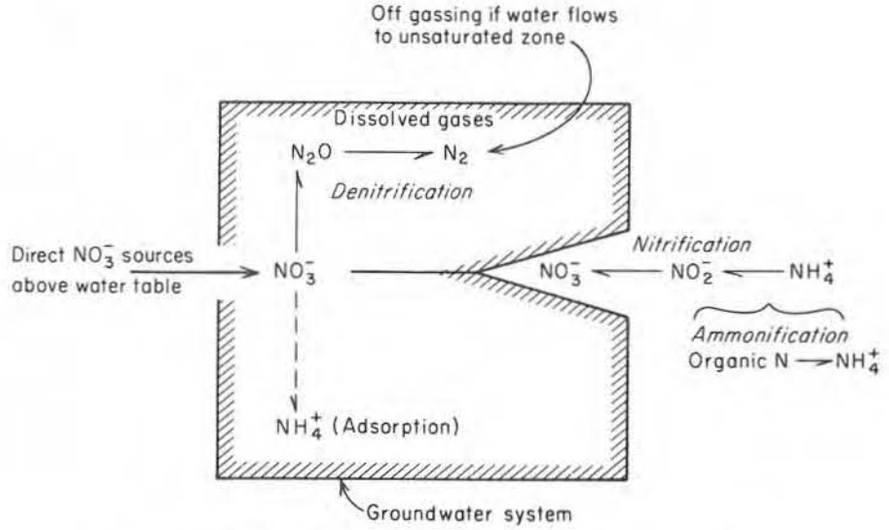

Figure 9.18 Nitrogen inputs and transformations in the groundwater system.

25°C. At this redox potential, the water would be devoid of dissolved O_2 (i.e., below the detection limit). The NO_3^- is reduced to N_2O and then, if the redox potential declines further, the N_2O is reduced to N_2. These reaction products exist as dissolved species in the groundwater. If the water moves into the unsaturated zone, a portion of the N_2O or N_2 may be lost by off-gassing to the soil air (Figure 9.18).

Figure 9.18 indicates that in addition to the denitrification pathway for the reduction of NO_3, there is a pathway that leads to NH_4^+. For biochemical reasons only a small fraction of the NO_3^- that undergoes reduction follows this reduction path. If NH_4^+ is produced in groundwater by this process, most of it would eventually be adsorbed on clay or silt-sized particles in the geologic materials.

From a water-quality viewpoint, denitrification in groundwater is a desirable process. Increased concentrations of dissolved N_2 and N_2O are not detrimental to drinking water. In contrast, NO_3^- at concentrations above 45 mg/ℓ renders water unfit for consumption by human infants. If water has more than 450 mg/ℓ of NO_3^-, it is unsuitable for consumption by livestock.

Denitrification is a process that has been observed in numerous investigations of soil systems in the laboratory and in the field. Given a source of organic matter and abundant NO_3^-, bacterial systems in soil are capable of denitrifying large amounts of NO_3^-. Denitrification in the groundwater zone, however, is a process about which little is known. It appears that a lack of suitable types or amounts of organic matter in the groundwater zone commonly inhibit the growth of denitrifying bacteria in groundwater. This limits the rate of denitrification, even if the redox system has evolved toward reducing conditions. However, since groundwater

commonly flows at low velocity, a slow rate of denitrification may nevertheless be significant with respect to the nitrate budget of the subsurface environment. For discussions of field situations in which evidence indicating denitrification in aquifers is presented, the reader is referred to Edmunds (1973) and Gillham and Cherry (1978).

Trace Metals

In recent years the mobility of trace metals in groundwater has received considerable attention. Of special interest are the trace metals for which maximum permissible or recommended limits have been set in drinking water standards. These include Ag, Cd, Cr, Cu, Hg, Fe, Mn, and Zn (see Table 9.1). During the next decade this list may grow as more is learned about the role of trace metals in human health and ecology. Although these elements rarely occur in groundwater at concentrations large enough to comprise a significant percentage of the total dissolved solids, their concentrations can, depending on the source and hydrochemical environment, be above the limits specified in drinking water standards. Most of the elements listed above are in an elemental group referred to by chemists as the *transition elements*. Many of these elements are also known as *heavy metals*.

Trace metals in natural or contaminated groundwaters, with the exception of iron, almost invariably occur at concentrations well below 1 mg/ℓ. Concentrations are low because of constraints imposed by solubility of minerals or amorphous substances and adsorption on clay minerals or on hydrous oxides of iron and manganese or organic matter. Isomorphous substitution or coprecipitation with minerals or amorphous solids can also be important.

A characteristic feature of most trace metals in water is their tendency to form hydrolyzed species and to form complexed species by combining with inorganic anions such as HCO_3^-, CO_3^{2-}, SO_4^{2-}, Cl^-, F^-, and NO_3^-. In groundwater environments contaminated with dissolved organic compounds, organic complexes may also be important. Expressed in terms of the products of hydrolysis, the total concentration of a trace metal M_T that in the unhydrolyzed form exists as M^{n+} is

$$M_T = (M^{n+}) + (MOH^{(n-1)+}) + (M(OH)_2^{(n-2)+}) + \dots$$

If the total concentration, M_T, is known, the concentrations of the other species can be computed using mass-action equations with equilibrium constants derived from thermodynamic data (Leckie and James, 1974). Using zinc as an example, the hydrolyzed species *and* inorganic complexes that would form would include $ZnOH^+$, $Zn(OH)_2^\circ$, $Zn(OH)_4^{2-}$, $ZnCl^-$, $ZnSO_4^\circ$, and $ZnCO_3^\circ$. The occurrence and mobility of zinc in groundwater requires consideration of these and other dissolved species. Chemical analyses of zinc in groundwater provide direct information only on the total zinc content of water. The percent of the total concentration existing as hydrolyzed species increases with increasing pH of the water. Complexes of zinc with Cl^-, SO_4^{2-}, and HCO_3^- increase with increasing concentrations of these anions in solution. In Section 3.3, it was shown that dissolved species in groundwater resulting from the formation of complexes with major ions can be computed from analyses of total concentrations of major constituents. In much the same manner, the concentration of trace-metal complexes can be computed using concentration data from laboratory analyses. Capability to predict the mobility of trace metals in groundwater can depend on the capability for prediction of the concentrations of the most important complexes formed by the element in the water. Although information on the free and complexed forms are often required for an understanding of the mobility of trace metals, the concentration values listed in water quality standards are total concentrations.

Nearly all the trace metals of interest in groundwater problems are influenced by redox conditions, as a result either of changes in the oxidation state of the trace metal or of nonmetallic elements with which it forms complexes. The redox environment may also indirectly influence trace-metal concentrations as a result of changes in solid phases in the porous medium that cause adsorption of the trace metal. In the following discussion, mercury is used for illustration of the influence of redox conditions and complexing. Diagrams of pE–pH for Hg, in water that contains Cl^- and dissolved sulfur species, are shown in Figure 9.19. Figure 9.19(a) indicates

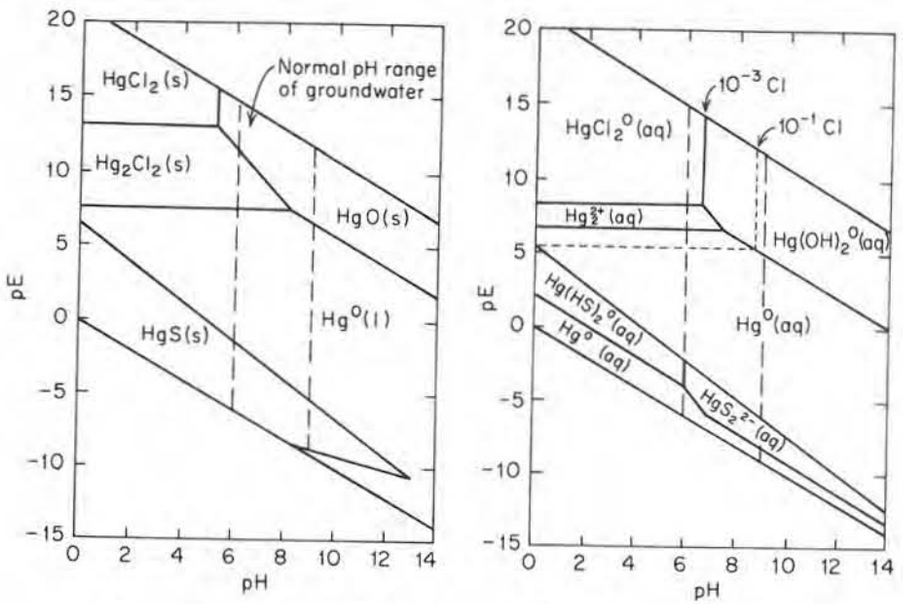

Figure 9.19 Stability fields of solid phases and aqueous species of mercury as a function of pH and pE at 1 bar total pressure. (a) Solid phases calculated for conditions of 10^{-3} molal Cl^- and SO_4^{2-} in solution; (b) aqueous species calculated for conditions of 10^{-3} molal SO_4^{2-} and 10^{-3} and 10^{-1} molal Cl^-. Fine dashed line indicates expanded boundary of $HgCl_2^\circ$(aq) field at higher Cl^- concentration (after Leckie and James, 1974).

the main solid compounds of mercury that occur in the various pH–pE stability fields and the field in which liquid mercury occurs. The dominant aqueous Hg species in equilibrium with these solid phases containing appreciable concentrations of SO_4^{2-} and Cl^- are shown in Figure 9.19(b). In high-Cl^- water, $HgCl_2^\circ$ is the dominant dissolved species of Hg in the normal pH range of groundwater under oxidizing conditions. At low Cl^- concentrations, HgO is the equilibrium solid phase and $Hg(OH)_2^\circ$ is the dominant dissolved species at high redox potential. The main equilibrium reaction in this pH-pE environment is

$$HgO + H_2O = Hg(OH)_2^\circ \tag{9.19}$$

At 25°C, log K for this reaction is −3.7. The equilibrium $Hg(OH)_2^\circ$ concentration from this reaction is therefore 47 mg/ℓ. This concentration is 4 orders of magnitude above the maximum permissible level for drinking water. In most of the pH-pE domain below the HgO(s) stability field, solubility constraints produce equilibrium concentrations of total dissolved mercury considerably below this level. In much of the redox domain, the equilibrium concentrations are below the maximum levels permitted in drinking water.

Some of the other trace metals also have large equilibrium concentrations in waters with high redox potential. In anaerobic groundwaters, the relative insolubility of sulfide minerals can limit trace metals to extremely low concentrations. In nonacidic groundwaters with high concentrations of dissolved inorganic carbon, solubility of carbonate materials will, if equilibrium is achieved, maintain concentrations of metals such as cadmium, lead, and iron at very low levels. This is the case provided that excessive amounts of inorganic or organic complexing substances are not present in the water.

In addition to the constraints exerted by solubilities of solid substances and the effects thereon caused by the formation of dissolved complexes, the occurrence and mobility of trace metals in groundwater environments can be strongly influenced by adsorption processes. In some groundwaters, many of the trace metals are maintained by adsorption at concentrations far below those that would exist as a result only of solubility constraints. Trace-metal adsorption in subsurface systems occurs because of the presence of clay minerals, organic matter, and the other crystalline and amorphous substances that make up the porous media. In some geologic materials trace-metal adsorption is controlled by crystalline or amorphous substances that are present in only small quantities. For example, Jenne (1968) indicates that hydrous oxides of Fe and Mn furnish the principal control on the fixation of Co, Ni, Cu, and Zn in soils and freshwater sediments. In oxidizing environments, these oxides occur as coatings on grains and can enhance the adsorptive capability of the medium far out of proportion to their percent occurrence relative to the other solids. The hydrous oxide coatings can act as scavengers with respect to trace metals and other toxic constituents.

Hydrous iron and manganese oxide precipitates are usually denoted as $Fe(OH)_3$(s) and MnO_2(s). FeOOH(s) is sometimes used to designate the iron oxide

precipitates. The oxides of iron and manganese may be X-ray amorphous (i.e., noncrystalline) or crystalline. In crystalline form hydrous iron oxide is known as the mineral goethite, or if the composition is Fe_2O_3, as hematite. Hydrous iron oxide precipitates are generally mixtures of different phases. Crystalline forms such as goethite and hematite form as a result of long-term aging of amorphous precipitates (Langmuir and Whittemore, 1971).

A pH–Eh diagram for iron in water that contains dissolved inorganic carbon and dissolved sulfur species is shown in Figure 9.20. Within the pH range typical of groundwater, $Fe(OH)_3$(s) is thermodynamically stable at moderate to high pE values. In groundwaters with appreciable dissolved inorganic carbon and sulfur, $FeCO_3$(s) (siderite) and FeS_2(pyrite or marcasite) are stable at lower pE values. In Figure 9.20 the boundaries of the $Fe(OH)_3$(s) field have considerable uncertainty because of uncertainty in free-energy data for $Fe(OH)_3$(s). Nevertheless, the pH–pE diagram serves to illustrate that the existence of $Fe(OH)_3$(s) is dependent on

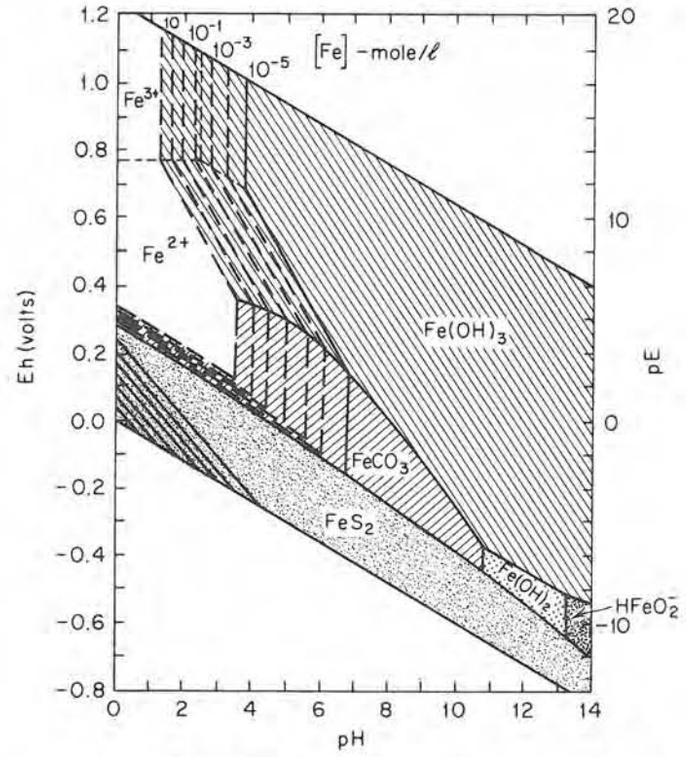

Figure 9.20 Stability fields for main solid phases and aqueous species of iron in water as a function of pH and pE, 25°C and 1 bar. Dashed lines represent solubility of iron. Stability fields and iron solubility calculated for conditions of total dissolved sulfur = 10^{-4} mol/ℓ and bicarbonate = 10^{-2} mol/ℓ (after Hem, 1967).

the redox conditions. From this it follows that the trace-metal adsorption capability of a groundwater system may vary greatly from one zone to another. If man's activities disturb the pH–pE regime, a zone that initially has a strong capability for trace-metal adsorption may lose this capability, or the reverse situation may occur.

In summary, it can be concluded that the environmental chemistry of trace metals is complex. It is difficult to predict their transport behavior within groundwater flow systems. In many subsurface environments adsorption and precipitation reactions cause fronts of these elements to move very slowly relative to the velocity of the groundwater. It is not surprising, therefore, that relatively few instances of trace-metal pollution of groundwater have been reported (Kaufman, 1974). In situations where trace-metal contamination does occur, however, the consequences can be serious.

More comprehensive reviews of trace-metal behavior in aqueous systems are provided by Leckie and James (1974) and Leckie and Nelson (1977). The occurrence and controls of trace metals in natural and contaminated groundwaters have been reviewed by Matthess (1974).

Trace Nonmetals

Of the many nonmetals listed in the periodic table of the elements, only a few have received much attention in groundwater investigations. These include carbon, chlorine, sulfur, nitrogen, fluorine, arsenic, selenium, phosphorus, and boron. Dissolved forms of carbon (HCO_3^-, CO_3^{2-}, CO_2, H_2CO_3), of chlorine (Cl^-), and of sulfur (SO_4^{2-}, HS^-, H_2S) occur in abundance in most natural and contaminated groundwaters. The geochemical origin and behavior of these constituents is described in Chapters 3 and 7 and need not be pursued here. Nitrogen in groundwater was discussed previously in this chapter. Our purpose here is to briefly review the hydrochemical behavior of the other important nonmetallic, inorganic constituents that occur as contaminants or as toxic natural constituents in groundwater. The following constituents will be considered: arsenic, fluoride, selenium, boron, and phosphate. These constituents are rarely present in natural or contaminated waters at concentrations above 1 mg/ℓ. Limits for the first four constituents on this list are included in the drinking water standards (Table 9.1).

Arsenic and its compounds have been widely used in pigments, as insecticides and herbicides, as an alloy in metals, and as chemical warfare agents (Ferguson and Gavis, 1972). Synthetic organic compounds have now replaced arsenic in most of these uses, but because of past usage and contributions from ore processing wastes and from natural sources, arsenic is still an element of interest in terms of environmental quality. Based on a review of arsenic data from water supply and surface water environments, Ferguson and Gavis (1972) concluded that arsenic concentrations in natural waters often approach or exceed the limits specified in drinking water standards.

The geochemistry of arsenic has been described by Onishi and Sandell (1955). Ferguson and Gavis (1972) have reviewed the arsenic cycle in natural waters. Arsenic occurs in four oxidation states, +V, +III, 0, and −III. The −III state

is stable only at extremely low pE values. In the pH range typical of groundwater, the stable solid arsenic forms are As_2O_5(s) and As_2O_3(s). These solids are soluble enough for dissolved arsenic species to exist at concentrations well above the permissible concentration in drinking water. Under oxidizing conditions, the following species of dissolved arsenic are stable: $H_3AsO_4^\circ$, $H_2AsO_4^-$, $HAsO_4^{2-}$, and AsO_4^{3-}. Under mildly reducing conditions, $H_3AsO_3^\circ$, $H_2AsO_3^-$, and $HAsO_3^{2-}$ are predominant. At low pE values in waters with moderate or large concentrations of dissolved sulfur species, the sulfides As_2S_3 and AsS are stable. Under these conditions, total dissolved arsenic is limited by solubility constraints to concentrations far below the limit for drinking water. At higher pE conditions, however, dissolved arsenic species can occur at equilibrium concentrations that are much above the permissible limit for drinking water. The fact that the dominant dissolved species are either uncharged or negatively charged suggests that adsorption and ion exchange will cause little retardation as these species are transported along groundwater flow paths.

Of the various nonmetals for which maximum permissible limits are set in drinking water standards, two of these, fluoride and selenium, are of interest primarily because of contributions from natural sources rather than from man-derived sources. Although within the strict usage of the term, these constituents derived from natural sources are not *contaminants* even if they do occur at toxic levels, their occurrence will be discussed in this section.

Selenium is a nonmetallic element that has some geochemical properties similar to sulfur. Selenium can exist in the +VI, +IV, and −II oxidation states, and occurs in appreciable concentrations in such rocks as shale, in coal, in uranium ores, and in some soils (Lewis, 1976). The aqueous solubilities of selenium salts are in general greater than those of sulfate salts. In dissolved form in groundwater, selenium is present primarily as SeO_3^{2-} and SeO_4^{4-} ions. Experimental studies by Moran (1976) indicate that selenium concentrations in groundwater can be controlled by adsorption on coatings or colloidal particles of hydrous iron oxide. In many groundwater systems, however, there is so little selenium present in the rocks or soils that availability is the main limiting factor. There are, however, exceptions to this generalization. For example, Moran (1976) has described an area in Colorado in which waters from many wells have selenium concentrations that exceed the permissible limits for drinking water.

Fluoride, because of the beneficial effects on dental health that have been claimed for it and consequently because of its use as a municipal water-supply additive in many cities, is a constituent that has received much attention in recent decades. Fluoride is a natural constituent of groundwater in concentrations varying from less than 0.1 mg/ℓ to values as high as 10–20 mg/ℓ. Maximum permissible limits specified for drinking water range from 1.2 to 2.4 mg/ℓ (Table 9.1), depending on the temperature of the region. Concentrations recommended for optimum dental health are close to 1 mg/ℓ, but also vary slightly depending on the temperature of the region. Natural concentrations of F^- in groundwater depend on the availability of F^- in the rocks or minerals encountered by the water as it moves

along its flow paths and on solubility constraints imposed by fluorite (CaF_2) or fluorapatite, $Ca_3(PO_4)_2 \cdot CaF_2$. Equilibrium dissolution-precipitation relations for these minerals in water are

$$K_{\text{flourite}} = [Ca^{2+}][F^-]^2 \qquad \log K_{25°C} = -9.8 \qquad (9.20)$$

$$K_{\text{flourapatite}} = [Ca^{2+}]^5[F^-][PO_4^{3-}]^3 \qquad \log K_{25°C} = -80 \qquad (9.21)$$

Because of the lack of PO_4^{3-} in most groundwater environments, CaF_2 is probably the mineral phase that exerts the solubility constraint in situations where F^- is available from the host rock. However, as can be determined by substituting values in Eq. (9.20), Ca^{2+} concentrations of many hundreds of milligrams per liter are required for this solubility constraint to limit F^- concentrations to levels below drinking water standards. The fact that nearly all groundwaters are undersaturated with respect to fluorite and fluorapatite suggests that the F^- content of groundwater is generally limited by the availability of F^- in the rocks and sediments through which the groundwater moves rather than by the solubility of these minerals. Groundwater with F^- contents that exceed drinking water standards is common in the Great Plains region of North America and in parts of the southwestern United States. This suggests that F^- is more readily available from the rocks of these regions than in most other areas of North America.

Although phosphorus is not a harmful constituent in drinking water, its presence in groundwater can be of considerable environmental significance. Phosphorus additions to surface-water bodies in even small amounts can, in some circumstances, produce accelerated growth of algae and aquatic vegetation, thereby causing eutrophication of the aquatic system. Because of this, phosphorus is regarded as a pollutant when it migrates into ponds, lakes, reservoirs, and streams. The occurrence and mobility of phosphorus in groundwater is important in situations where there is a potential for groundwater to feed phosphorus into surface-water environments. Through the widespread use of fertilizers and disposal of sewage on land, the potential for phosphorus influx to surface-water systems as a result of transport through the groundwater zone is increasing.

Dissolved inorganic phosphorus in water occurs primarily as H_3PO_4, $H_2PO_4^-$, HPO_4^{2-}, and PO_4^{3-}. Since H_3PO_4 is a polyprotic acid [see discussion in Section 3.3 and Figure 3.5(b)], the relative occurrence of each of these forms of dissolved phosphorus is pH-dependent. In the normal pH range of groundwater, $H_2PO_4^-$ and HPO_4^{2-} are the dominant species. Because these species are negatively charged, the mobility of dissolved phosphorus in groundwater below the organic-rich horizons of the soil zone is not strongly limited by adsorption. The dominant control on phosphorus in the groundwater zone is the solubility of slightly soluble phosphate minerals.

Solubility control is usually attributed to one or more of the following minerals: hydroxylapatite, $Ca_5(OH)(PO_4)_3$; strengite, $FePO_4 \cdot 2H_2O$; and varisite, $AlPO_4 \cdot 2H_2O$. From the law of mass action, equilibrium expressions for precipitation-dissolution reactions of these minerals in water can be expressed as

$$K_n = [Ca^{2+}]^5[OH^-][PO_4^{3-}]^3 \qquad \log K_n = -58.5 \qquad (9.22)$$

$$K_s = [Fe^{3+}][H_2PO_4^-][OH^-]^2 \qquad \log K_s = -34.9 \qquad (9.23)$$

$$K_v = [Al^{3+}][H_2PO_4^-][OH^-]^2 \qquad \log K_v = -30.5 \qquad (9.24)$$

where K_n, K_s, and K_v are the equilibrium constants for hydroxylapatite, strengite, and varisite, respectively. The log K values are for 25°C and 1 bar. These solubility relations indicate that the concentrations of Ca^{2+}, Fe^{3+}, and Al^{3+} can control the equilibrium concentration of dissolved phosphorus in solution. Equilibrium concentrations of total dissolved phosphorus computed from the solubility relations above are shown in Figure 9.21. Since the solubilities of hydroxylapatite, strengite,

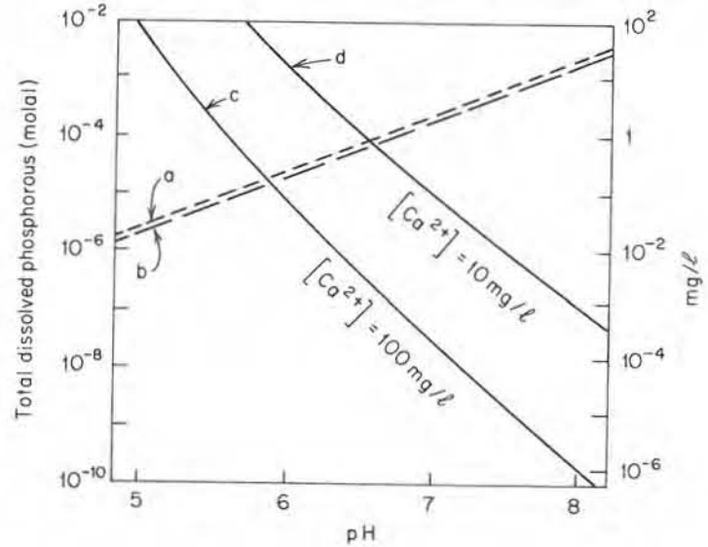

Figure 9.21 Total phosphate solubility as a function of pH. Dissolved phosphate in equilibrium with (a) variscite; (b) strengite; (c) and (d) hydroxylapatite at two calcium activities.

and varisite depend on the concentrations of Ca^{2+}, Fe^{3+}, and Al^{3+}, respectively, each solubility line is valid only for a specified concentration of these ions. Two solubility lines for hydroxylapatite (lines c and d) are shown in order to illustrate the influence of Ca^{2+} on the equilibrium phosphate concentration. The varisite solubility line (line a) is based on the assumption that the Al^{3+} concentration is governed by the solubility of gibbsite, $Al(OH)^3(s)$. For strengite solubility (line b) it is assumed that $Fe(OH)_3(s)$ limits the Fe^{3+} concentration.

From Figure 9.21 it is apparent that equilibrium concentrations of total dissolved phosphate are large in waters that have low Ca^{2+} concentrations and pH

values near or below 7. In anerobic groundwater, Fe^{2+} rather than Fe^{3+} is the dominant form of dissolved iron. In this situation strengite solubility is not a limiting factor in phosphate occurrence. Groundwaters with these characteristics, namely, low Ca^{2+} concentrations and reducing redox conditions, occur in many regions that are underlain by crystalline igneous rocks or by deposits derived from these rocks. In regions such as the Precambrian Shield region of Michigan, Minnesota, and parts of Canada, migration of dissolved phosphorus from septic systems through shallow groundwater regimes into clear-water lakes poses a significant water-quality problem. Small increases in phosphorus influx to many of these lakes can cause extensive growth of algae and undesirable aquatic vegetation. Phosphorus mobility in groundwater can be a significant factor in the environmental impact of cottage and recreational developments near lakes.

For a more extensive review of the hydrochemical controls on phosphorus in aqueous systems and soils, the reader is referred to Stumm and Morgan (1970) and Beek and De Haan (1974).

Organic Substances

In Chapter 3, it was indicated that all groundwater normally contains small amounts of dissolved organic substances of natural origin. These substances, which are referred to as humic and fulvic acids, are of little concern from a water quality viewpoint. Organic substances produced by man, however, are of great concern. The number of identified man-made organic compounds now totals near 2 million and is growing at a rate of about 250,000 new formulations annually, of which 300–500 reach commercial production (Giger and Roberts, 1977).

Increasing numbers of these substances are relatively resistant to biological degradation. Many resist removal in sewage treatment plants. It is estimated that up to one-third of the total production of today's synthetic organic compounds eventually enters the biosphere (Iliff, 1973). More than 1200 individual man-made organic substances have been identified in drinking water supplies (Shackelford and Keith, 1976). This number is increasing rapidly as investigations of organic compounds in water supplies are intensified.

The question that should be addressed here is: To what extent and under what circumstances are organic compounds causing degradation of groundwater quality? Unfortunately, this question cannot be answered at present. Since there have been so few investigations of organic compounds in groundwater, it is not possible at the present time to draw any general conclusions. Our purpose here is to briefly review some of the factors that are expected to play a major role in the migration of organic compounds into groundwater systems.

Organic chemicals make their way to the land surface as a result of the use of pesticides, the use of land for sewage disposal, the use of sanitary landfills or refuse dumps for disposal of organic compounds, burial of containers with organic compounds at special burial sites, leakage from liquid waste storage ponds, and accidental spills along highways or other transportation routes. There are hundreds of

thousands of locations in North America and Europe in which organic compounds may be a threat to groundwater quality.

Fortunately, there are several mechanisms that tend to prevent or retard the migration of most organic substances from the land surface or soil zone into deeper parts of the subsurface environment. These mechanisms include chemical precipitation, chemical degradation, volatilization, biological degradation, biological uptake, and adsorption.

Many organic substances have extremely low solubility in water. This generally limits the possibility for appreciable migration of large quantities in groundwater. However, because many of these substances are toxic at very low concentrations, solubility constraints are often not capable of totally preventing migration at significant concentration levels. For example, comparison of the solubilities and maximum permissible concentrations in drinking water of some of the common pesticides (Table 9.3) indicates that the solubilities generally exceed the permissible concentrations of these pesticides. A more comprehensive description of pesticide compositions and solubilities is presented by Oregon State University (1974).

Table 9.3 Comparison of Maximum Permissible Concentration Limits in Drinking Water and the Solubilities of Six Pesticides

Compound	Maximum permissible concentration (mg/ℓ)	Solubility in water (mg/ℓ)
Endrine	0.0002	0.2
Lindane	0.004	7
Methoxychlor	0.1	0.1
Toxaphene	0.005	3
2,4-D	0.1	620
2,4,5-TP silvex	0.01	—

NOTE: Solubilities from Oregon State University, 1974.

Many organic substances are lost from the soil zone as a result of volatilization (i.e., conversion to the vapor state). When the substances transform from the solid phase or from the dissolved phase to the vapor phase, they are lost by diffusion to the atmosphere. This process can greatly reduce the concentrations available for transport in subsurface water. For volatilization to occur, however, a gas phase must be present. Therefore, this process cannot be effective if the compounds migrate below the water table, where species occur only in dissolved form.

Nearly all pesticides and many other organic substances that make their way to the land surface and hence into the soil zone undergo biochemical degradation. The soil zone contains a multitude of bacteria that can convert and consume countless numbers of organic compounds. If it were not for these organisms, the biosphere would long ago have become intolerably polluted with organic com-

pounds. In terms of environmental contamination, the major concern is focused on those organic substances that are not readily degraded by bacteria, either in the soil zone or in sewage treatment facilities. These substances are known as *refractory compounds*. Their presence in the surface environment is becoming increasingly pervasive.

The organic substances that pose the greatest threat to the quality of groundwater resources are those that are relatively soluble, nonvolatile, and refractory. The main mechanism that prevents most of these compounds from readily migrating from the land surface into aquifer systems is adsorption. Minerals and amorphous inorganic and organic substances in the soil zone and in deeper geologic materials all provide surfaces for adsorption of organic compounds. Unfortunately, adsorption isotherms are available for only a small percentage of the existing organic chemicals that are entering the biosphere. These isotherms relate to only a small number of permeable geological materials under a limited range of hydrochemical conditions. Because of this paucity of adsorption data, it is not possible to draw general conclusions on the potential magnitude of the hazard to groundwater resources posed by increasing use and dependence on organic chemicals.

For readers interested in obtaining more information on the occurrence, classification, and movement of organic substances in groundwater and surface waters, the following introduction to the literature may be useful. Giger and Roberts (1977) describe the problems associated with characterizing refractory organic compounds in contaminated waters. A classification scheme for organic compounds in water is presented by Leenheer and Huffman (1977). The chemical, ecological, and adsorptive properties of a wide variety of insecticides and herbicides are described by the Oregon State University (1974). Malcolm and Leenheer (1973) indicate the usefulness of dissolved organic carbon measurement as a contamination indicator in groundwater and surface-water investigations. Based on an extensive literature review, Shackelford and Keith (1976) summarized the reported occurrences of organic compounds in groundwater and other waters used for drinking water supplies. The behavior of petroleum substances such as oil and gasoline in water is described by McKee (1956). Adsorption isotherms for several organic compounds in selected soils are described by Kay and Elrick (1967), Hamaker and Thompson (1972), Davidson et al. (1976), and Hague et al. (1974).

9.4 Measurement of Parameters

Velocity Determination

There are three groups of methods for determination of the velocity of groundwater. The first group includes all techniques that are directly dependent on use of the Darcy equation. The second group involves the use of artificial tracers. The third group consists of groundwater age-dating methods using environmental isotopes such as tritium and carbon 14. Darcy-based techniques require information on the hydraulic conductivity, hydraulic gradient, and porosity in the portion of

the flow field in which velocity estimates are desired. From these data the average linear velocity $\bar{v}$ can be computed using Eq. (2.82). Methods by which field values of hydraulic conductivity, hydraulic gradient, and porosity are determined are described in Chapters 2, 6, and 8. They need not be pursued here, other than to note that velocity estimates based on use of these parameters in Darcy-based equations have large inherent uncertainties that generally cannot be avoided. In field situations hydraulic conductivity determinations often have large uncertainties. Errors in hydraulic conductivity measurements combined with the errors associated with determination of the gradient and porosity result in considerable error being associated with the computed velocity. In some situations better accuracy can normally be achieved by use of artificial groundwater tracers, although this may involve greater expense.

The most direct method for groundwater velocity determination consists of introducing a tracer at one point in the flow field and observing its arrival at other points. After making adjustments for the effect of dispersion, the groundwater velocity can be computed from the travel time and distance data. The literature is replete with descriptions of experiments of this type. Many types of nonradioactive and radioactive tracers have been used, ranging from such simple tracers as salt (NaCl or $CaCl_2$), which can be conveniently monitored by measurements of electrical conductance, to radioisotopes such as ^{3}H, ^{131}I, ^{29}Br, and ^{51}Cr-EDTA (an organic complex with ^{51}Cr), which can be accurately monitored using radioactivity detectors. Radioisotopes have the disadvantage of government licensing requirements for their use and of being hazardous when used by careless workers. Fluorescent dyes (fluoroscein and rhodamine compounds) have been used by many investigators. In field tests, visual detection of the dye can sometimes yield adequate results. Dye concentrations can be measured quantitatively to very low concentrations when necessary. Recent work suggests that Freon (Cl_3CF) may be one of the best of the artificial tracers for use in groundwater velocity tests (Thompson et al., 1974). It is nonreactive with geologic materials and can be used in extremely small concentrations that are nonhazardous in public waters. For reviews of tracer techniques in groundwater investigations, the reader is referred to Knutson (1966), Brown et al. (1972), and Gaspar and Oncescu (1972).

The direct tracer method of groundwater velocity determination described above has four main disadvantages: (1) because groundwater velocities are rarely large under natural conditions, undesirably long periods of time are normally required for tracers to move significant distances through the flow system; (2) because geological materials are typically quite heterogeneous, numerous observation points (piezometers, wells, or other sampling devices) are usually required to adequately monitor the passage of the tracer through the portion of the flow field under investigation; (3) because of (1), only a small and possibly nonrepresentative sample of the flow field is tested; and (4) because of (2), the flow field may be significantly distorted by the measuring devices. As a result of these four factors, tracer experiments of this type commonly require considerable effort over extended periods of time and are rarely performed.

A tracer technique that avoids these disadvantages was developed in the USSR in the late 1940's. This technique, which has become known as the borehole dilution or point-dilution method, is now used extensively in Europe. Borehole dilution tests can be performed in relatively short periods of time in a single well or piezometer. The test provides an estimate of the horizontal average linear velocity of the groundwater in the formation near the well screen. A schematic representation of a borehole dilution test is shown in Figure 9.22(a). The test is performed in a segment of a well screen that is isolated by packers from overlying and underlying portions of the well. Into this isolated well segment a tracer is quickly introduced and is then subjected to continual mixing as lateral groundwater flow gradually removes the tracer from the well bore. The combined effect of groundwater through-flow and mixing within the isolated well segment produces a dilution versus time relation as illustrated in Figure 9.22(b). From this relation the average horizontal velocity of groundwater in the formation beyond the sand or gravel pack

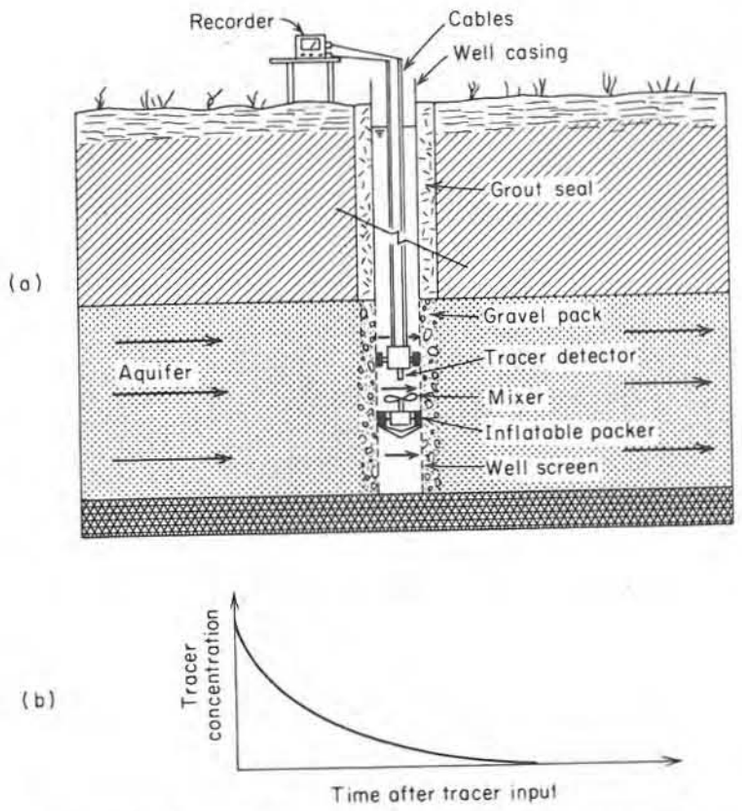

Figure 9.22 Borehole dilution test. (a) Schematic diagram of apparatus; (b) dilution of tracer with time.

but close to the well screen is computed. The theory on which the computational methods are based is described below.

Although adjustments in field technique and analytical methods can be made to take into account the effects of flow with a significant vertical component, the borehole dilution method is best suited for velocity determination in steady-state lateral flow regimes. We will proceed on this basis and with the additional stipulation that complete mixing of the tracer in the well-screen segment is maintained with no significant disturbance of the flow conditions in the formation.

The effect of the well bore and sand pack in a lateral flow regime is shown in Figure 9.23. The average linear velocity of the groundwater in the formation

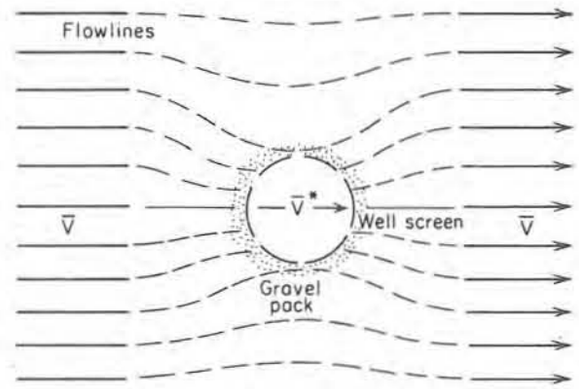

Figure 9.23 Distortion of flow pattern caused by the presence of the well screen and sand or gravel pack.

beyond the zone of disturbance is $\bar{v}$. The average bulk velocity across the center of the well bore is denoted by $\bar{v}^*$. It will be assumed that the tracer is nonreactive and that it is introduced instantaneously at concentration C_0 into the isolated segment of the well screen. The vertical cross-sectional area through the center of the isolated segment is denoted as A. The volume of this well segment is W. At time $t > 0$, the concentration C in the well decreases at a rate

$$\frac{dC}{dt} = -\frac{A \cdot \bar{v}^* \cdot C}{W} \tag{9.25}$$

which, upon rearrangement, yields

$$\frac{dC}{C} = -\frac{A \cdot \bar{v}^* \cdot dt}{W} \tag{9.26}$$

Integration and use of the initial condition, $C = C_0$ at $t = 0$, leads to

$$\bar{v}^* = -\frac{W}{A \cdot t} \ln\left(\frac{C}{C_0}\right) \tag{9.27}$$

Thus, from concentration versus time data obtained during borehole dilution tests, values of $\bar{v}^*$ can be computed. The objective of the test, however, is to obtain estimates of $\bar{v}$. This is accomplished using the relation

$$\bar{v} = \frac{\bar{v}^*}{n\bar{\alpha}} \tag{9.28}$$

where n is the porosity and α is an adjustment factor that depends on the geometry of the well screen, and on the radius and hydraulic conductivity of the sand or gravel pack around the screen. The usual range of α for tests in sand or gravel aquifers is from 0.5 to 4 (Drost et al., 1968).

Borehole dilution tests performed at various intervals within a well screen can be used to identify zones of highest groundwater velocity. These zones are often of primary interest because contaminants can move through them at velocities much higher than in other parts of the system. Identification of the high-velocity zones, which may occur in only a thin segment of an aquifer system, can provide for efficient design of monitoring networks for groundwater quality.

The borehole dilution method is described in detail by Halevy et al. (1967) and Drost et al. (1968). In most borehole dilution tests described in the literature, radioactive tracers were used. The recent advent of commercially available electrodes for use with portable pH meters for rapid down-hole measurement of Cl^- or F^- has made it feasible to conduct borehole-dilution tests with these readily available tracers in a more convenient manner than was previously the case. An example is described by Grisak et al. (1977). An even simpler approach involves the use of salt as the tracer with down-hole measurement of electrical conductance as the salt is flushed from the well screen. Borehole dilution tests, like many other types of field tests used in groundwater studies, can be accomplished using simple, inexpensive equipment or more elaborate instrumentation. The choice of method depends on factors such as the hydrogeologic setting, availability of instrumentation, and the experimental precision and reproducibility that is desired.

Dispersivity

From a measurement point of view, the most elusive of the solute transport parameters is dispersivity. Longitudinal dispersivity can be measured in the laboratory by passing a nonreactive tracer through cylindrical samples collected from boreholes or excavations. These experiments produce break-through curves as illustrated in Figure 9.1(c). The dispersivity of the sample can be computed by fitting solutions of the advection-dispersion equation to the experimentally determined breakthrough curve. If the breakthrough curve is obtained from a column test with step-function tracer input, Eq. (9.5) can be used in the analyses of the curve. The velocity is obtained by dividing the specific discharge of water through the column by the porosity. Dispersivity is then obtained as the remaining unknown in the equation. Dispersivity values obtained from column tests on disturbed or undisturbed samples of unconsolidated geological materials invariably yield values

in the range 0.01–2 cm. Based on 2500 column dispersion tests of this type, Klotz and Moser (1974) observed that values of longitudinal dispersivity depend on grain size and grain-size distribution and are independent of grain shape, roughness, and angularity.

Longitudinal dispersivity values determined by column tests are generally viewed as providing little indication of the *in situ* dispersivity of the geologic materials. Dispersivity has the distinction of being a parameter for which values determined on borehole-size samples are commonly regarded as having little relevance in the analysis of problems at the field scale.

It is generally accepted that longitudinal and transverse dispersivities under field conditions are larger than those indicated by tests on borehole samples. In other words, tracer or contaminant spreading in the field as a result of dispersion is greater than is indicated by laboratory measurements. This difference is normally attributed to the effects of heterogeneities on the macroscopic flow field. Since most heterogeneities in geological materials occur at a larger scale than can be included in borehole samples, dispersivity values from tests on small samples can be viewed as representing a property of the medium but at a scale of insufficient size for general use in prediction of dispersion in the field.

Studies of contaminant migration under field conditions require dispersivity measurements in the field. Although this premise is generally accepted, there is little agreement on the types of field dispersivity tests or methods for test analysis that are most appropriate. This state of affairs may be the result of the fact that relatively few detailed field dispersivity tests have been conducted, rather than a result of excessive difficulties of the task. It has only been in recent years that dispersivity at the field scale has received much attention. In comparison to the many thousands of field hydraulic conductivity and transmissivity tests that have been conducted in the common types of geologic materials, only a few tens of field dispersivity tests are reported in the literature.

There are four main types of field dispersivity tests. These are (1) single-well withdrawal-injection tests, (2) natural-gradient tracer tests, (3) two-well recirculating withdrawal-injection tests, and (4) two-well pulse tests. In each of these tests a nonreactive tracer is introduced into the groundwater system. In the single-well test, the tracer is pumped in for a set time period followed by pumping from the well and monitoring the concentration levels. The dispersivity of the formation near the well screen is computed from the concentration response data (Percious, 1969; Fried et al., 1974). In the natural-gradient test the tracer is introduced into the system without much disturbance of the flow regime. Its migration is then monitored at one or more sampling points (Fried, 1976). In the two-well recirculating test, the tracer is injected into the flow regime at one well. It is pumped out of a second well and then recirculated through the withdrawal-injection system. The concentration versus time response at the withdrawal well serves as a basis for computation of the dispersivity using analytical or numerical models (Grove and Beetem, 1971; Pickens et al., in press). In the two-well pulse test a tracer is introduced into a well situated within the drawdown cone caused by pumping of a

second well. Concentration data from the pumping well are used for calculation of a dispersivity value for the segment of the formation between the two wells (Zuber, 1974).

Fried (1975) presents an outline of the test methods and the mathematical basis for analysis of data from the first three types of tests indicated above. In each case dispersivity values are obtained by fitting an analytical or numerical model to the experimental data. Zuber (1974) emphasizes that the dispersivity value obtained from a given field experiment depends, sometimes to a high degree, on the mathematical model used in the analysis, and on the scale of the experiment. Aquifers are commonly stratified and tracers travel at different rates through the different layers. Even though the differences in hydraulic conductivity between layers may be almost imperceptible, the design of wells used for sampling can exert a dominant influence on the dispersivity values computed from concentration response data. Tests in which monitoring wells with large screened intervals are used can yield large apparent dispersivities because of mixing in the well screen. Pickens et al. (in press) describe a multilevel point-sampling device that is well suited for use in dispersion tests in sandy aquifers. Castillo et al. (1972) show that the dispersive nature of fractured rocks can exhibit great complexities in comparison with that expected of granular materials.

Chemical Partitioning

Reactive contaminants transported by groundwater are distributed between the solution phase and other phases. Reactions between the dissolved species and the geological materials may cause a portion of the dissolved species to be transferred to the solids as a result of adsorption or ion exchange. Reactions primarily among the contaminant, other dissolved constituents, and the geological materials may cause a portion of the contaminant concentration to be incorporated into a solid form as a result of chemical precipitation. Above the capillary fringe, where a continuous gas phase normally exists in part of the void space, reactions may cause some of the contaminant mass to be transferred from the solution phase to the gas phase, such as occurs during denitrification in the unsaturated zone. In each of these processes the contaminant is partitioned between the solution and other phases. The ultimate fate of the contaminant in the subsurface zone can depend on the degree of irreversibility of the reactions. Prediction of the rate and concentrations at which a contaminant will be transported in groundwater requires knowledge of the rates and extent to which this partitioning will occur.

In this brief discussion of this broad topic, we will focus on the partitioning of contaminants between the liquid and solid phases. There are four main approaches to the determination of this type of partitioning. These include (1) use of computational models based primarily on thermodynamically derived constants or coefficients for equilibrium systems, (2) laboratory experiments in which the contaminant in solution is allowed to react under controlled conditions with samples of the geologic materials of interest, (3) field experiments in which the degree of partitioning is determined during passage of contaminant solutions through

a small segment of the groundwater system and (4) studies of existing sites at which contamination has already occurred.

Insight into the computational approach based on equilibrium thermodynamics can be acquired from Chapters 3 and 7. If it is expected that the concentration of the contaminant in solution is controlled by precipitation-dissolution reactions and if the necessary thermodynamic data on the aqueous and solid components of the system are available, the equilibrium concentration of the contaminant in solution under specified conditions can be computed. Although the necessary computational techniques are well developed, this method has limited application for many types of contaminants because of uncertainties with regard to chemical composition and the free energies of the controlling solid phases or because of sluggish rates of the dominant reactions. In many cases the contaminant species of interest are transported in solutions that are chemically very complex. The presence of organic compounds can cause contaminant mobility to be enhanced considerably beyond that predicted based on inorganic considerations alone.

In the laboratory, the degree of contaminant partitioning is determined in *column experiments* and in what are known as *batch experiments*. In column experiments (Figure 9.1), prepared solutions or natural waters to which the contaminant is added are passed through cylindrical samples of the geologic materials of interest. If the flow rate and input water chemistry is regulated to approximate the field conditions and if disturbance of the sample prior to emplacement in the column has not caused the material to acquire properties that deviate significantly from field conditions, the degree of partitioning and retardation obtained from this type of experiment provides an indication of what will take place in the field. Column experiments, however, are rarely conducted with adherence to all of these requirements. There is considerable uncertainty, therefore, in application of the results to field situations. Column experiments are described by Rovers and Farquhar (1974) and Griffin et al. (1976) using sanitary landfill leachate, by Routson and Serne (1972) using trace concentrations of radionuclides, by Kay and Elrick (1967) and Huggenberger et al. (1972) using lindane (a pesticide), by Doner and McLaren (1976) using urea, and by many other investigators using various chemical constituents.

In batch experiments the contaminated solution and the geologic material in a disaggregated state are brought into contact in a reaction vessel. After a period of time that normally ranges from hours to days, the degree of partitioning of the contaminant between the solution and the geologic materials is determined. For partitioning data from these experiments to be applied with confidence in the analysis of field situations, comparisons with results of column or field tests are necessary. Batch tests have the advantage of being relatively quick and inexpensive to conduct. For some contaminants, the batch test is a standard method for establishing adsorption isotherms or selectivity coefficients in ion exchange reactions. Sample disturbance and the lack of representation of field flow conditions can detract from the validity of the results in the analysis of field situations. Samples used in batch tests are usually exposed to oxidizing conditions (i.e., to oxygen in

the air) during sample preparation and during the tests. Since the adsorptive capabilities of oxidized materials can be much different than reduced materials, the test results can be invalid for analysis of contaminant behavior in field systems.

The most direct but rarely the most convenient method for determining the partitioning and retardation of the contaminant is to conduct field tests. Injection of a solution of appropriate composition into a small segment of the groundwater system followed by monitoring of its behavior can provide, in favorable circumstances, a basis for prediction of contaminant behavior elsewhere in the system. Field tests of this type can be time-consuming and expensive. In order to obtain adequate information, numerous tests may be required. In some situations the need to obtain reliable information on contaminant behavior is great enough to justify this effort.

Another approach for obtaining information on the partitioning and retardation of contaminants during transport in groundwater is to conduct investigations at existing sites where groundwater pollution has already occurred. For results of these investigations to have more than site-specific significance, not only must the distributions of the contaminants in the water and on the porous media be determined, but the factors that influence these distributions must also be investigated. During recent years an appreciable number of detailed studies of sites with subsurface contamination have been reported in the literature. Some of the more notable examples are those by McKee et al. (1972), Childs et al. (1974), Suarez (1974), Ku et al. (1978), Goodall and Quigley (1977), and Gillham and Cherry (1978).

9.5 Sources of Contamination

Land Disposal of Solid Wastes

In North America approximately 3 kg of refuse per capita is produced daily. More than 20,000 landfills across the continent accommodate more than 90% of the solid waste that is produced by municipal and industrial activities. According to Yen and Scanlon (1975), a city of 1 million people generates refuse with an annual volume equivalent to 80 ha covered 5 m deep. Although materials recovery and incineration may eventually decrease the amount of waste that is disposed of by landfilling, landfills will continue to be the primary method of disposal of these wastes during at least the next few decades.

The design, construction, and operational aspects of land disposal of refuse are described by Mantell (1975). For purposes of this discussion this information is not required, other than to recognize that much of the solid waste (refuse) that is now disposed of on land is emplaced in engineered disposal systems known as *sanitary landfills*. In sanitary landfills, solid waste is reduced in volume by compaction and then is covered with earth. Ideally, the earth cover is placed over the refuse at the conclusion of each day's operation, but in practice less frequent cover application is common. The landfill, consisting of successive layers of compacted waste

and earth, may be constructed on the ground surface or in excavations. In North America a large number of the older sites that receive municipal wastes are open dumps or poorly operated landfills. Newer sites are generally better situated and better operated. It is estimated that 90% of the industrial wastes that are considered to be hazardous are landfilled, primarily because it is the least expensive waste management option.

Our purpose here is to consider some of the effects that refuse disposal can have on the groundwater environment. With the exception of arid areas, buried refuse in sanitary landfills and dumps is subject to leaching by percolating water derived from rain or snowmelt. The liquid that is derived from this process is known as *leachate*. Table 9.4 indicates that leachate contains large numbers of inorganic contaminants and that the total dissolved solids can be very high. Leachate also contains many organic contaminants. For example, Robertson et al. (1974) identified more than 40 organic compounds in leachate-contaminated groundwater in a sandy aquifer in Oklahoma. These authors concluded that many of these compounds were produced by leaching of plastics and other discarded manufactured items within the refuse. Not only do the leachates emanating from

Table 9.4 Representative Ranges for Various Inorganic Constituents in Leachate From Sanitary Landfills

Parameter	Representative range (mg/ℓ)
K^+	200–1000
Na^+	200–1200
Ca^{2+}	100–3000
Mg^+	100–1500
Cl^-	300–3000
SO_4^{2-}	10–1000
Alkalinity	500–10,000
Fe (total)	1–1000
Mn	0.01–100
Cu	<10
Ni	0.01–1
Zn	0.1–100
Pb	<5
Hg	<0.2
NO_3^-	0.1–10
NH_4^+	10–1000
P as PO_4	1–100
Organic nitrogen	10–1000
Total dissolved organic carbon	200–30,000
COD (chemical oxidation demand)	1000–90,000
Total dissolved solids	5000–40,000
pH	4–8

SOURCES: Griffin et al., 1976; Leckie et al., 1975.

landfills contain contaminants derived from solids, but many leachates contain toxic constituents from liquid industrial wastes placed in the landfill.

Concern has developed in recent years with regard to the effect of landfills on the quality of groundwater resources. Garland and Mosher (1975) cite several examples where groundwater pollution has been caused by landfills. A case where leachate migration caused serious pollution of a large aquifer used as a city's water supply is described by Apgar and Satherthwaite (1975). It is expected that the cost of rectifying this situation will eventually total many millions of dollars.

Numerous investigations in North America and Europe have shown that in nonarid regions, infiltration of water through refuse causes water table mounding within or below the landfill. The mounding process is similar to that described in Section 8.11. Water-table mounding causes leachate to flow downward and outward from the landfill as illustrated in Figure 9.24. Downward flow of leachate may threaten groundwater resources. Outward flow normally causes leachate springs at the periphery of the landfill or seepage into streams or other surface-water bodies. If the paths of leachate migration do not lead to aquifers containing potable water, downward movement of leachate will not pose a threat to groundwater resources.

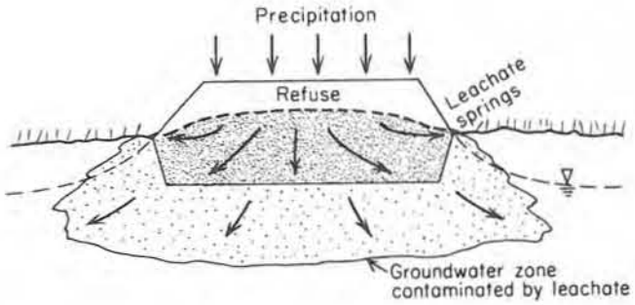

Figure 9.24 Water-table mound beneath a landfill, causing leachate springs and migration of contaminants deeper into the groundwater zone.

In situations where landfills are located in relatively permeable materials such as sand, gravel, or fractured rock, leachate migration may cause contamination over areas many times larger than the areas occupied by the landfills. An example of such a case is shown in Figure 9.25. At this landfill site on moderately permeable glaciodeltaic sand, a large plume of leachate-contaminated water, represented in Figure 9.25 by the Cl^- distribution, has penetrated deep into the aquifer and has moved laterally several hundreds of meters along the paths of groundwater flow. This contamination developed over a period of 35 years. Infiltration of water through the landfill will continue to produce leachate for many decades. Transport by groundwater flow in the sand will cause the zone of contamination to greatly expand. In this particular case, however, the aquifer is not

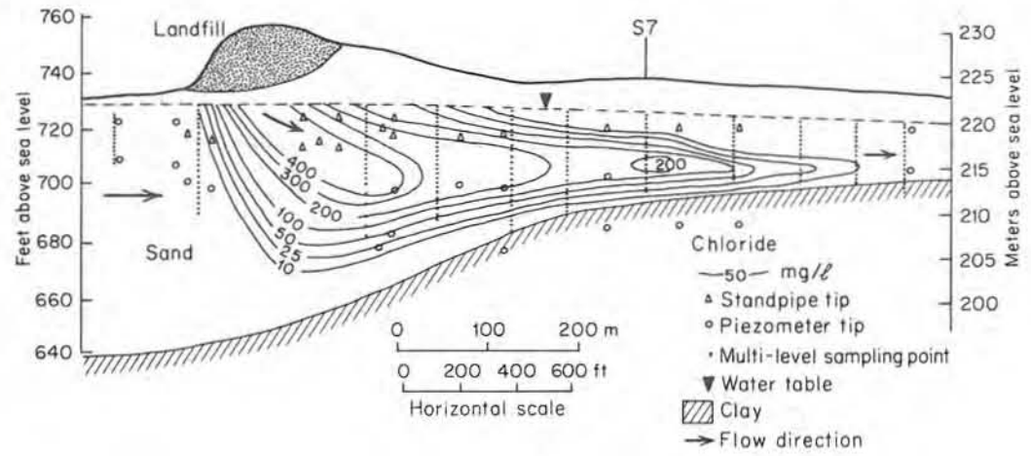

Figure 9.25 Plume of leachate migrating from a sanitary landfill on a sandy aquifer; contaminated zone is represented by contours of Cl^- concentration in groundwater.

used for water supply. The spreading contaminant plume is therefore not regarded as a significant problem. At a landfill on sand and gravel on Long Island, N.Y., Kimmel and Braids (1974) delineated a leachate plume that is more than 3000 m long and greater than 50 m in depth. These two examples and others described in the literature indicate that if leachate has access to active groundwater flow regimes, pollution can spread over very large subsurface zones. Physical and chemical processes are sometimes incapable of causing appreciable attenuation of many of the toxic substances contained within the leachate plume.

If landfills are situated in appropriate hydrogeologic settings, both groundwater and surface-water pollution can be avoided. It is commonly not possible, however, to choose sites with ideal hydrogeologic characteristics. In many regions land of this type is not available within acceptable transportation distances, or it may not be situated in an area that is publicly acceptable for land filling. For these and other reasons most landfills are located on terrain that has at least some unfavorable hydrogeologic features.

Although it is well established that landfills in nonarid regions produce leachate during at least the first few decades of their existence, little is known about the capabilities for leachate production over much longer periods of time. In some cases leachate production may continue for many decades or even hundreds of years. It has been observed, for example, that some landfills from the days of the Roman Empire are still producing leachate. Many investigators have concluded that at the present time there have been very few occurrences of leachate contamination of aquifers that are used for water supply. Whether or not it will be possible to draw similar conclusions many years from now remains to be established.

Farvolden and Hughes (1976) have concluded that solid waste can be buried at almost any site without creating an undue groundwater pollution hazard, provided that the site is properly designed and operated. A testing program to define the hydrogeological environment is essential. These authors indicate that if uncontrolled leachate migration is unacceptable, the leachate should be collected and treated as a liquid waste. One feasible way to ensure that no leachate leaves the site is to establish a hydraulic gradient toward the site, perhaps by pumping. Liners for emplacement beneath landfills are currently being evaluated as a control method but have not yet been established in practice. Some examples of controls on leachate migration using drains or wells are shown in Figure 9.26. These types of control measures require that the collected leachate be treated or otherwise managed in an appropriate manner.

In addition to the production of leachate, infiltration of water into refuse causes gases to be generated as biochemical decomposition of organic matter

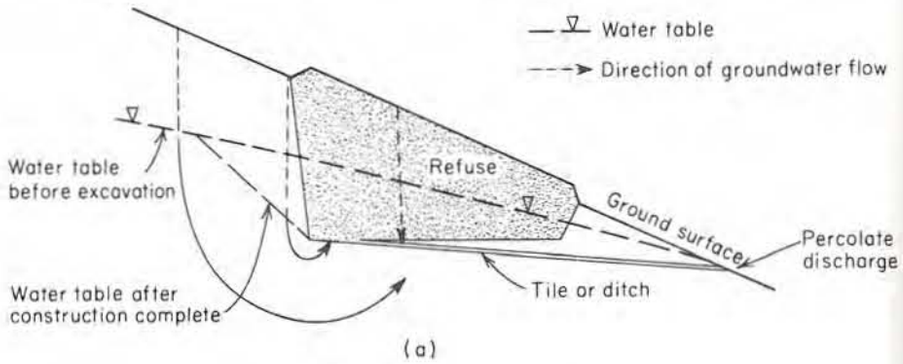

Figure 9.26 Control of leachate in a sanitary landfill by (a) tile drain or ditch and (b) pumped well (after Hughes et al., 1971).

occurs. Gases such as CO_2, CH_4, H_2S, H_2, and N_2 are commonly observed. CO_2 and CH_4 are almost invariably the most abundant of these gases. CH_4 (methane) has a low solubility in water, is odorless, and generally is of little influence on groundwater quality. In the environmental impact of landfills, however, it can be of great importance because of its occurrence in gaseous form in the zone above the water table. It is not uncommon for CH_4 to attain explosive levels in the refuse air. In some situations CH_4 at dangerous levels can move by gaseous diffusion from the landfill through the unsaturated zone in adjacent terrain. Migration of CH_4 at combustible levels from landfills through soils into residences has occurred in urban areas. In recent years, installation of gas vents in landfills to prevent buildup of methane in the zone above the water table has become a common practice.

In addition to hazards caused by the potential for methane explosion, gaseous migration from landfills can result in extensive damage to vegetation and odor problems. Case histories of gas migration from landfills have been described by Flower (1976). Mohsen (1975) has presented a theoretical analysis of subsurface gas migration from landfill sources. The interactions of the various factors that influence gas production in landfills have been described by Farquhar and Rovers (1973).

Sewage Disposal on Land

Sewage is placed on or below the land surface in a variety of ways. Widespread use of septic tanks and drains in rural, recreational, and suburban areas contributes filtered sewage effluent directly to the ground. Septic tanks and cesspools are the largest of all contributors of wastewater to the ground and are the most frequently reported sources of groundwater contamination in the United States (U.S. Environmental Protection Agency, 1977). Twenty-nine percent of the U.S. population disposes of its domestic waste through residential disposal systems. An increasing percentage of the municipal sewage in industrialized countries is being processed in primary and secondary sewage treatment plants. Although this decreases surface-water pollution, it produces large volumes of solid residual materials known as *sewage sludge*. In many areas this sludge, which contains a large number of potential contaminants, is spread on agricultural or forested lands. In some regions liquid sewage that has not been treated or that has undergone partial treatment is sprayed on the land surface. Application of liquid sewage and sewage sludge to the land provides nutrients such as nitrogen, phosphorus, and heavy metals to the soil. This can stimulate growth of grasses, trees, and agricultural crops. Land that is infertile can be made fertile by this practice. One of the potential negative impacts of this type of sewage disposal is degradation of groundwater quality.

Primary- and secondary-treated sewage is being spread on forested land and crop land in an increasing number of areas in Europe and North America. For example, in Muskegon County, Michigan, more than 130 million liters per day of sewage effluent is sprayed on the land surface (Bauer, 1974). For many decades cities such as Berlin, Paris, Milan, Melbourne, Fresno, and many others have been

using sewage for irrigation of crops. Not only are the nutrients in sewage effluent valuable, but the water itself is a valuable resource in many regions. In some situations intensely treated sewage effluent may be used as a source of artificial recharge for aquifers that serve for municipal water supply. Injection of treated sewage into coastal aquifers may serve as a means of controlling the intrusion of salt water.

Considering the many ways in which liquid and solid constituents from sewage reach the land surface and subsurface zones, it is reasonable to expect that over the long term the quality of groundwater resources in many areas will reflect the extent to which hydrogeologic factors are considered in the overall planning and operation of sewage management systems. In a textbook of this type it is not feasible to look specifically at the hydrogeologic and geochemical factors that are important in each of the land-application or disposal-of-sewage options that are in use. Before proceeding to other topics, however, we will provide a brief guide to some of the more important studies that have been conducted. For a detailed guide to the literature in this area, the reader is referred to the U.S. Environmental Protection Agency (1974a).

During the 1950's and early 1960's it was observed that one of the most serious consequences of land disposal of sewage by way of septic systems was contamination of groundwater by alkyl benzene sulfonate (ABS), which was a major component of household detergents. ABS is relatively nonbiodegradable and exists in water in anionic form. In the 1960's, numerous cases of shallow contamination of sand and gravel aquifers were reported. The problem was most acute in areas where septic systems were draining into unconfined aquifers in which there were numerous shallow water supply wells. Case histories of this type of problem in Long Island and in Southern California are described by Perlmutter et al. (1964) and Klein (1964).

In the mid-1960's the detergent industry replaced ABS with linear alykl sulfonate (LAS), a compound that is readily biodegradable in aerobic environments. Cases of LAS and ABS contamination of wells have been a rare occurrence since LAS gained widespread use, a somewhat surprising situation considering that many septic systems drain into anaerobic groundwater environments where the effects of biodegradation are probably minimal. LAS may undergo considerable retardation as a result of adsorption.

Effluent from septic systems includes many other types of contaminants. One of the most frequently reported of these contaminants in groundwater is nitrate. As indicated in Section 9.3, nitrate commonly does not undergo complete biochemical reduction to N_2 even if the groundwater system is anaerobic. Nitrate emanating from septic systems into groundwater is transported along the groundwater flow paths. A detailed case history of the migration of nitrate and other contaminants in groundwater as a result of discharge from septic systems was presented by Childs et al. (1974).

In some areas the primary concern with regard to contaminant migration from septic systems is surface-water quality rather than groundwater quality.

This is particularly the case in areas of recreational lakes where cottages and tourist facilities use septic systems located near lakes. Transport of nitrogen and phosphorus through the groundwater zone into lakes can cause lake eutrophication manifested by accelerated growth of algae and decrease in water clarity. Some examples of hydrogeologic investigations in recreational lake environments are described by Dudley and Stephenson (1973) and Lee (1976).

Another concern associated with the disposal of treated or untreated sewage on or below the land surface revolves around the question of how far and how fast pathogenic bacteria and viruses can move in subsurface flow systems. This problem is also crucial in the development of municipal water supplies by extraction of water from wells located adjacent to polluted rivers. The literature is replete with investigations of movement of bacteria through soils or granular geological materials. As bacteria are transported by water flowing through porous media, they are removed by straining (filtering), die-off, and adsorption. The migration of the bacterial front is greatly retarded relative to the velocity of the flowing water. Although bacteria can live in an adsorbed state or in clusters that clog parts of the porous medium, their lives are generally short compared to groundwater flow velocities. In medium-grained sand or finer materials, pathogenic and coliform organisms generally do not penetrate more than several meters (Krone et al., 1958). Field studies have shown, however, that in heterogeneous aquifers of sand or gravel, sewage-derived bacteria can be transported tens or hundreds of meters along the groundwater flow paths (Krone et al., 1957; Wesner and Baier, 1970).

Viruses are very small organic particles (0.07–0.7 μm in diameter) that have surface charge. There is considerable evidence from laboratory investigations indicating that viruses are relatively immobile in granular geological materials (Drewry and Eliassen, 1968; Robeck, 1969; Gerba et al., 1975; Lance et al., 1977). Adsorption is a more important retardation mechanism than filtering in highly permeable granular deposits. Problems associated with sampling and identification of viruses in groundwater systems have restricted the understanding of virus behavior under field conditions. Advances in sampling technology (Wallis et al., 1972; Sweet and Ellender, 1972) may lead to a greatly improved understanding of virus behavior in aquifers recharged with sewage effluent.

Although there is considerable evidence indicating that bacteria and viruses from sewage have small penetration distances when transported by groundwater through granular geologic materials, similar generalizations cannot be made for transport in fractured rock. It is known that these microorganisms can live for many days or even months below the water table. In fractured rocks, where groundwater velocities can be high, this is sufficient time to produce transport distances of many kilometers.

As man relies more heavily on land application as a means of disposal for municipal sewage effluent and sludge, perhaps the greatest concern with regard to groundwater contamination will be the mobility of dissolved organic matter. Sewage effluent contains many hundreds of dissolved organic compounds, of which very little is known about their toxicity and mobility. Some of these com-

pounds may eventually be shown to be more significant in terms of degradation of groundwater quality than nitrate, trace metals, bacteria, or viruses.

Agricultural Activities

Of all the activities of man that influence the quality of groundwater, agriculture is probably the most important. Among the main agricultural activities that can cause degradation of groundwater quality are the usage of fertilizers and pesticides and the storage or disposal of livestock or fowl wastes on land. The most widespread effects result from the use of fertilizer. In industrialized countries most fertilizer is manufactured chemically. This type of fertilizer is known as inorganic fertilizer. In less developed countries, animal or human wastes are widely used as organic fertilizer.

Fertilizers are categorized with respect to their content of nitrogen (N), phosphorus (P), and potassium (K). These are the three main nutrients required by crops. The annual application rates of fertilizers vary greatly from region to region and from crop to crop. Nitrogen applications, (expressed as N), generally vary from about 100 to 500 kg/ha·yr. Because fertilizer is used year after year, it is to be expected that in many areas some of the N, P, or K is carried by infiltrating water downward to the water table, where it can migrate in the groundwater flow regime. For reasons explained in Section 9.3, nitrogen in the form of NO_3^- is generally much more mobile in subsurface flow systems than dissolved species of phosphorus. Cation exchange causes K^+ to have low mobility in most nonfractured geologic materials.

Of the three main nutrients in fertilizer, N in the form of NO_3^- is the one that most commonly causes contamination of groundwater beneath agricultural lands. High NO_3^- concentrations have been delineated in extensive areas in many parts of the world, including Israel (Saliternik, 1972), England (Foster and Crease, 1972), Germany (Groba and Hahn, 1972), California (Calif. Bureau Sanitary Eng., 1963; Nightingale, 1970; Ayers and Branson, 1973), Nebraska (Spalding et al., 1978), southern Ontario, and southern Alberta. Many wells in these areas have NO_3^- concentrations that exceed the recommended limit for drinking water. In areas where NO_3^- contamination is areally extensive, fertilizer rather than animal wastes from feedlots or lagoons or septic field seepage is usually identified as the primary nitrogen source. Nitrate is the principal dissolved nitrogen component, with ammonium and organic nitrogen present in much lower concentrations. Although in many aquifers that are contaminated by NO_3^-, the concentrations are below the limits recommended for drinking water, it is disturbing to note that gradual increases in NO_3^- have been observed. The widespread use of inorganic fertilizers began after World War II. The major impact on groundwater quality resulting from this change in agricultural practice is probably not yet fully developed. Nitrate contamination is rarely reported at depths of more than about 10–100 m below the water table. As time goes on, however, NO_3^- contamination may extend to greater depth in areas where there are significant downward flow components. For example, NO_3^- in deep wells in California, ranging in depth from 240 to 400 m below

ground surface, increased from approximately 1 mg/ℓ in 1950 to 10–17 mg/ℓ in 1962 (Broadbent, 1971). The extent to which denitrification occurs as water moves along regional flow paths is a major uncertainty inherent in predictions of long-term NO_3^- increases in aquifers.

In England, NO_3^- contamination of a large regional carbonate-rock aquifer is widespread. Analysis of the occurrence and movement of NO_3^- in this aquifer is complicated by the fact that NO_3^- is carried in groundwater flowing in a network of joints and solution channels, while some of the NO_3^- is lost from the active flow regime as a result of diffusion into the porous matrix of the limestone (Young et al., 1977). If at some time in the future the NO_3^- concentration in the flow network declines, NO_3^- will diffuse from the matrix back into the flow regime.

Although extensive NO_3^- contamination of shallow groundwater can often be attributed to leaching of fertilizer, NO_3^- in shallow groundwater in large areas in southern Alberta (Grisak, 1975), southern Saskatchewan, Montana (Custer, 1976), and Texas (Kreitler and Jones, 1975) is not caused by fertilizer use. In these areas it appears that most of the NO_3^- is derived by oxidation and leaching of natural organic nitrogen in the soil. The greater abundance and deeper penetration of oxygen into the soil has occurred as a result of cultivation. In some areas the initial turning of the sod as settlers moved on the land was probably a major factor. In other areas continual deep cultivation during the modern era of farming has been a major influence.

In many agricultural areas shallow groundwater has become contaminated locally as a result of leaching of NO_3^- from livestock and fowl wastes. The conversion of organic nitrogen in these wastes to NO_3^- takes place through biochemical processes. Relatively small source areas such as farm manure piles, fowl-waste lagoons, and feedlots contribute NO_3^- to groundwater, but if these contaminant sources are not directly underlain by aquifers, the contamination is rarely very significant. Specific cases of groundwater contamination from animal wastes are reported by Hedlin (1972) and by Gillham and Webber (1969). In agricultural areas contamination of shallow wells by NO_3^- and other consituents commonly occurs because of faulty well construction. If wells are not properly sealed by grout or clay along the well bore above the screen, contaminated runoff can easily make its way to the aquifer zone near the well screen.

Concurrent with the widespread increase in the use of chemical fertilizers since World War II has been the rapid development and use of a multitude of organic pesticides and herbicides. In a report on groundwater pollution in the southwestern United States, Fuhriman and Barton (1971) concluded that pollution by pesticides must be listed as an important potential hazard. However, they obtained no direct evidence indicating significant pesticide contamination of groundwater. Kaufman (1974), in a review of the status of groundwater contamination in the United States, indicates that this conclusion appears to characterize today's situation—that of a potential but as-yet-unrealized problem. Based on a literature review and field studies in Kent, England, Croll (1972) arrived at a similar conclusion. It is well known from laboratory experiments that many

pesticides and herbicides with appreciable solubility in water have significant mobility in some types of geologic materials, particularly clean sands and gravels (Burns and Mclaren, 1975; Adams, 1973). It is not unreasonable to expect that the use of these chemicals in agriculture will eventually cause parts of some aquifers to become contaminated. Davidson et al. (1976) have pointed out that because of the immense size to which the pesticide industry has grown, the problems associated with the disposal of surplus and waste pesticide materials and empty or partially empty pesticide containers has become acute. High concentrations of pesticides in groundwater can result in greater mobility than at lower concentrations. At higher concentrations, the exchange sites are more readily saturated with the pesticide, or the biodegradation capabilities of the medium may be exceeded.

Petroleum Leakage and Spills

In industrialized countries hundreds of thousands of steel gasoline storage tanks lie buried at filling stations. Many thousands of kilometers of underground pipelines carry petroleum products across continents. Tanker trucks with oil and gasoline are continually on the move. It is not surprising, therefore, that leakages and spills from these sources are an increasing threat to groundwater quality. Most of the buried storage tanks at filling stations were placed in the ground since World War II. Because stringent requirements for tank testing and replacement are only gradually being implemented in most countries, leakage problems caused by older tanks are common, particularly in regions of high water tables and frequent infiltration.

Contamination of groundwater by petroleum products from leaky tanks, from pipelines, or from spills is a much different type of problem than those described elsewhere in this chapter. The major difference lies in the fact that oils and gasoline are less dense than water and are *immiscible* in water. As a consequence of this, oil or gasoline from leakages or spills migrate almost exclusively in the unsaturated zone. The processes of petroleum movement in the unsaturated zone have been described in detail by Schwille (1967), van Dam (1967), and Dietz (1971). The following discussion is based primarily on these references.

Figure 9.27 illustrates the main subsurface migration stages that occur when oil seeps in the ground. In this case, the hydrogeologic conditions are simple. There is appreciable depth of unsaturated zone beneath the level of oil entry into the system. The term "oil" is used here to refer to both crude oil proper and its liquid derivatives, such as gasoline.

In the first migration stage, the oil movement is primarily downward under the influence of gravitational forces. During this seepage stage, capillary forces produce some lateral migration. This causes a zone, referred to as the *oil wetting zone*, around the core of the infiltration body. It is comparable in origin to the natural capillary fringe on the water table. In the oil wetting zone, the degree of oil saturation decreases outwardly and capillary forces (surface tension) are dominant. In the main seepage zone, only gravitational forces exist.

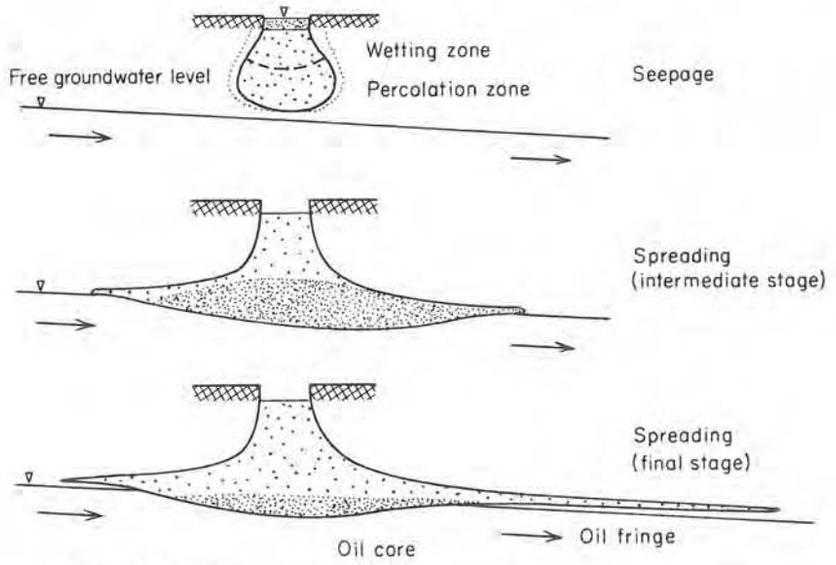

Figure 9.27 Stages of migration of oil seeping from a surface source (after Schwille, 1967).

Downward seepage of oil ceases when the seepage front reaches the water table. Although it might be expected that the oil would spread laterally on top of the capillary fringe rather than along the water table, experimental and field evidence indicates that considerable migration occurs within the capillary fringe at or very near the water table. Since oil is immiscible in water and is less dense than water, it may slightly depress the water table. Except for small amounts of hydrocarbons that go into solution, the oil does not penetrate below the water table. As oil accumulates on the water table, the oil zone spreads laterally, initially under the influence of gradients caused by gravity and later in response mainly to capillary forces. Capillary spreading becomes very slow and eventually a relatively stable condition is attained. In theory, stability occurs when a condition known as *residual oil saturation* or *immobile saturation* is reached. The experience of oil production engineers is that below a certain degree of saturation, oil is held in a relatively immobile state in the pore spaces. If the percent oil saturation is reduced further, isolated islands or globules of oil become the dominant mode of oil occurrence. Over the range of pressure gradients that can occur, these islands are stable. As the mass of oil spreads laterally due to capillary forces, the residual oil saturation condition must eventually be attained, provided that the influx of oil from the source ceases. This is referred to as the *stable* stage.

When the oil spill or leakage volume is small relative to the surface available for contact as the oil moves through the zone above the water table, the oil migration zone may attain residual saturation and become immobile before penetrating

to the water table. The volume of porous medium required to immobilize a given amount of oil depends on two factors: the porosity and the nature of the hydrocarbons that comprise the oil. The volume B of porous geologic materials that is required to immobilize a spill or leakage volume can be estimated from the relation

$$B = \frac{B_0}{nS_0} \tag{9.29}$$

where B_0 is the volume of oil entering the system, n the porosity, and S_0 the residual oil saturation. If the depth to water table and values for n and S_0 are known, this relation can be used to estimate the likelihood that spilled oil will penetrate to the water table (American Petroleum Institute, 1972). Van Dam (1967) presents equations that describe the shape of the stable layer of oil if penetration to the water table occurs. In practice, however, it is generally not possible in field situations to obtain sufficient data on the distribution of relative permeabilities for more than a qualitative analysis to be made (Dietz, 1971). Laboratory model experiments by Schwille (1967) have demonstrated that minor differences in permeabilities laterally or vertically can cause strong distortions in the shape of the oil migration zone.

Because oil leakages or spills usually do not involve large fluid volumes of oil, and because migration is limited by residual oil saturation, one might expect that oil is not a significant threat to groundwater quality. This is unfortunately not the case. Crude oil and its derivatives contain hydrocarbon components that have significant solubility in water. In general, the lighter the petroleum derivative, the greater is the solubility. Commercial gasoline, for example, has solubility of 20–80 mg/ℓ. It can be detected by taste and odor at concentrations of less than 0.005 mg/ℓ (Ineson and Packham, 1967). Because the solubility of the lighter hydrocarbons greatly exceeds the concentration levels at which water is considered to be seriously polluted, it is not difficult to envision situations where the effect of hydrocarbon dissolution is of much greater concern in terms of groundwater quality than the localized immobile zone of immiscible hydrocarbons on and above the water table. For example, in the situation represented in Figure 9.28, the lateral flow of groundwater beneath the zone of immobilized oil could cause soluble hydrocarbons to be transported large distances along the groundwater flow paths.

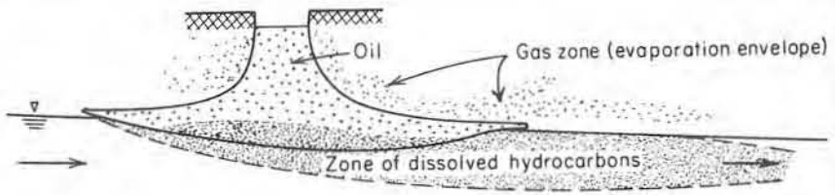

Figure 9.28 Migration of dissolved and gaseous hydrocarbons from a zone of oil above the water table (after Schwille, 1967).

In situations where oil penetrates to the water-table zone and then spreads out and becomes relatively immobile, the effect of water table fluctuations can be important. If the water table falls, much of the oil remains in the newly created zone as a thin coating on the surface of the porous medium. This film is not removed by water flushing or air ventilation. The problem can be ameliorated by the effect of bacteria. There exist species of aerobic and anaerobic bacteria that grow rapidly in the presence of oil or gasoline if the other necessary nutrients are also available. In favorable circumstances, bacterial oxidation can consume much of the oil or gasoline that accumulates above the water table as a result of leakages or spills. A fluctuating groundwater table is believed to promote the processes of biodegradation.

Of the many examples of petroleum contamination of groundwater that have been reported, the case history described by McKee et al. (1972) is particularly illustrative of the problems and processes involved and remedial measures that can be used to minimize the damage to subsurface water quality. Control and remedial procedures are described by the American Petroleum Institute (1972).

Disposal of Radioactive Waste

It has been several decades since nuclear engineers and scientists at an Idaho research station watched four household light bulbs flicker to life as a result of man's first generation of electricity from atomic energy. From this modest beginning, nuclear-power-generating facilities have grown to the point where they now produce more than 15% of the electricity in the United States and Canada and larger percentages in some European countries. By the turn of this century it is expected that in North America and Europe, the percentages will be much larger. Feared by many as a threat to mankind's future and hailed by others as the answer to the world's energy problems, nuclear generation of electricity has sparked controversy around the globe. At the present time there are several uncertainties inherent in activities associated with the generation of nuclear power. One of them is man's capability to safely isolate radioactive wastes from the biosphere for long periods of time. Because of its hydrogeologic nature, this nuclear-power-related topic is worthy of discussion in this text.

The hydrogeologic aspects of the nuclear power industry will be considered within the framework of the *nuclear fuel cycle*. This expression refers to all the stages in the nuclear power industry in which nuclear fuel is developed and used and in which radioactive wastes are generated. This includes uranium mining, milling, refining, uranium enrichment, fuel fabrication, fuel consumption in reactors, fuel reprocessing, waste solidification, and burial of solidified waste or unreprocessed spent fuel in deep geological repositories. The "front end" of the nuclear fuel cycle involves mining and milling of uranium ore. An undesirable by-product of these activities is the production of large volumes (hundreds of millions of cubic meters per year in North America) of waste rock from mining and tailings from milling. Waste rock and tailings are usually placed in piles on the land surface or as fill material in topographic depressions confined by small earth embankments

or dams. Because they contain isotopes of uranium, thorium, and radium, waste rock and tailings are a form of solid low-level radioactive waste. Radium 226 (^{226}Ra), with a half-life of 1620 years, poses the greatest environmental hazard. Table 9.1 indicates that the maximum permissible concentration of ^{226}Ra in drinking water is 3 pCi/ℓ, which is equivalent to 10^{-9} mg/ℓ. This concentration is so small that it is orders of magnitude below the maximum permissible concentrations for trace metals such as lead, mercury, or cadmium (Table 9.1). Extremely small amounts of ^{226}Ra leached from waste rock or tailings into groundwater can therefore cause the water to be unfit for human consumption. Uranium mining in North America generally occurs in areas remote from population centers and from industrial or agricultural developments. In these areas, groundwater quality has, until recently, not been a subject of significant concern. The extent to which ^{226}Ra and other hazardous constituents from waste rock or tailings are entering groundwater and their fate within groundwater flow systems is not known. We can expect, however, that in the next decade hydrogeological factors will play a much greater role in the design and evaluation of disposal sites for uranium mining and milling wastes than has previously been the case.

The next stage in the nuclear fuel cycle is uranium refining, a process in which the mill product is upgraded in preparation for uranium enrichment into nuclear fuel (the U.S. and European approach) or unenriched fuel fabrication (the Canadian approach). In the refining process, small quantities of solid or semisolid, low-level radioactive wastes are generated. The chemical nature of these wastes varies from refinery to refinery, but the wastes generally contain ^{226}Ra, ^{230}Th, and ^{238}U in what are normally small but significant concentrations. As in the case of mining and milling wastes, ^{226}Ra is the isotope of main concern. The refinery wastes are assigned to near-surface burial grounds that are located near the refineries. After more than 20 years of use, the burial ground at the principal uranium refinery in Canada (Port Hope, Ontario) was found in the mid-1970's to be emitting leachate with ^{226}Ra, as well as other nonradioactive contaminants. Although no aquifers were in jeopardy, remedial measures include excavation of the wastes with subsequent reburial at a site with hydrogeologic capability for longer-term isolation of the wastes from the biosphere.

The next major waste-generation stage in the nuclear fuel cycle is the operation of nuclear reactors for power production, weapons production, or research. In this stage, low-level solid radioactive wastes in the form of discarded equipment, assorted slightly radioactive refuse, and ion-exchange materials from decontamination facilities are produced. These wastes are known as *reactor wastes*. The term "low-level" is used here in a qualitative sense to distinguish these wastes from the very highly radioactive materials in used nuclear fuel or material derived directly from the used fuel.

Since the start of nuclear power production on a commercial basis in North America, the total volume of accumulated reactor wastes has amounted to about 40,000 m^3 (as of 1975). These wastes have been emplaced in shallow burial sites at 11 major locations in the United States and four major locations in Canada.

In the United States, the volume is expected to rise to 50,000 m^3 by 1980 and then to more than 300,000 m^3 by the year 2000 (*Nuclear News*, 1976). By use of existing and economically viable technology, the projected volumes can be reduced by a factor of 2 or 3. It is hoped, of course, that new waste processing methods will be developed to provide further volume reduction.

In spite of the improvements that may develop, the volumes of reactor waste are expected to be enormous in comparison with the volumes that have been handled in the past. Since the standard method of managing reactor wastes is to assign them to shallow burial sites, these mounting waste volumes can be viewed as a potential source of contamination to groundwater and other environments. The past history of shallow low-level waste burial in the United States is less than satisfactory. Of the 11 existing sites at which radioactive wastes resulting from commercial power production have been buried, three are leaking radioactive constituents to the environment (*Ground Water Newsletter*, 5, no. 3, 1976). Although at present this leakage to subsurface flow systems does not present a hazard to potable water supplies, it is striking evidence that undesirable consequences of inadequate hydrogeologic studies of waste management sites can become evident many years or decades after site usage begins. There is now little doubt that at the time most of these sites were established many years ago, more attention was given to the economics of handling the wastes, the ready availability of land for burial use, and proximity to transportation routes than was given to the ultimate fate of the wastes. With these lessons in hand, the problem facing hydrogeologists now is to ensure, through use of proper site search and evaluation methodologies, that future sites for shallow burial of solid low-level wastes have adequate radionuclide containment capabilities and that proper subsurface monitoring facilities are installed and operated.

Reactor wastes contain a variety of radionuclide species, with half-lives ranging from seconds to many decades or longer. Of these nuclides, ^{137}Cs, ^{90}Sr, and ^{60}Co, with half-lives of 28, 33, and 6 years, respectively, are usually regarded as posing the most significant environmental hazard. Wastes with these radionuclides need several hundred years to decay to very low radioactivity levels.

Figure 9.29 illustrates several types of waste-burial options. Although other situations exist, these will serve as a basis for discussion of some of the main concepts used in the development of burial facilities. In Figure 9.29(a), the wastes are placed in strong engineered containers constructed of materials such as concrete and steel situated on the ground surface. In these containers they can remain in storage in areas from which the public is excluded. Deterioration of the containers can be readily monitored. If problems arise, the containers can be repaired or the wastes can be placed in new containers, provided, of course, that a responsible organization remains in charge of the facilities. The facilities shown in Figure 9.29(b) are similar, except that the storage containers are covered with earth materials. If these materials are properly designed, they will protect the containers from weathering and thereby extend their life expectancy. The earth materials can be thought of as an engineered hydrogeological environment. In Figure 9.29(c) and

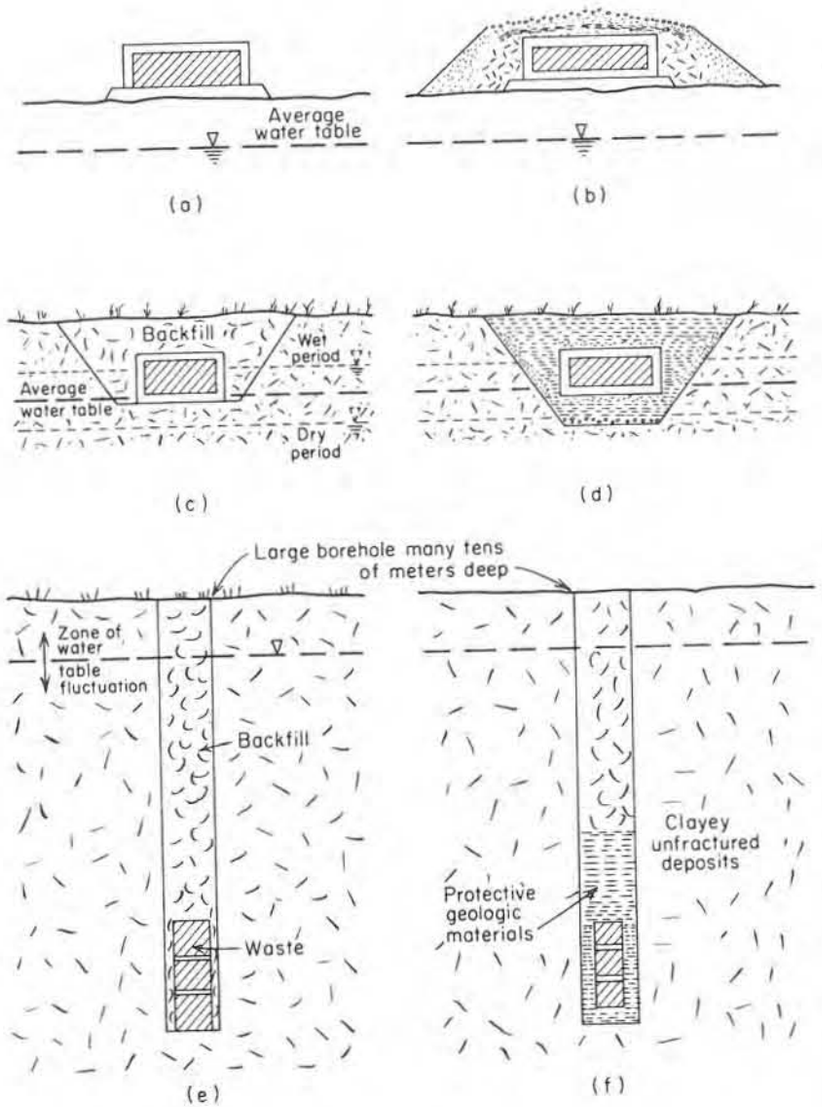

Figure 9.29 Schematic diagrams illustrating methods of low-level radioactive waste storage or disposal in shallow-water-table areas. (a) Above ground container storage; (b) above ground container storage with protection by geologic materials; (c) shallow burial in trench with backfill; (d) shallow burial in trench with additional containment provided by engineered zone of special geological materials; (e) deeper burial with backfill; (f) deeper burial in large-diameter borehole with protection by high-retardation geologic material.

(d), the wastes are stored in containers situated a few meters below ground surface, either above or below the water table. In the case shown in Figure 9.29(c), earth material from the excavation is used as backfill around the containers. In Figure 9.29(d), part of the fill in the excavation is designed to provide enhanced containment capabilities for the system. If the containers are located above the water table and if there is good reason to believe that during periods of water-table fluctuation, the water table will not rise into the burial zone, there will be little possibility of radionuclides escaping into the environment. If the water table fluctuates within the zone of burial, the containers are subjected to variable hydraulic and geochemical conditions. Their life expectancy and the fate of radionuclides in the event of container failure is much less certain than in the case of burial entirely above the water table.

In Figure 9.29(e) and (f), the containers are buried in large holes about 10 to 20 m deeper than in the previous examples. In nonarid regions the permanent water table in these situations would normally be above the containers. In the case depicted in Figure 9.29(e), the hole is simply backfilled with material originally removed from the site. In Figure 9.29(f) the excavated zone around the containers is packed with geological material such as bentonitic clay chosen to improve the long-term containment capabilities of the burial facility.

Nearly all of the burial sites for reactor wastes in the United States and Canada are in the category represented by Figure 9.29(c), with the water table within or just slightly below the burial zone. Some of the wastes have been placed directly in the ground without the protection of watertight containers. Most of the sites are located in poor hydrogeologic settings. It is not surprising, therefore, that subsurface migration of radionuclides from the burial zones is a common circumstance.

To avoid problems of subsurface radionuclide migration at future sites, numerous investigators have proposed that future sites be located in hydrogeologic environments that are shown to have long-term containment capability. To achieve this capability, the site should have the following characteristics: geomorphic and structural stability, isolation from fractured bedrock or other subsurface flow regimes that are too complex for development of reliable pathway analyses (i.e., the site should have a simple hydrogeologic framework), absence of subsurface flowlines that lead directly to the biosphere or to subsurface zones of potable water, and low predicted radionuclide velocities resulting from favorable combinations of groundwater velocity and chemical retardation. In addition to hydrogeologic criteria such as these, various investigators have indicated that the water table should be deep enough to permit waste burial to occur entirely in the unsaturated zone (Cherry et al., 1974). The predicted upper level of the range of water-table fluctuation over many centuries should be below the bottom of the burial zone. The criteria outlined above, if adhered to, would lead to the development of waste-burial facilities that would provide considerably better long-term containment than is the case for existing sites. Unfortunately, in most humid and semi-humid regions of North America, this desired ideal combination of hydrogeologic properties is rare, or even nonexistent, within areas that also meet social and

economic criteria. Water-table depth is generally shallow, which prevents establishment of burial zones at appreciable depth below ground surface. Wastes that are buried within a few meters, or even within 5–10 m of ground surface, are generally not considered to be in isolation from future generations during the hundreds of years or more that will be necessary for decay to reduce radioactivity in the waste to low levels.

As an alternative approach to the siting of burial grounds for low-level solid radioactive waste, Cherry et al. (in press) proposed that in humid and semihumid regions, burial zones be located in unfractured clayey aquitards in the manner represented in Figure 9.29(f). According to this scheme, burial would occur at the bottom of large (2–5 m in diameter) auger holes more than 15 m below ground surface. The burial zone would be at considerable depth below the water table and below the zone of active weathering. The wastes would therefore be isolated from the biosphere in a hydrogeologic environment in which groundwater velocity is extremely low and chemical retardation is great. Accidental unearthment of the waste by future generations would be much less probable than is the case for shallow, above-water-table waste burial. For this approach to be evaluated in detail it will be necessary to direct research toward the hydrogeologic properties of clayey aquitards such as clayey till, glaciolacustrine clay, and soft shale.

For additional information on the hydrogeologic aspects of the management of low-level solid radioactive waste (primarily reactor waste), the reader is referred to Peckham and Belter (1962), Richardson (1962a, 1962b), Mawson and Russell (1971), Cherry et al. (1973), and Pferd et al. (1977).

In the nuclear reactors that are currently used for power production, fuel rods composed of solid uranium oxide undergo fission reactions that release heat and decay particles. After a period of time in the reactor, the fuel rods are replaced. The *spent fuel* contains a wide variety of toxic radioactive isotopes produced from the uranium and from other elements. The ultimate fate of these man-made radionuclides is the core of what has become known as the *high-level radioactive waste disposal problem*. Numerous proposed solutions to this problem have been suggested, each with the objective of isolating the radionuclides from the biosphere for the life span of their radioactivity. This is the final stage of the nuclear fuel cycle.

Disposal options such as burial within the Antarctic ice cap, emplacement in the ocean floor at locations where natural burial beneath migrating continental plates will occur, and rocket transport beyond the earth's gravity field have been excluded because of impracticalities during the next few decades. It is now generally hoped that a satisfactory solution can be obtained by emplacing the radioactive material in an engineered repository in geologic strata in which it will be isolated from zones of active groundwater flow. This approach is commonly referred to as *terminal storage*. This implies that for a generation or two the repository environment will be monitored, and that if all goes well the wastes will then be regarded as having been permanently disposed.

In the United States, four main hydrogeologic possibilities are being investi-

gated for suitability for respository development. These are (1) deep salt beds, (2) deep crystalline igneous rocks, (3) deep shale strata, and (4) thick unsaturated zones in arid regions. Because of differences in climate, option (4) is not available in Canada or in European countries. The most critical question in the evaluation of these options is whether or not the wastes will be isolated from the biosphere for periods of time that are considered to be acceptable.

The waste will contain numerous radionuclide species, but by the year 2020, 99% of the projected accumulation of radioactivity will be due to the presence of ^{90}Sr and ^{137}Cs (Gera and Jacobs, 1972) which have half-lives of 28 and 33 years, respectively, and which will decay to very low levels within about 1000 years. Much longer periods of time, however, are required for decay to low levels of long-lived transuranic nuclides in the waste, namely, ^{238}Pu, ^{239}Pu, ^{240}Pu, ^{241}Am, and ^{243}Am, with half-lives ranging from 89 years for ^{238}Pu to 24,000 years for ^{239}Pu. Radioactive decay of these elements in the waste produces other radionuclides, known as daughter products (^{237}Np, ^{226}Ra, ^{129}I, ^{99}Tc, and others). If these are taken into account, the material will remain hazardous for millions of years, although at much lower radioactivity levels than will occur during the first thousand years.

The radionuclides can be placed in the repository in their original form as spent fuel or they may be incorporated into other materials after the spent fuel has been *reprocessed*. Reprocessing is a chemical treatment in which spent fuel is dissolved in acid and plutonium is separated from the other radionuclides. Plutonium is viewed by the nuclear power industry as a valuable commodity because it can be used to produce power in fast-breeder reactors. After the extraction of plutonium, a hot, highly radioactive waste solution containing the remaining radionuclide species and some plutonium residue remains as waste. It is now generally agreed by the nuclear regulatory agencies in the various countries working on the problem that these wastes must be solidified and incorporated into solid relatively inert materials such as ceramics or glass. This must be done before proceeding with commitment to any scheme for long-term subsurface storage or disposal. From the chemical reprocessing plant the waste will proceed, after a period of interim storage, through a solidification plant. After being solidified and encapsulated, the waste will then be ready for emplacement in a subsurface geological repository. Although reprocessing removes most of the plutonium from the spent fuel, the waste that remains after reprocessing is still highly radioactive. From a hydrogeological viewpoint, isolation of spent fuel or isolation of solidified waste from reprocessing are fundamentally the same problem.

For a subsurface repository to be viewed as satisfactory within the above-mentioned time framework, it must be capable of protecting the wastes from the effects of landscape erosion caused by wind, water, and even glaciers. It must be located in an area that does not have a significant seismic hazard or potential for volcanic activity. The protective materials within which the wastes are placed in the repository and the hydrogeologic environment outside the repository must be capable, within an exceptionally high degree of predictive confidence, of

preventing migration of radionuclides in groundwater from the repository into the biosphere. It is this latter criterion that is the most difficult to establish at the level of confidence that is required. Never before in the history of mankind have engineers and scientists been asked to provide safety analyses relevant to such a long period of time. The feasibility of achieving long-term waste isolation in each of the four hydrogeologic repository options listed above is currently under evaluation. The deep-salt option is discussed by Bradshaw and McClain (1971) and by Blomeke et al. (1973). The potential for repository development in shale is described by Ferro et al. (1973). Winograd (1974) reviewed the hydrogeologic aspects of the arid region/unsaturated zone option. For a broader view of the high-level radioactive-waste-disposal problem, the reader is referred to Kubo and Rose (1973) and Cohen (1977).

Deep-Well Disposal of Liquid Wastes

Injection of liquid wastes, mainly of industrial origin, has been widely adopted as a waste disposal practice in North America. The purpose of this procedure is to isolate hazardous substances from the biosphere. As the discharge of pollutants to rivers and lakes has become increasingly objectionable, and as legislation for protection of surface water resources has become more stringent, the use of deep permeable zones for liquid waste disposal has become an increasingly attractive waste management option for many industries. Inventories of industrial liquid-waste injection wells in the United States were conducted in 1964, 1967, 1968, 1972, and 1973. During this period the number of waste injection wells increased from 30 in 1964 to at least 280 in 24 states in 1973 (Warner and Orcutt, 1973). In Canada in 1976 at least 80 injection wells were in use. Injection wells used for return of brines extracted during oil or gas field pumping are normally not categorized as waste injection wells. There are more than 100,000 of these wells in North America. Chemical, petrochemical, and pharmaceutical companies are the largest users of waste injection wells. Other important users are petroleum refineries, gas plants, steel mills, potash mines, uranium mills, and processing plants. In Florida, Hawaii, Louisiana, and Texas, injection of sewage effluent into saline-water aquifers occurs on a minor scale. Nearly all the waste injection wells are in the depth range of 200–4000 m. Most are between 300 and 2000 m deep. The injection zones are generally located in sandstones, carbonate rocks, and basalt.

Most injection wells are operated at injection pressures less than 7×10^3 kN/m^2. The trend in recent years is toward lower injection pressures and injection rates in the range of 500–1400 ℓ/min. The effect of an injection well on the hydrodynamic conditions in a hypothetical horizontal aquifer in which there is regional flow, are shown in Figure 9.30. The injection well causes a mound in the potentiometric surface. The mound extends unsymmetrically in the direction of regional flow in the aquifer. As injection continues the areal extent of the mound spreads to occupy an ever-increasing area. This process can be viewed as the inverse of the effect of a pumping well in a confined aquifer, and in fact is described mathematically by the same equations, modified for the effect of injection rather than pumping (Warner, 1965). If injection wells are located close together, the potentiometric mounds coalesce in a manner analogous to the drawdown interface in fields of pumping wells. The spread of the front of the potentiometric mound is very rapid in comparison to the spread of the zone of injected waste. The front of the potentiometric mound spreads by pressure translation. The front of the waste zone spreads as volume displacement occurs. The waste zone spreads in direct proportion to the cumulative volume of waste that is forced into the aquifer. The interface between the formation water and the waste will be gradational as a result of dispersion.

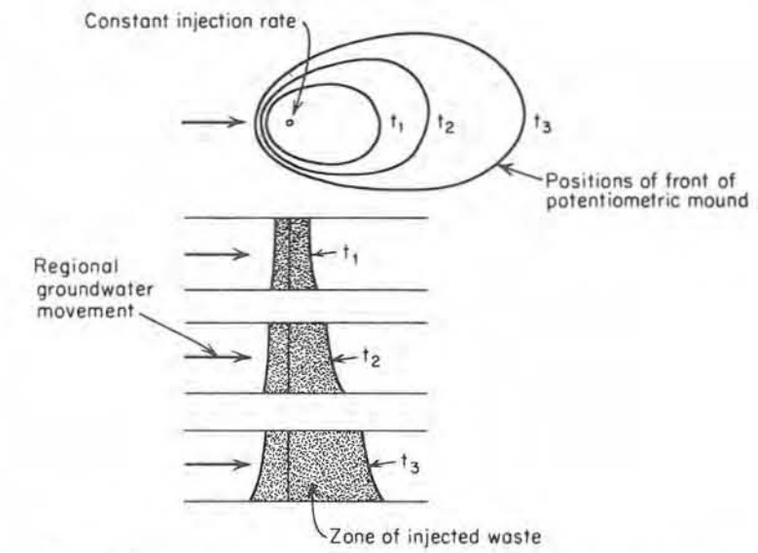

Figure 9.30 Potentiometric mound caused by waste disposal well and expansion of zone occupied by waste. Positions at times t_1, t_2, and t_3 (after Kazmann, 1974).

Based on reviews of status and impact of waste injection practices in the United States and Canada, Warner and Orcutt (1973) and Simpson (1976) concluded that documented cases of even minor disposal system failure and related contamination of surface and near-surface waters are rare. This may not continue to be the case, however, as waste injection becomes an increasingly common waste disposal practice and as the length of time that strata have received wastes increases. One of the few reported instances in which waste injection has caused surface contamination occurred in southern Ontario near Sarnia, where most of the Canadian petrochemical industry is located. Contamination was caused by five injection wells, the first of which was drilled in 1958 and the others in 1960. Refinery caustic and phenolic waters were injected down the wells at rates less than 400

ℓ/min into carbonate rock strata at depths between 200 and 260 m below surface. In the late 1960's and early 1970's, phenol occurrences in fluids reaching the surface in the Sarnia district were observed (Simpson, 1976). It is believed that the contamination occurred because of upward leakage of the wastes through abandoned unplugged wells. There may be as many as 30,000 unplugged wells in southwestern Ontario in the vicinity of Sarnia (van Everdingen and Freeze, 1971). Many of these were drilled decades ago before plugging of abandoned wells was required. The hazard represented by unplugged wells in areas of waste injection is a particularly insidious one because the location of many of the wells is unknown. Some no longer even exist at ground surface but provide vertical connections below ground surface. There may be more than 1 million unplugged, unlocated wells in North America. In regard to the long-term effect of deep-well injection of noxious wastes, van Everdingen and Freeze (1971) have suggested that vertical connections provided by unplugged wells may well be the most important hazard.

Another major hazard associated with the practice of waste injection is the inducement of earthquakes as a result of increasing pore-water pressures along faults. This topic is discussed in Chapter 11.

As a concluding statement on deep-well disposal, the comments by A. M. Piper (1970) of the United States Geological Survey seem appropriate:

> In its predilection for grossly oversimplifying a problem and seeking to resolve all variants by a single massive attack, the United States appears to verge on accepting deep injection of wastes as a certain cure for all the ills of water pollution (p. 2).
>
> Injection does not constitute permanent disposal. Rather, it detains in storage and commits to such storage—for all time in the case of the most intractable wastes—under-ground space of which little is attainable in some areas, and which definitely is exhaustible in most areas (p. 6).
>
> Admittedly, injecting liquid wastes deep beneath the land surface is a potential means for alleviating pollution of rivers and lakes. But, by no stretch of the imagination is injection a panacea that can encompass all wastes and resolve all pollution even if economic limitations should be waived. Limitations on the potentials for practical injection are stringent indeed—physical, chemical, geologic, hydrologic, economic and institutional (including legal) limitations (p. 5).

Other Sources

There are many other sources that contribute contaminants to the groundwater zone. In the northern United States and in Canada large quantities of salts are applied to roads to combat adverse ice conditions during the winter months. Contamination of shallow aquifers along roads that receive salt is not uncommon in these regions. Since salts such as NaCl and $CaCl_2$ are highly soluble and relatively mobile in groundwater, there is little that can be done to prevent this situation, other than to decrease the amount of salt usage.

Activities of the mining industry are another potential cause of groundwater contamination. The effects range from changes in groundwater chemistry caused by mining to infiltration of leachate from tailings and other wastes. The extensive occurrence of acid water drainage from abandoned coal mines in the Appalachian region of the United States is the most visible example of adverse effects of mining on groundwater and surface water.

Seepage from industrial waste lagoons is another cause of groundwater contamination. Across North America there are thousands of artificial ponds and lagoons that contain countless types of liquid wastes. In many cases the lagoons are not lined with impermeable barriers, thereby providing opportunity for seepage of wastes downward into the subsurface environment. In situations where potable-water aquifers are located nearby, this can cause serious problems. Many years may pass, however, before the extent of the problem becomes evident.

In some regions urbanization is spreading into the recharge areas of major aquifers. Even if centralized sewage treatment facilities rather than septic systems are used, urban activities produce numerous sources of contamination to the ground. Prediction of the long-term effect of urbanization on groundwater quality is a difficult task but a necessary one if we are to develop methods of land use planning that will minimize adverse impacts on the groundwater environment.

As an introduction to the literature on groundwater contamination and related topics, the reader is referred to Hall (1972), Summers and Spiegal (1974), Todd and McNulty (1976), and Wilson et al. (1976). An indication of the nature and regional extent of groundwater contamination in the United States is presented in the reviews by Fuhriman and Barton (1971), Scalf et al. (1973), Miller et al. (1974), and Scalf (1977). A summary of waste disposal practices and their effects on groundwater in the United States has been described by U.S. Environmental Protection Agency (1977). A review of recent research activities related to chemical problems in hydrogeology has been presented by Back and Cherry (1976).

Suggested Readings

BAETSLÉ, L. H. 1969. Migration of radionuclides in porous media, *Progress in Nuclear Energy, Series XII, Health Physics*, ed. A. M. F. Duhamel. Pergamon Press, Elmsford, N.Y., pp. 707–730.

CHERRY, J. A., R. W. GILLHAM, and J. F. PICKENS. 1975. Contaminant hydrogeology: Part 1: Physical processes, *Geosci. Can.*, 2, pp. 76–84.

FRIED, J. J. 1976. *Ground Water Pollution.* Elsevier, Amsterdam, pp. 1–47.

OGATA, AKIO. 1970. Theory of dispersion in a granular medium. *U.S. Geol. Surv. Prof. Paper 411-I*, p. 134.

U.S. Environmental Protection Agency. 1977. Waste disposal practices and their effects on ground water. *The Report to Congress*, pp. 81–107.

Problems

1. A chemical analysis of groundwater yields the following results (mg/ℓ): $K^+ = 3$, $Na^+ = 110$, $Ca^{2+} = 80$, $Mg^{2+} = 55$, $HCO_3^- = 420$, $Cl^- = 220$, $SO_4^{2-} = 35$, $NO_3^- = 15$, Fe(total) = 0.8, Mn(total) = 0.2, $F^- = 0.6$, As = 0.03, Pb = 0.08, B = 0.9. Comment on the suitability of this water for the following uses:
   (a) Municipal water supply.
   (b) Irrigation of vegetable crops.
   (c) Livestock.
   (d) Brewing of beer.

2. Would water with the composition indicated in Problem 1 normally be softened for household use? How would the process of water softening be expected to alter the composition?

3. Using a cylindrical column (10 cm in diameter and 30 cm long) of relatively homogeneous sand, an experiment with a step-function input of a nonreactive tracer is conducted (see Figure 9.1). The porosity of the sand is 35%, the steady-state flow rate is 1 ℓ/h, and the hydraulic gradient is 0.1. The $C/C_0 = 0.5$ point on the breakthrough curve arrived 0.8 h after the tracer initially entered the column. The $C/C_0 = 0.25$ point arrived at 0.7 h and the $C/C_0 = 0.75$ point at 0.9 h. Estimate the dispersivity of the sand.

4. A contaminant zone is migrating through an aquifer composed of medium-grained sand. The average hydraulic gradient is 0.01. A representative value of the hydraulic conductivity of the sand is 1×10^{-5} m/s. Is the movement of nonreactive contaminants influenced primarily by advection and mechanical dispersion or by molecular diffusion? Explain.

5. A sanitary landfill is located on a deposit of dense clay that is 5 m thick overlying an aquifer that provides drinking water to a small town. A zone of leachate-contaminated groundwater has accumulated at the base of the landfill on the clay surface. Observations in the aquifer indicate a steady piezometric level of 250.5 m above mean sea level. The surface of the water table in the landfill is at about 251.3 m. The hydraulic conductivity of the clay is approximately 2×10^{-11} m/s, and the porosity is 19%. Estimate how long it will take for nonreactive contaminants to move through the clay into the aquifer. Express your answer as a range of values that you consider to be reasonable in light of the available data.

6. As a result of the rupture of a storage tank, 10 m^3 of liquid waste containing 100 kg of dissolved arsenic rapidly infiltrated into a shallow, unconfined, sandy aquifer in which the flow is horizontal. The average groundwater velocity in the aquifer is 0.5 m/day, the dispersivity is 0.1 m, and the coefficient of molecular diffusion is 2×10^{-10} m^2/s. As the contaminated zone moves through the

aquifer, the arsenic does not undergo significant adsorption or precipitation. Estimate the maximum arsenic concentration after the contaminant cloud has moved a distance of 500 m. What will be the approximate dimensions of the cloud? Assume that the leakage from the storage tank can be approximated as a point source and that the aquifer can be treated as a homogeneous medium with uniform flow.

7. High-level radioactive waste is buried in a cavern in unfractured shale at a depth of 1000 m below ground surface. The burial zone is separated from the nearest overlying aquifer by a vertical thickness of 100 m of shale. The shale has a hydraulic conductivity of the order of 10^{-12} m/s and vertical hydraulic gradient of about 10^{-2} directed upward. In the shale, nonreactive radionuclides have effective diffusion coefficients in the order of 10^{-10} m^2/s. It is expected that the wastes will become wet at some time during the next 1000 years and will then move slowly out into the shale. Is it reasonable to expect that radionuclides will remain entirely within the shale during the next 100,000 years? Ignore the potential effects of faulting, glaciation, and so on, as a cause of radionuclide transfer through the shale. Consider only the influence of flow, mechanical dispersion, and molecular diffusion.

8. Field observations in a granitic area indicate bulk hydraulic conductivities on the order of 10^{-6} cm/s. The granite has a cubic array of joints with a representative spacing of 10 cm between joint planes. Estimate the average groundwater velocity for a zone in which the flow is horizontal and the hydraulic gradient is 10^{-2}.

9. In laboratory experiments using a pesticide and samples from a sandy aquifer, it is observed that when water with the pesticide is equilibrated at various concentrations with the sand samples, the partitioning of the pesticide between the liquid and solid phases is as follows: test 1, 100 μg/g adsorbed at 10 mg/mℓ in solution; test 2, 300 μg/g adsorbed at 220 mg/mℓ in solution; test 3, 600 μg/g adsorbed at 560 μg/mℓ in solution; test 4, 1000 μg/g adsorbed at 1000 mg/mℓ in solution. What distribution coefficient is indicated by these data? Express your answer in milliliters per gram. In sand (porosity = 35%) below the water table, estimate the relative velocity at which the pesticide would migrate in an advection-controlled system.

10. Studies of the behavior of a toxic chemical compound in a sandstone aquifer indicate the following parameter values: porosity 10%, average linear velocity 0.1 cm/day, and distribution coefficient 75 mℓ/g. Estimate the velocity at which the center of mass of a zone contaminated with the compound would travel.

11. Hydrogeological studies of a site for a proposed lagoon for storage of toxic liquid wastes indicate that the hydraulic gradient at the site is downward. The water table is located at a depth of 4 m below the ground surface. Samples from

piezometers at depths of 5, 10, 15, 20, 25, 30, 40, and 50 m below ground surface have tritium concentrations of 75, 81, 79, 250, 510, 301, 50, and 10 tritium units. The site is located in the interior of North America. The piezometers are situated in a thick deposit of shale. Provide an interpretation of the tritium data. What is the nature of the permeability of the shale?

12. Groundwater in a sandstone aquifer at a temperature of 25°C has the following composition (mg/ℓ): $K^+ = 12$, $Na^+ = 230$, $Ca^{2+} = 350$, $Mg^{2+} = 45$, $HCO_3^- = 320$, $Cl^- = 390$, and $SO_4^{2-} = 782$; pH 7.6. If F^- is supplied to the water from minerals in the aquifer and if the F^- concentration is not limited by availability, will solubility constraints be expected to maintain the F^- concentration at a level below the limit specified for drinking water? Explain.

13. Effluent from a septic (sewage disposal) system infiltrates into an unconfined gravel aquifer. Upon mixing with the groundwater, the contaminated part of the aquifer has the following content of inorganic constituents (mg/ℓ): $K^+ = 3.1$, $Na^+ = 106$, $Ca^{2+} = 4.2$, $Mg^{2+} = 31$, $HCO_3^- = 81$, $Cl^- = 146$, and $SO_4^{2-} = 48$; pH 6.3, $Eh = -0.1$ V, DO = 0, temperature 23°C. Assuming that equilibrium occurs and that mineral precipitation-dissolution reactions control the concentration of dissolved inorganic phosphorus, indicate (a) the mineral that would provide the solubility constraint on the phosphorus concentration; (b) the dominant dissolved species of inorganic phosphorus; (c) the equilibrium concentration of dissolved phosphorus.

14. A borehole-dilution test is conducted in a well with an inside diameter of 10 cm. The packer-isolated interval in which the tracer is introduced is 100 cm long. After 2 h the tracer concentration declines to one-half of its initial value. The flow in the formation is horizontal, the well has no sand or gravel pack, and the tracer is nonradioactive and nonreactive. Estimate the average linear velocity in the formation.

15. A disposal well for liquid industrial waste commences operation in a horizontal isotropic confined limestone aquifer that has the following characteristics: thickness = 10 m, secondary porosity = 0.1%, bulk hydraulic conductivity = 5×10^{-5} m/s, specific storage = 10^{-6} cm^{-1}. The injection rate is 100 ℓ/min.

(a) To what distance from the injection well will the front of the potentiometric mound have extended after 1 month?

(b) To what distance from the injection well will the front of contamination have moved after 1 month? Neglect the effects of regional groundwater flow and dispersion. Assume that the aquifer is homogeneous and that the primary permeability of the limestone matrix is negligible.

16. Studies of an unconfined aquifer indicate a shallow zone that contains dissolved oxygen in the range 2–6 mg/ℓ and NO_3^- in the range 30–50 mg/ℓ. The source of the NO_3^- is fertilizer. Below this zone there is no detectable dissolved oxygen and no detectable NO_3^-. Hydraulic-head data indicate that groundwater

flows from the upper zone to the lower zone. All the water in the aquifer is very young. Suggest a hydrochemical hypothesis to account for the large decrease in NO_3^- as the water moves downward in the aquifer. What additional data would be desirable as a basis for testing your hypothesis?

17. Salt (as NaCl only) applied to a highway during the winter for prevention of icing problems has caused contamination of a shallow unconfined aquifer near the highway. It has been observed that the Cl^- content of water from many domestic wells, which was formerly soft, has become hard as the Cl^- has risen. The large increase in hardness can be attributed to the effect of road-salt contamination. Outline a geochemical hypothesis to explain the hardness increase.

18. Natural water in a deep sandstone aquifer composed of quartz, feldspar, and a small amount of clay has the following composition (mg/ℓ): $K^+ = 18$, $Na^+ = 850$, $Ca^{2+} = 41$, $Mg^{2+} = 120$, $HCO_3^- = 820$, $Cl^- = 470$, and $SO_4^{2-} = 1150$; pH 8.1. Wastewater that contains abundant dissolved organic matter is put into the aquifer through a disposal well. After injection commences, observation wells in the aquifer near the disposal well yield water in which abundant H_2S and CH_4 are detected. Prior to waste injection, the observation wells showed no detectable H_2S and CH_4. The wastewater injected into the aquifer did not contain these gases. Outline a geochemical hypothesis to account for the occurrence of H_2S and CH_4 in the observation wells. Would you expect the pH of the water to increase or decrease? Explain, with the aid of appropriate chemical equations.

19. An unlined lagoon is used intermittently for recharge of water from a secondary sewage treatment plant. The water has moderate concentrations of major ions (K^+, Na^+, Ca^{2+}, Mg^{2+}, Cl^-, SO_4^{2-}, and HCO_3^-) and an appreciable content of NH_4^+, bacteria, and organic matter. The treated sewage infiltrates from the lagoon downward into a sandy aquifer. Observation wells used to monitor the change in groundwater chemistry caused by the artificial discharge system indicate that the aquifer water in the zone of influence has total hardness, nitrate, and dissolved inorganic carbon concentrations that are considerably above the natural levels in the aquifer. No bacteria are detected in the aquifer. The NH_4^+ concentrations are very low. Account for these chemical characteristics of the water. Include appropriate chemical equations as part of your explanation.

20. In an area of strip mining for coal, the noncoal geologic materials removed during mining (referred to as cast overburden) are returned to the stripped areas as part of a land reclamation program. The average porosity of the cast overburden is 30%. The average degree of saturation of the material is 40%. Assuming that the water and entrapped air in the voids do not migrate, and assuming that all the oxygen in the air and water in the voids is consumed by

oxidation of pyrite, estimate the following:

(a) The SO_4^{2-} content of the pore water.
(b) The pH of the pore water (assume that no carbonate-mineral buffering occurs.
(c) The amount (weight percent) of calcite that would be necessary in the cast overburden to neutralize the acid product by pyrite oxidation.
(d) The amount of pyrite necessary for consumption of all the oxygen by the oxidation reaction.
(e) Would the amounts of calcite and pyrite obtained in parts (c) and (d) be noticeable by normal means of examination of the geologic materials?

CHAPTER 10

Groundwater and Geotechnical Problems